

Functionalization of Polymeric Materials to Control the Kinetics of Pharmaceutical Crystallization

by

Derek S. Frank

A dissertation submitted in partial fulfillment
of the requirements for the degree of
Doctor of Philosophy
(Macromolecular Science and Engineering)
in the University of Michigan
2019

Doctoral Committee:

Professor Adam J. Matzger, Chair
Associate Professor Kenichi Kuroda
Professor Anne J. McNeil
Associate Professor Anish Tuteja

Derek S. Frank

dsfrank@umich.edu

ORCID iD: 0000-0002-0564-074X

© Derek S. Frank 2019

Acknowledgements

First and foremost, I would like to acknowledge my research advisor, Professor Adam J. Matzger. None of the work presented in this thesis could have been completed without his mentorship and guidance. I hope to carry his scientific approach, confident leadership, and clarity of thinking into my own career, and I am indebted to him for crafting me from a student to a scientist. Thank you Professor Matzger for your leadership and trust throughout my graduate school career. I would also like to acknowledge Professor William W. Roberts and Professor Khurshid R. Ghani. Although the work I performed under their guidance is not in this thesis, I have learned a great deal and thoroughly enjoyed working under them in our collaboration project investigating the laser lithotripsy of kidney stones. On that note, I would also like to thank Dr. Ali A. Aldoukhi for being a patient collaborator, thoughtful scientist, and great friend throughout this collaboration.

I am also thankful for my committee members: Professor Anne J. McNeil, Professor Anish Tuteja, and Professor Kenichi Kuroda. Their guidance and support are much appreciated over the past four years. Additionally, I have had a number of fantastic teachers and mentors both during and prior to graduate school. Professor Richard Robertson, Professor Jinsang Kim, Professor Melanie Sanford, Professor Stewart Novick, Professor Brian Northrop, and Professor T. David Westmoreland (and countless others not listed here): I thank you all for inspiring me to seek beauty in science and the joy that knowledge and discovery bring each and every day.

Graduate school was not only a period of intellectual growth but personal as well. I would not be the person I am today if not for the friends and colleagues I've had at Michigan. I'd

especially like to thank the entire Matzger group for their support and friendship—especially my collaborators Dr. Shalini and Amy Zhu—and Brian R. Thompson for his advice, empathy, and humor over the past four years. Finally, I would not be here at all if not for my family. This thesis is dedicated to my parents, who have given me the freedom, support, guidance, and love to make my life exactly as I see it. I love you both. I also want to thank my sisters, Rachel and Ellie (who I apologize for pulling down this path), and my cousins, aunts, uncles, and grandparents who love to see me succeed.

Table of Contents

Acknowledgements	ii
List of Schemes	vii
List of Tables	viii
List of Figures	x
Abstract	xviii
Chapter 1. Introduction	1
1.1 Controlling the Kinetics of Pharmaceutical Crystallization	1
1.2 Nucleation and Crystal Growth	2
1.3 Crystallization Kinetics	3
1.4 Additives to Control Crystallization	4
1.5 Outline of Thesis	6
1.6 References	8
Chapter 2. Influence of Chemical Functionality on the Rate of Polymer-Induced Heteronucleation	12
2.1 Introduction	12
2.2 Methods	13
2.3 Results/Discussion	14
2.4 Conclusion	18
2.5 Supporting Information	19
2.5.1 Synthesis of functionalized Merrifield Resin	19
2.5.2 Raman spectroscopy of functionalized Merrifield Resin	20
2.6 References	27

Chapter 3. Inhibiting or Accelerating Crystallization of Pharmaceuticals by Manipulating Polymer Solubility	29
3.1 Introduction	29
3.2 Methods	30
3.3 Results and Discussion	32
3.4 Supporting Information	40
3.4.1 Synthesis of Functionalized Merrifield Resin	40
3.4.2 Synthesis of Water-Soluble Copolymers	45
3.4.3 Gel Permeation Chromatography of PHEAM Polymers	51
3.4.4 Induction Times to Crystallization of Pyrazinamide and Hydrochlorothiazide containing Functionalized Polymeric Materials	53
3.4.5 Induction Times to Crystallization of Pyrazinamide and Hydrochlorothiazide containing Small-Molecule Additives	66
3.4.6 Solubility of Pharmaceutical Solutes in Presence of PHEAM Polymers	67
3.4.7 Polymorphic Phase of Pharmaceutical Solutes	68
3.4.8 Average Intermolecular Bond Lengths from the Cambridge Structural Database	70
3.4.9 Electrostatic Potential Surfaces of APIs and Polymer Functionalities	71
3.5 References	73
Chapter 4. Effect of Polymer Hydrophobicity on the Stability of Amorphous Solid Dispersions and Supersaturated Solutions of a Hydrophobic Pharmaceutical	77
4.1 Introduction	77
4.2 Experimental	80
4.3 Results/Discussion	81
4.4 Conclusion	89
4.5 Supporting Information	90
4.5.1 Synthesis and characterization of poly(N-hydroxyethyl acrylamide)	90
4.5.2 Functionalization of PHEAM polymers	92
4.5.3 Thermal analysis of ethenzamide, pure polymers, and amorphous solid dispersions	95
4.5.4 Theoretical solubility of amorphous ethenzamide	97
4.5.5 Statistical analysis of precipitation kinetics of ethenzamide	98

4.5.6	Powder X-ray diffraction of ethenzamide amorphous solid dispersions	100
4.5.7	Dynamic vapor sorption of pure PHEAM polymers	104
4.5.8	CSD Interaction Survey	104
4.6	References	107
Chapter 5. Probing the Interplay between Amorphous Solid Dispersion Stability and Polymer Functionality 111		
5.1	Introduction	111
5.2	Experimental	113
5.3	Results	115
5.4	Discussion	121
5.5	Conclusion	124
5.6	Supporting Information	125
5.6.1	Synthesis and functionalization of poly(chloromethylstyrene-co-styrene)	125
5.6.2	Raman spectroscopy and PXRD of functionalized polymers	132
5.6.3	GPC of functionalized polymers	135
5.6.4	Transmission IR Spectroscopy of amorphous solid dispersions	136
5.6.5	Methodology and statistical significance of induction time measurements	137
5.6.6	Polarized light microscopy of amorphous solid dispersion crystallization	141
5.6.7	Prediction of T _g of dispersions by the Fox Equation	142
5.6.8	Powder X-Ray Diffraction of nabumetone crystallized from amorphous solid dispersions	143
5.6.9	Melting point depression of nabumetone	144
5.7	References	144
Chapter 6. Conclusions and Future Directions		149
6.1	Summary of Work	149
6.2	Future Directions	151

List of Schemes

Scheme 2.1 Coupling between Merrifield Resin and phenols to synthesize heteronuclei. The R group indicates the position of functional group variation that was controlled to build the structure-property relationships in this study.....	13
Scheme 3.1 Synthesis of (a) insoluble polymer heteronuclei to accelerate crystallization (black dot represents MFR) and (b) water-soluble polymers to inhibit crystallization. Functionalization with (c) substituted phenols thymol, raspberry ketone, and tyrosol modulates the potency of the polymer to speed or slow crystallization.	31
Scheme 4.1 Functionalization of poly(N-hydroxyethyl acrylamide) to tether hydrophobic phenyl groups to side chains on the polymer.....	79

List of Tables

Table 2.1 Full listing of induction times (in minutes) for acetaminophen crystallization in the presence of insoluble heteronuclei. Values shaded in grey were discarded from statistical analysis—these represent cases where no crystallization occurred over five cycles for an individual vial.	21
Table 2.2 Average intermolecular bond length to resin functionalities, shown with the standard error of measurement and the number of structures included in the averaging. Structures were constrained to those containing intermolecular contacts no more than 4 Å apart.	27
Table 3.1. Induction times (minutes) to crystallization of aqueous pyrazinamide with heteronuclei and water-soluble polymer additives.	54
Table 3.2. Induction times (minutes) to crystallization of aqueous hydrochlorothiazide (7.05 mM, 30 °C) with heteronuclei and water-soluble polymer additives.....	61
Table 4.1 Glass transition temperatures of pure PHEAM polymers and amorphous solid dispersions of polymer and ethenzamide (10 wt% drug) as measured by inflection points by modulated DSC (see Supporting Information for additional details, each value the average of two measured transition temperatures). Water content was measured as total weight loss by TGA below 125 °C for amorphous dispersions stored at ambient temperature and humidity for 24 hours. Dispersions were verified to be amorphous prior to TGA by polarized light microscopy.	85
Table 4.2. ANOVA with Fisher LSD and Tukey HSD tests to determine statistical significance between mean induction times at the 0.05 level. Differences which were judged to be statistically	

significant (probability of null hypothesis > 0.05) are colored in green and differences which are not are shown in red. 98

Table 5.1 Glass transition temperatures for pure functionalized polymers, predicted T_g of polymeric dispersions from the Fox equation, and onset crystallization temperature of nabumetone dispersions (measured by DSC) compared with nucleation rate of dispersions. Values recorded by DSC shown with standard errors are the average of two experimental runs. 118

Table 5.2. Recorded induction times (in minutes) to crystallization for amorphous solid dispersion samples prepared in this work. 137

List of Figures

Figure 1.1. Free energy of a molecular aggregate forming. At sizes beyond the critical radius, an aggregate undergoes nucleation.....	3
Figure 1.2. Reaction coordinate diagram representing crystallization. The kinetics of crystallization can be altered by adjusting the kinetic barrier to nucleation, represented by the red ΔG	4
Figure 2.1 Induction time data of polymer induced heteronucleation of acetaminophen crystallization in water (136 mM at 30 °C). The plot in black represents acetaminophen crystallization without added heteronucleant and colored lines depict crystallization in the presence of the functionalized resins (color coded and shown underneath). The inset in the bottom right shows probability of crystallization in the initial 25 minutes.....	15
Figure 2.2 Statistical analysis of induction time data for polymer-induced heteronucleation. The median induction time is shown on the left in a lighter color, and the time at which 50% vials have undergone crystallization is shown in a darker color on the right.....	15
Figure 2.3 The average induction time is presented with the standard error of measurement for the four functionalized polymers which induced crystallization in all vials before 300 minutes. Below are the average intermolecular bond distances between a phenolic hydroxy functionality and hydrogen bond accepting functionalities (hydroxy to carbonyl oxygen atom for AP-MFR, ACM-MFR, and MACM-MFR; hydroxy to aniline nitrogen for AN-MFR) as averaged over materials in the Cambridge Structural Database (CSD) containing intermolecular bonds between	

the relevant functionalities (see Supporting Information for additional details). Also listed is the average bond length to a water molecule from these functionalities as found in crystalline hydrates. 18

Figure 2.4 Raman spectra of functionalized Merrifield Resins. Each colored plot corresponds with the functionalized resin pictured at the left in the diagram..... 20

Figure 3.1 Pharmaceuticals (a) pyrazinamide and (b) hydrochlorothiazide were employed to study the effects of additives on crystallization. 32

Figure 3.2 Percent of trials crystallized over time of aqueous pyrazinamide (30 °C, 203 mM) containing Merrifield Resin (solid lines) and poly(hydroxyethyl acrylamide-co-chloromethylstyrene) (dashed lines) functionalized with thymol (shown in green), raspberry ketone (red), and tyrosol (blue). Crystallization without additives is shown by the black trace. . 34

Figure 3.3 Percent of trails crystallized of aqueous hydrochlorothiazide (30 °C, 7.05 mM, giving a supersaturation ratio of 2.554) with Merrifield Resin (solid lines) and poly(hydroxyethyl acrylamide-co-chloromethylstyrene) (dashed lines) additives functionalized with thymol (shown in green), raspberry ketone (red), and tyrosol (blue). Crystallization without additives is shown in black. 38

Figure 3.4. Raman spectroscopy of functionalized Merrifield Resins with substituted phenols. Chloromethyl substitution confirmed by the loss of the band at 676 cm^{-1} in the unfunctionalized MFR. 43

Figure 3.5. FT-IR spectra of functionalized Merrifield Resin between (a) $2600\text{-}4000\text{ cm}^{-1}$ and between (b) $400\text{-}2000\text{ cm}^{-1}$. Each colored trace in (b) corresponds to the compounds drawn in the same color on the left in (a). 45

Figure 3.6. GPC of functionalized PHEAM polymers. 52

Figure 3.7. Survival plots for pyrazinamide crystallization, where survival represents the ability of a supersaturated solution to maintain supersaturation without crystallization, drawn with 95% confidence intervals, comparing a) control (neat) pyrazinamide crystallization and crystallization with added MFR, and b) pyrazinamide crystallizations with 1 wt% functionalized PHEAM polymers..... 60

Figure 3.8. Survival plots for hydrochlorothiazide crystallization, where survival represents the ability of a supersaturated solution to maintain supersaturation without crystallization, drawn with 95% confidence intervals, comparing a) control (neat) hydrochlorothiazide crystallization and crystallization with added MFR, and b) crystallizations with 1 wt% functionalized PHEAM polymers..... 65

Figure 3.9. Aqueous crystallization kinetics of pyrazinamide (shown in black, 203 mM, 30 °C) in the presence of 1 mol% small-molecule additives thymol (green), raspberry ketone (red), and tyrosol (blue), pictured in the lower right of the figure. 66

Figure 3.10. Clear point temperature (with standard error) upon heating of a) pyrazinamide (25 mg/mL) and b) hydrochlorothiazide (2.1 mg/mL) in the presence of 1 wt% soluble polymer (denoted under the x-axis on the plot) and in aqueous solution (denoted as control group). 68

Figure 3.11. Raman spectroscopy of pyrazinamide crystallized from aqueous solution (black trace), aqueous solution with PHEAM (dotted colored traces, following the coloring scheme for functionalized polymers used throughout the manuscript), and aqueous solution with PHEAM (solid colored traces). All crystals were found to be alpha pyrazinamide. 69

Figure 3.12. Raman spectroscopy of hydrochlorothiazide crystallized from aqueous solution (black trace), aqueous solution with PHEAM (dotted colored traces, following the coloring

scheme for functionalized polymers used throughout the manuscript), and aqueous solution with PHEAM (solid colored traces). All crystals were found to be hydrochlorothiazide Form I. 69

Figure 3.13. Histogram of interaction distances between aliphatic hydroxyl group and water (shown in upper panel in blue) and ketone functionality and water (shown in lower panel in red). 71

Figure 3.14. Electrostatic potential maps of a) pyrazinamide, b) hydrochlorothiazide, and polymers functionalized with c) thymol, d) raspberry ketone, and e) tyrosol (functionalization is represented by replacement of the phenol with a benzyl ether) calculated using density functional theory at the B3LYP/6-31+G** level of theory (regions of negative potential represented by red, positive potential presented by blue, and neutral represented by green). 72

Figure 4.1 Average induction time of aqueous ethenzamide (3 mg/mL, 18 mM) crystallization at 30 °C (shown with standard error) with 300 µg/mL poly(hydroxyethyl acrylamide) polymers as crystallization additives. 82

Figure 4.2 Powder X-ray diffraction data of amorphous solid dispersions over time. Crystalline content of a dispersion containing 10 wt% ethenzamide in PHEAM over one week is shown on the left (in green), as compared to ethenzamide in PHEAM-3% (blue) and ethenzamide in PHEAM-10% (in purple). Diffraction patterns have been background subtracted and baseline corrected to remove signal from amorphous polymer and glass substrate. 83

Figure 4.3 Percent uptake of water vapor by pure polymeric materials. PHEAM is shown with green squares, PHEAM-3% is shown with blue circles, and PHEAM-10% is shown with purple triangles. 86

Figure 4.4 Average intermolecular bond distance between amide or water groups and carbamate and primary alcohol groups as determined by an arithmetic average of bond distances from

crystal structures from the CSD, shown with standard error. Interaction distances with alcohol functionalities are shown in blue and interaction distances with carbamate functionalities are shown in red..... 89

Figure 4.5. Elution time of PHEAM in tetrahydrofuran through GPC column with a flow rate of 1 mL/min. Molecular weights were calculated relative to polystyrene standards in tetrahydrofuran using UV-vis detection at 264 nm..... 92

Figure 4.6. DSC thermogram of 0.9 mg pure ethenzamide melting and recrystallization at a 20 °C/minute scanning rate..... 95

Figure 4.7. Glass transition temperatures of a) PHEAM, b) PHEAM-3%, and c) PHEAM-10% as measured by MDSC..... 96

Figure 4.8. Glass transition temperatures of dispersions of ethenzamide with a) 90 wt% PHEAM, b) 90 wt% PHEAM-3%, and c) 90 wt% PHEAM-10% as measured by MDSC after vitrification at 140 °C. 96

Figure 4.9. Theoretical amorphous solubility of ethenzamide determined by equating expressions for $\Delta G_{a \rightarrow c}$ 97

Figure 4.10. Box plot showing median, 25-75th percentile range (limits to the box), and 5-95th percentile ranges (denoted by error bars) of the induction time to crystallization of aqueous ethenzamide in the presence of polymer additives. 99

Figure 4.11. PXRD patterns of amorphous dispersions of ethenzamide and PHEAM polymers (90 wt%) over time. Each amorphous solid dispersion contains the polymer shown above each set of powder patterns. Samples stored during the same time period are compared across the x-axis. 102

Figure 4.12. PXRD patterns of PHEAM ethenzamide dispersions (90 wt% polymer) stored under ambient conditions (green on the left) and stored in desiccator (shown in yellow on the right). 103

Figure 4.13. Histogram of interaction distances between functional groups as shown above.

Hydrogen bonding in the crystal structures was found predominately in the regions between 2.5 and 3.5 Å. 105

Figure 4.14. Average intermolecular bond distances between amide groups or water molecules and primary alcohol or carbamate groups as determined from averaging interaction distances from a survey of known crystal structures. Structures were restricted to those with intermolecular contacts between 2.5 to 3.5 Å, 3D coordinates determined, no ions, and only organic structures using CSD version 5.38 (updated May 2016). 107

Figure 5.1 a) Series of statistical copolymers studied as crystallization inhibitors in amorphous solid dispersions with b) nabumetone. Each is given a name corresponding to functional groups on the polymers; polyCMS is the parent poly(chloromethylstyrene-*co*-styrene) polymer, polyPH has a phenyl group, polyACM bears an acetaminophen ligated through the phenol, polyMACM has bears a methylated acetaminophen, polyBA has a benzyl alcohol functionality, and polyBME has a benzyl methyl ether moiety. 113

Figure 5.2 Crystal appearance of nabumetone dispersed in polymer (shown here in polyBME). As seen in the sample indicated with a red circle, within three minutes of initial nucleation ($t = 33$ min), crystallization occurs throughout the entire dispersion. Thus the induction time to nucleation is designated as the time to first crystal appearance in dispersions and delays due to growth rates are assumed to be negligible. The two samples at the bottom of the slide remain amorphous over this time period, and the other samples have undergone crystallization earlier in the trial. 114

Figure 5.3 Rate of crystallization for nabumetone dispersed in each of the functionalized polymers at 30 °C. The black trace shows pure nabumetone crystallization from the amorphous state and each colored trace represents a 50 wt% dispersion of nabumetone in the corresponding colored polymer, ordered left-to-right according to their relative ability to inhibit crystallization. 116

Figure 5.4 Overlaid transmission IR spectra of dispersions ranked top-to-bottom by decreasing peak frequency of the nabumetone carbonyl stretch, highlighted in red. 120

Figure 5.5 Probability plot of nabumetone nucleation from amorphous solid dispersions containing 16 wt% (dotted lines) and 50 wt% (solid lines) of polyACM (blue) and polyMACM (purple). Pure nabumetone crystallization is shown in black. 123

Figure 5.6. Raman spectra of functionalized poly(chloromethylstyrene-*co*-styrene) polymers used in this study, labeled by side-chain functionality. 133

Figure 5.7. PXRD of functionalized polymers labelled by chemical name as designed in Figure 1 in the manuscript text. 134

Figure 5.8. GPC traces for functionalized poly(chloromethylstyrene-*co*-styrene) polymers. 135

Figure 5.9. Transmission IR spectra comparing pure polymer (dotted line) and dispersion with nabumetone (solid line). 136

Figure 5.10. Average induction times to crystallization as determined by linear regression—standard errors were determined by standard error to slopes regressed in $\ln P = -t/\tau$. Plot a) compares across all polymers used as inhibitors in this study, while plot b) compares the fastest crystallizing samples. 140

Figure 5.11. Measured T_g of nabumetone dispersions in polyCMS with extrapolated plot to determine the T_g for pure nabumetone. 142

Figure 5.12. PXRD traces for nabumetone crystallites formed from amorphous dispersions—
plots correspond to the dispersion labeled above to each curve. 143

Figure 5.13. DSC of nabumetone Form I showing melting point depression in the presence of
polymers..... 144

Abstract

Crystallization is ubiquitous in the pharmaceutical industry and is employed in the design, development, and manufacturing of drugs. In particular, controlling the kinetics of crystallization can improve the efficiency of batch crystallization processes and ensure the physical stability of metastable drug products. Although the crystallization rate of a small-molecule pharmaceutical is often tuned by altering parameters such as pharmaceutical concentration, temperature, or solvent, there is a considerable demand for additives that can alter crystallization kinetics without changing the thermodynamic solubility of a pharmaceutical. However, the relationship between the molecular structure and impact of an additive on crystallization kinetics is still poorly understood. This dissertation presents structure-function relationships dictating how polymers can be engineered to most effectively increase or decrease the crystallization rate of small-molecule pharmaceuticals in solution and in the amorphous phase. Insoluble, crosslinked polymers are demonstrated to accelerate acetaminophen nucleation in solution. Maximizing interaction strength between polymer and acetaminophen while minimizing interaction strength between polymer and water leads to polymers best able to induce crystallization. These insoluble crystallization accelerators are leveraged to discover water-soluble polymers to inhibit crystallization. Functionalities that rapidly accelerate crystallization when tethered to soluble polymers are shown to be strong inhibitors of crystallization when attached to

water-soluble polymers. This methodology of screening functionalities on insoluble polymers to determine their interaction strength with a target pharmaceutical streamlines the discovery of polymers to inhibit crystallization. The relationship between polymers designed to inhibit crystallization in solution and in the solid-state is also explored. Using a common set of polymeric materials, it is shown that increasing polymer hydrophobicity improves both the physical stability of supersaturated solutions and the physical stability of amorphous solid dispersions. Finally, the relationship between polymer functionality and physical stability is investigated for amorphous solid dispersions of the hydrophobic drug nabumetone. The solubility of polymer excipient in amorphous nabumetone is demonstrated to have a crucial effect in determining the ability of polymers to stabilize amorphous solid dispersions. Throughout all of these studies, postpolymerization functionalization is used to synthesize libraries of polymers containing a range of functional group chemistry without changing physical parameters of polymers such as number-average chain length or backbone chain chemistry to isolate the effects of polymer chemistry on the ability of a polymer to alter crystallization rates. Fundamental parameters, including interaction strength between polymer and drug, interaction strength between polymer and solvent, and cohesive polymer-polymer interactions, are shown to dictate the ability of a polymer to speed or slow crystallization, and the effect of polymers to either speed or slow crystallization is compared and contrasted for crystallizations in solution and in the amorphous phase.

Chapter 1. Introduction

1.1 Controlling the Kinetics of Pharmaceutical Crystallization

Crystallization is a physical transformation used across a range of chemical industries. Reflecting its overwhelming importance in the purification and processing of small molecules, crystallization is a widely researched phenomenon both in academia and industry.¹ Understanding the factors that dictate the kinetics of crystallization is necessary for scientists and engineers to best plan and execute crystallizations in manufacturing settings.² Furthermore, as is true for many chemical and physical transformations, a detailed understanding of crystallization kinetics provides insights into its mechanism and therefore a window to control. Unlike many chemical transformations, crystallization is a stochastic process—in other words, whether a crystallization will occur after a given amount of time cannot be known beyond some probability.³ An optimally controlled crystallization is one in which the kinetics have been accelerated or inhibited to such an extent that the probability of crystallization becomes sufficiently large (or small) that crystallization can be nearly guaranteed to occur (or completely avoided). Controlling crystallization is crucial in the pharmaceutical industry. For instance, drug products containing amorphous active pharmaceutical ingredient must be stabilized from crystallization in their amorphous phase, as crystallization leads to dramatic changes in the oral bioavailability of these drug products, potentially rendering a potent medication unable to exert sufficient therapeutic effect.⁴ This introduction will discuss fundamental theories concerning crystallization as well as the use of molecular additives with the goal of controlling crystallization kinetics.

1.2 Nucleation and Crystal Growth

Crystallization is composed of two distinct physical processes: nucleation and crystal growth. Nucleation is the initial formation of a crystalline material from some homogeneous fluid medium, be it the solution state or the amorphous phase.³ At the mechanistic level, nucleation is an understudied process, and this is a natural result of the extremely small length scales of nuclei. In place of an experimentally validated mechanism, classical nucleation theory (which is inspired by the process of liquid condensation from the vapor phase) posits that nucleation occurs when molecular aggregates coalesce in spheres with sizes greater than that of the critical radius. At these sizes, the stabilizing negative free energy of the aggregate volume is greater than the destabilizing positive free energy associated with the interfacial tension between the aggregate and the surrounding medium (see Figure 1.1). As a result, these aggregates continue to grow and molecules within the aggregate adopt the arrangement of a regular, ordered lattice. The exact molecular arrangement of pre-nucleation clusters prior to crystallization is not well known, although recent work has proposed models for how molecules come together to undergo nucleation from disordered phases.⁵⁻⁶ Nucleation arises from density fluctuations which result in regions of high concentration and the formation of molecular aggregates with sizes beyond the critical radius. A single nucleation event often leads to widescale crystallization of a medium via mechanisms such as secondary nucleation or crystal growth. Because this initial primary nucleation event occurs due to random density fluctuations in a medium, it is impossible to predict the exact moment nucleation will occur, and as a result, nucleation is a stochastic phenomenon. Nucleation often—if not always at lab scale—occurs via a heteronucleation pathway, meaning that pre-nuclei in solution are stabilized by foreign particles in the crystallization medium which reduce interfacial free energy.⁷

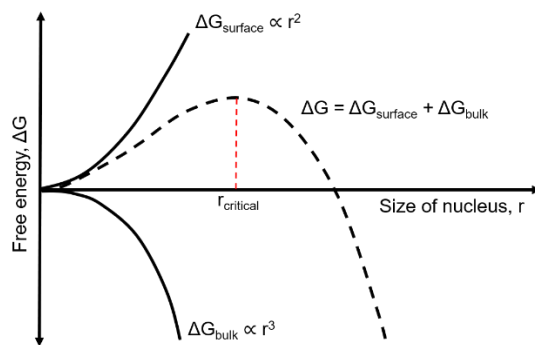


Figure 1.1. Free energy of a molecular aggregate forming. At sizes beyond the critical radius, an aggregate undergoes nucleation.

Once nucleation has occurred, crystallites in contact with a high energy phase (supersaturated solution or amorphous melt) undergo crystal growth. There are many pathways for crystal growth.^{3, 8} Crystal growth rates are a function of a variety of parameters such as concentration, diffusivity, pressure, and temperature.³ The relative rates of crystal growth along each crystal face modulate crystal morphology, and the overall rates of crystal growth can control other properties of crystals, such as solvent inclusion and crystallographic defects.

1.3 Crystallization Kinetics

The most common method to alter the kinetics of crystallization is by changing the concentration of solute. This change can also be achieved by modifying the temperature or solvent used in a crystallization. However, although altering the concentration of a solute or temperature changes the kinetics of crystallization, it also changes a number of other parameters relevant to a crystallization, such as the equilibrium concentration and solute activity. In contrast, a more controlled way to increase or decrease crystallization rates is by modifying the kinetic barrier to crystallization (see reaction coordinate diagram in Figure 1.2). Lowering the kinetic barrier accelerates nucleation while raising the barrier inhibits nucleation. This method of altering crystallization kinetics has been leveraged to select for particular crystal polymorphs of a compound by facilitating formation of one polymorph or restricting formation of another. This

approach does not change the supersaturation ratio (ratio between solute concentration and the equilibrium solubility) and as a result does not affect the overall yield during crystallization. As a result, there is a significant interest in developing methods to control the kinetic barrier to crystallization as a method to control crystallization kinetics.

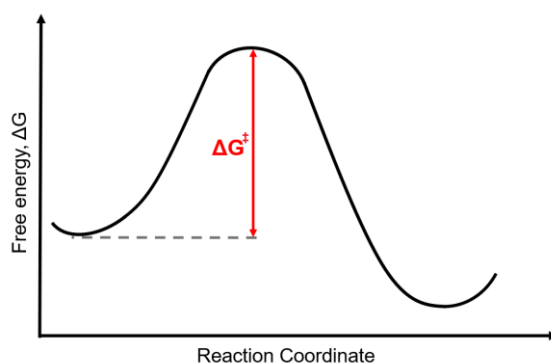


Figure 1.2. Reaction coordinate diagram representing crystallization. The kinetics of crystallization can be altered by adjusting the kinetic barrier to nucleation, represented by the red ΔG^\ddagger .

The nucleation rates for pharmaceuticals have been predicted and rationalized for a number of compounds.⁹⁻¹⁶ In general, it has been shown that compounds of high molecular weight, containing many rotatable bonds, and forming strong molecular interactions with solvent, show relatively slow nucleation rates when controlled for solubility. Crystal growth kinetics for pharmaceutical have also been investigated are also controlled by properties such as temperature, viscosity, and crystallization solvent. Similar to nucleation, crystal growth can be inhibited or accelerated by altering the kinetic barrier associated with adsorption of molecules on a high-energy crystal face.¹ In amorphous systems, differences between crystal growth rates at the surface and within the bulk of glasses have been observed experimentally.¹⁷

1.4 Additives to Control Crystallization

There have been a variety of developments in the design of additives to alter and control the kinetics of crystallization.¹⁸⁻²⁰ Additives range in their physical properties, such as molecular

weight, solubility, and polarity. This section will discuss additives to accelerate and inhibit nucleation as well as additives to speed or slow the crystal growth rates for pharmaceuticals.

The ability of additives to speed nucleation has been observed for crystallization from solution as well as from the amorphous phase.²⁰⁻²¹ Both soluble and insoluble additives have been shown to act as nucleation accelerators. Insoluble crystallization additives accelerate nucleation by providing insoluble surfaces to promote heterogeneous nucleation,^{3, 22} and soluble additives can accelerate nucleation by modifying the structural organization of a crystallizing molecule to promote the formation of nucleation clusters.^{19, 23} It has been demonstrated that factors such as interaction strength between an insoluble surface and crystallization solute correlate with heteronucleation rates.²⁴⁻²⁸ Other parameters such as structural lattice matching between insoluble surfaces and a target crystal have been proposed to facilitate acceleration of nucleation as well.^{24, 29} The ability of crystallization additives to promote nucleation by other mechanisms has also been explored.³⁰ One well-documented instance is the ability of water to speed crystallization from the amorphous phase, which occurs due to increases in molecular mobility upon the absorption of water, which catalyzes crystallization.³¹⁻³³

Inhibition of nucleation can also be achieved using molecular additives. One difference between additives that suppress and those that accelerate nucleation is that inhibitors tend to be soluble in the crystallization medium whereas accelerators tend to be insoluble. Inhibition of nucleation has been explored both in solution and in the amorphous solid-state due to its direct application in the formulation of amorphous solid dispersions of hydrophobic pharmaceuticals. Crystallization inhibitors have been proposed to function by interrupting the formation of nucleation clusters.¹⁴ Additives to inhibit nucleation in solution tend to be linear, water-soluble polymers,³⁴⁻³⁶ but small molecules have also been shown various degrees of effectiveness,³⁷⁻⁴⁰ and more recent work has

investigated polymer micelles to prevent nucleation in solution as well.⁴¹⁻⁴² In the amorphous phase, water-soluble linear polymers have also been commonly used to stabilize against nucleation;⁴³⁻⁴⁴ however, water-solubility is by no means necessary for an excipient to stabilize the amorphous phase, and neither is large molecule weight, evident by the many small molecules which have also been shown to stabilize the amorphous phase from crystallization.⁴⁵⁻⁴⁹

The effects of additives on crystal growth are equally as divergent as those found for nucleation. Some additives have also been demonstrated to accelerate crystal growth rates;⁵⁰⁻⁵² however, far more common is that additives inhibit crystal growth rates in solution^{26, 53-56} and the amorphous phase.⁵⁷⁻⁶⁰ Regulating crystal growth by molecular additives has been leveraged in crystallization techniques as spherical crystallization⁶¹⁻⁶² and nanocrystallization⁶³⁻⁶⁴ which have direct applications to improve both processing and performance of crystalline therapeutics. However, from the standpoint of developing excipients to restrict crystallization in amorphous drug products, restricting nucleation is far more important than restricting crystal growth, as even minute amounts of crystalline material can have dramatic effects on oral bioavailability.⁶⁵

1.5 Outline of Thesis

This thesis describes the use of polymeric additives to modulate the crystallization rate of pharmaceuticals. Polymers are compounds of high molecular weight composed of small, chemically linked (and often repeating) subunits.⁶⁶ Polymers are advantageous as kinetic modifiers of crystallization given their range of functional group chemistry, controllable molecular weight, and ease of separation relative to small-molecular crystallization additives. Although many studies have empirically investigated the ability of polymers to modulate the crystallization propensity of pharmaceutical compounds, for the most part, these studies have used commercially available water-soluble polymers.^{35, 44} As a result, the currently existing structure-function relationships

dictating how functional groups impact crystallization rely on a relatively small range of functional group chemistries. The work in this thesis employs post-polymerization functionalization to alter the side-chain functionality on a polymer without changing its number-average chain length or backbone chain chemistry to elucidate the relationship between functional group chemistry on a polymer and its ability to impact the crystallization of pharmaceuticals. The following chapters in this dissertation illustrate design principles for polymers to impact crystallization in a number of contexts, including the use of polymers to speed crystallization, the use of polymers to inhibit precipitation, and the use of polymers to stabilize amorphous pharmaceutical against crystallization. It is demonstrated that the fundamental parameters governing how a polymer impacts crystallization are vastly similar in each of these situations. This work in total serves to deepen the design and engineering of polymeric additives to impact crystallization rate, ultimately with the goal of a totally controlled crystallization for pharmaceutical compounds. Chapter 2 describes the design of insoluble polymers to act as heterogeneous sites to catalyze nucleation. The structure-function relationships dictating the impact of polymer chemistry on heteronucleation are explored. Chapter 3 contains a study on the engineering of water-soluble polymers to inhibit crystallization. Here, it is shown that functionalities identified as potent crystallization accelerators when tethered to insoluble polymers are effective inhibitors of crystallization when attached to water-soluble precipitation inhibitors. This insight reduces the bottleneck associated with measuring crystallization inhibition, which can often take months or years to accomplish, by quantifying the ability of functionalities to accelerate crystallization via heteronucleation, which occurs on the timescale of minutes. Such technology can lead to a more efficient discovery of polymer chemistries to be used in pharmaceutical formulation to ensure long-term stability. Chapters 4 and 5 discuss stabilization against crystallization in the amorphous phase. Chapter 4

compares the polymers optimized to inhibit crystallization in solution and those designed to inhibit amorphous crystallization. It is found that many chemical factors which allow an additive to enhance the stability of supersaturated solutions also lead to long-term stability of amorphous solid dispersions. Chapter 5 describes how post-polymerization functionalization leads to a deeper understanding of polymer design to inhibit the crystallization of amorphous solid dispersions. This work also demonstrates how many parameters used previously to predict the relative physical stability of amorphous solid dispersions—such as the onset crystallization temperature and the glass transition temperature—fail to predict stability when controlling for polymer properties such as chain length. A competing theory is presented that suggests that the solubility of polymers in the amorphous phase of pharmaceutical plays an essential role dictating the stability of amorphous solid dispersions against nucleation. Finally, Chapter 6 discusses future directions in this field, synthesizing conclusions from each chapter to propose how the data and insights presented in this thesis might lead to better pharmaceutical formulation and manufacturing technologies.

1.6 References

1. McCabe, W. L.; Smith, J. C.; Harriott, P., *Unit Operations of Chemical Engineering*; McGraw-Hill New York, 1993.
2. Variankaval, N.; Cote, A. S.; Doherty, M. F., From form to function: Crystallization of active pharmaceutical ingredients. *AIChE J.* **2008**, *54* (7), 1682-1688.
3. Mullin, J. W., *Crystallization*; Elsevier, 2001.
4. Yu, L., Amorphous pharmaceutical solids: preparation, characterization and stabilization. *Adv. Drug Delivery Rev.* **2001**, *48* (1), 27-42.
5. Gebauer, D.; Cölfen, H., Prenucleation clusters and non-classical nucleation. *Nano Today* **2011**, *6*(6), 564-584.
6. Erdemir, D.; Lee, A. Y.; Myerson, A. S., Nucleation of crystals from solution: classical and two-step models. *Acc. Chem. Res.* **2009**, *42* (5), 621-629.
7. Liu, X., Heterogeneous nucleation or homogeneous nucleation? *J. Chem. Phys.* **2000**, *112* (22), 9949-9955.
8. Davey, R.; Garside, J., *From Molecules to Crystallizers*; Oxford University Press, 2000.
9. Baird, J. A.; Van Eerdenbrugh, B.; Taylor, L. S., A classification system to assess the crystallization tendency of organic molecules from undercooled melts. *J. Pharm. Sci.* **2010**, *99* (9), 3787-3806.

10. Van Eerdenbrugh, B.; Baird, J. A.; Taylor, L. S., Crystallization tendency of active pharmaceutical ingredients following rapid solvent evaporation—classification and comparison with crystallization tendency from under cooled melts. *J. Pharm. Sci.* **2010**, *99* (9), 3826-3838.
11. Granberg, R. A.; Ducreux, C.; Gracin, S.; Rasmuson, Å. C., Primary nucleation of paracetamol in acetone–water mixtures. *Chem. Eng. Sci.* **2001**, *56* (7), 2305-2313.
12. Zeglinski, J.; Kuhs, M.; Devi, K. R.; Khamar, D.; Hegarty, A. C.; Thompson, D.; Rasmuson, Å. C., Probing Crystal Nucleation of Fenoxycarb from Solution through the effect of Solvent. *Cryst. Growth Des.* **2019**, *19* (4), 2037-2049.
13. Brandel, C.; ter Horst, J. H., Measuring induction times and crystal nucleation rates. *Faraday Discuss.* **2015**, *179*, 199-214.
14. Davey, R. J.; Schroeder, S. L.; ter Horst, J. H., Nucleation of organic crystals—a molecular perspective. *Angew. Chem. Int. Ed.* **2013**, *52* (8), 2166-2179.
15. Jiang, S.; ter Horst, J. H., Crystal nucleation rates from probability distributions of induction times. *Cryst. Growth Des.* **2010**, *11* (1), 256-261.
16. Khamar, D.; Zeglinski, J.; Mealey, D.; Rasmuson, Å. C., Investigating the Role of Solvent–Solute Interaction in Crystal Nucleation of Salicylic Acid from Organic Solvents. *J. Am. Chem. Soc.* **2014**, *136* (33), 11664-11673.
17. Wu, T.; Sun, Y.; Li, N.; de Villiers, M. M.; Yu, L., Inhibiting surface crystallization of amorphous indomethacin by nanocoating. *Langmuir* **2007**, *23* (9), 5148-5153.
18. Pino-García, O.; Rasmuson, Å. C., Influence of additives on nucleation of vanillin: experiments and introductory molecular simulations. *Cryst. Growth. Des.* **2004**, *4* (5), 1025-1037.
19. Anwar, J.; Boateng, P. K.; Tamaki, R.; Odedra, S., Mode of action and design rules for additives that modulate crystal nucleation. *Angew. Chem. Int. Ed.* **2009**, *48* (9), 1596-1600.
20. Nyvlt, J.; Ulrich, J., *Admixtures in Crystallization*; John Wiley & Sons, 2008.
21. Andronis, V.; Yoshioka, M.; Zografì, G., Effects of sorbed water on the crystallization of indomethacin from the amorphous state. *J. Pharm. Sci.* **1997**, *86* (3), 346-351.
22. Givargizov, E. I., *Oriented Crystallization on Amorphous Substrates*; Springer Science & Business Media, 2013.
23. Liu, X., Interfacial effect of molecules on nucleation kinetics. *J. Phys. Chem. B* **2001**, *105* (47), 11550-11558.
24. Diao, Y.; Harada, T.; Myerson, A. S.; Hatton, T. A.; Trout, B. L., The role of nanopore shape in surface-induced crystallization. *Nat. Mater.* **2011**, *10* (11), 867.
25. Diao, Y.; Myerson, A. S.; Hatton, T. A.; Trout, B. L., Surface design for controlled crystallization: The role of surface chemistry and nanoscale pores in heterogeneous nucleation. *Langmuir* **2011**, *27* (9), 5324-5334.
26. Pfund, L. Y.; Price, C. P.; Frick, J. J.; Matzger, A. J., Controlling pharmaceutical crystallization with designed polymeric heteronuclei. *J. Am. Chem. Soc.* **2015**, *137* (2), 871-875.
27. Caridi, A.; Kulkarni, S. A.; Di Profio, G.; Curcio, E.; Ter Horst, J. H., Template-induced nucleation of isonicotinamide polymorphs. *Cryst. Growth Des.* **2014**, *14* (3), 1135-1141.
28. Frostman, L. M.; Bader, M. M.; Ward, M. D., Nucleation and growth of molecular crystals on self-assembled monolayers. *Langmuir* **1994**, *10* (2), 576-582.
29. Tan, L.; Davis, R. M.; Myerson, A. S.; Trout, B. L., Control of heterogeneous nucleation via rationally designed biocompatible polymer surfaces with nanoscale features. *Cryst. Growth Des.* **2015**, *15* (5), 2176-2186.

30. Liu, X., Interfacial process of nucleation and molecular nucleation templator. *Appl. Phys Lett.* **2001**, *79* (1), 39-41.
31. Bhardwaj, S. P.; Suryanarayanan, R., Molecular mobility as an effective predictor of the physical stability of amorphous trehalose. *Mol. Pharmaceutics* **2012**, *9* (11), 3209-3217.
32. Mehta, M.; Kothari, K.; Ragoonanan, V.; Suryanarayanan, R., Effect of water on molecular mobility and physical stability of amorphous pharmaceuticals. *Mol. Pharmaceutics* **2016**, *13* (4), 1339-1346.
33. Mehta, M.; Suryanarayanan, R., Accelerated physical stability testing of amorphous dispersions. *Mol. Pharmaceutics* **2016**, *13* (8), 2661-2666.
34. Taylor, L. S.; Zhang, G. G., Physical chemistry of supersaturated solutions and implications for oral absorption. *Adv. Drug Delivery Rev.* **2016**, *101*, 122-142.
35. Trasi, N. S.; Oucherif, K. A.; Litster, J. D.; Taylor, L. S., Evaluating the influence of polymers on nucleation and growth in supersaturated solutions of acetaminophen. *CrystEngComm* **2015**, *17* (6), 1242-1248.
36. Raghavan, S.; Trividic, A.; Davis, A.; Hadgraft, J., Crystallization of hydrocortisone acetate: influence of polymers. *Int. J. Pharm.* **2001**, *212* (2), 213-221.
37. Heffernan, C.; Ukrainczyk, M.; Zeglinski, J.; Hodnett, B. K.; Rasmuson, Å. C., Influence of structurally related impurities on the crystal nucleation of curcumin. *Cryst. Growth Des.* **2018**, *18* (8), 4715-4723.
38. Pons Siepermann, C. A.; Huang, S.; Myerson, A. S., Nucleation inhibition of benzoic acid through solution complexation. *Cryst. Growth Des.* **2017**, *17* (5), 2646-2653.
39. Pons Siepermann, C. A.; Myerson, A. S., Inhibition of Nucleation Using a Dilute, Weakly Hydrogen-Bonding Molecular Additive. *Cryst. Growth Des.* **2018**, *18* (6), 3584-3595.
40. Hendriksen, B. A.; Grant, D. J., The effect of structurally related substances on the nucleation kinetics of paracetamol (acetaminophen). *J. Cryst. Growth* **1995**, *156* (3), 252-260.
41. Li, Z.; Lenk, T. I.; Yao, L. J.; Bates, F. S.; Lodge, T. P., Maintaining hydrophobic drug supersaturation in a micelle corona reservoir. *Macromolecules* **2018**, *51* (2), 540-551.
42. Li, Z.; Van Zee, N. J.; Bates, F. S.; Lodge, T. P., Polymer Nanogels as Reservoirs To Inhibit Hydrophobic Drug Crystallization. *ACS Nano* **2019**, *13* (2), 1232-1243.
43. Baghel, S.; Cathcart, H.; O'Reilly, N. J., Polymeric amorphous solid dispersions: a review of amorphization, crystallization, stabilization, solid-state characterization, and aqueous solubilization of biopharmaceutical classification system class II drugs. *J. Pharm. Sci.* **2016**, *105* (9), 2527-2544.
44. Konno, H.; Taylor, L. S., Influence of different polymers on the crystallization tendency of molecularly dispersed amorphous felodipine. *J. Pharm. Sci.* **2006**, *95* (12), 2692-2705.
45. Dengale, S. J.; Grohgan, H.; Rades, T.; Löbmann, K., Recent advances in co-amorphous drug formulations. *Adv. Drug Delivery Rev.* **2016**, *100*, 116-125.
46. Chiou, W. L.; Niazi, S., Phase diagram and dissolution-rate studies on sulfathiazole-urea solid dispersions. *J. Pharm. Sci.* **1971**, *60* (9), 1333-1338.
47. Summers, M.; Enever, R., Preparation and properties of solid dispersion system containing citric acid and primidone. *J. Pharm. Sci.* **1976**, *65* (11), 1613-1617.
48. Laitinen, R.; Löbmann, K.; Strachan, C. J.; Grohgan, H.; Rades, T., Emerging trends in the stabilization of amorphous drugs. *Int. J. Pharm.* **2013**, *453* (1), 65-79.
49. Suresh, K.; Mannava, M. C.; Nangia, A., A novel curcumin–artemisinin coamorphous solid: Physical properties and pharmacokinetic profile. *RSC Adv.* **2014**, *4* (102), 58357-58361.

50. Dowling, R.; Davey, R. J.; Curtis, R. A.; Han, G.; Poornachary, S. K.; Chow, P. S.; Tan, R. B., Acceleration of crystal growth rates: an unexpected effect of tailor-made additives. *Chem. Commun.* **2010**, 46 (32), 5924-5926.
51. Chen, C.-L.; Qi, J.; Tao, J.; Zuckermann, R. N.; DeYoreo, J. J., Tuning calcite morphology and growth acceleration by a rational design of highly stable protein-mimetics. *Sci. Rep.* **2014**, 4, 6266.
52. Powell, C. T.; Cai, T.; Hasebe, M.; Gunn, E. M.; Gao, P.; Zhang, G.; Gong, Y.; Yu, L., Low-concentration polymers inhibit and accelerate crystal growth in organic glasses in correlation with segmental mobility. *J. Phys. Chem. B* **2013**, 117 (35), 10334-10341.
53. Mirza, S.; Miroshnyk, I.; Heinämäki, J.; Rantanen, J.; Antikainen, O.; Vuorela, P.; Vuorela, H.; Yliruusi, J., Hydroxypropyl methylcellulose-controlled crystallization of erythromycin A dihydrate crystals with modified morphology. *Cryst. Growth Des.* **2008**, 8 (10), 3526-3531.
54. Klapwijk, A. R.; Simone, E.; Nagy, Z. K.; Wilson, C. C., Tuning crystal morphology of succinic acid using a polymer additive. *Cryst. Growth Des.* **2016**, 16 (8), 4349-4359.
55. Thompson, C.; Davies, M. C.; Roberts, C. J.; Tendler, S. J.; Wilkinson, M. J., The effects of additives on the growth and morphology of paracetamol (acetaminophen) crystals. *Int. J. Pharm.* **2004**, 280 (1-2), 137-150.
56. Simonelli, A.; Mehta, S.; Higuchi, W., Inhibition of sulfathiazole crystal growth by polyvinylpyrrolidone. *J. Pharm. Sci.* **1970**, 59 (5), 633-638.
57. Cai, T.; Zhu, L.; Yu, L., Crystallization of organic glasses: effects of polymer additives on bulk and surface crystal growth in amorphous nifedipine. *Pharm. Res.* **2011**, 28 (10), 2458-2466.
58. Kestur, U. S.; Taylor, L. S., Role of polymer chemistry in influencing crystal growth rates from amorphous felodipine. *CrystEngComm* **2010**, 12 (8), 2390-2397.
59. Mosquera-Giraldo, L. I.; Trasi, N. S.; Taylor, L. S., Impact of surfactants on the crystal growth of amorphous celecoxib. *Int. J. Pharm.* **2014**, 461 (1-2), 251-257.
60. Trasi, N. S.; Taylor, L. S., Effect of additives on crystal growth and nucleation of amorphous flutamide. *Cryst. Growth Des.* **2012**, 12 (6), 3221-3230.
61. Kawashima, Y., Development of spherical crystallization technique and its application to pharmaceutical systems. *Arch. Pharmacol Res.* **1984**, 7 (2), 145-151.
62. Paradkar, A.; Pawar, A.; Chordiya, J.; Patil, V.; Ketkar, A., Spherical crystallization of celecoxib. *Drug Dev. Ind. Pharm.* **2002**, 28 (10), 1213-1220.
63. Bajaj, A.; Rao, M. R.; Pardeshi, A.; Sali, D., Nanocrystallization by evaporative antisolvent technique for solubility and bioavailability enhancement of telmisartan. *AAPS PharmSciTech* **2012**, 13 (4), 1331-1340.
64. Shegokar, R.; Müller, R. H., Nanocrystals: industrially feasible multifunctional formulation technology for poorly soluble actives. *Int. J. Pharm.* **2010**, 399 (1-2), 129-139.
65. Purohit, H. S.; Trasi, N. S.; Osterling, D. J.; Stolarik, D. F.; Jenkins, G. J.; Gao, W.; Zhang, G. G.; Taylor, L. S., Assessing the impact of endogenously derived crystalline drug on the in vivo performance of amorphous formulations. *Mol. Pharmaceutics* **2019**, 16 (8), 3617-3625.
66. Cowie, J. M. G.; Arrighi, V., *Polymers: Chemistry and Physics of Modern Materials*; CRC press, 2007.

Chapter 2. Influence of Chemical Functionality on the Rate of Polymer-Induced Heteronucleation[†]

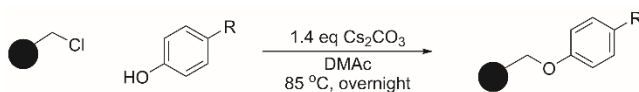
2.1 Introduction

Crystallization from a supersaturated solution is delayed by a significant energetic barrier associated with nucleation of the crystalline state.¹ The addition of a foreign surface, or heteronucleant, speeds nucleation by lowering the surface energy of molecular aggregates in solution.² Polymer-induced heteronucleation (PIHn) is such a technique where polymer libraries containing different functionalities in an insoluble resin are added to a solution to induce the formation of crystal polymorphs³⁻⁶ and multicomponent crystals,⁷ and to tune the rate of crystal nucleation.⁸⁻⁹ Polymers as heteronucleants are advantageous due to their stability in a range of solvents and ease of functionalization. Traditionally, to increase the rate of crystallization, polymer heteronuclei are designed to contain the same functionalities¹⁰⁻¹¹ as those present on a target molecule for crystallization. Through homomeric interaction, target molecules in solution are believed to form high density aggregates on the surface of heteronuclei and undergo nucleation.¹²⁻¹⁴ Although this method has shown success, the polymerization procedures implemented do not result in heteronuclei with uniform surface area or morphology—as a result, it can be difficult to compare crystallization rates induced by chemically different heteronuclei and therefore robust structure-property relationships are lacking. Herein we report a robust functionalization method applicable to cross-linked resins to produce uniform heteronucleants with varied functional

[†] Adapted from Frank, D. S.; Matzger, A. J. *Cryst. Growth Des.* **2017**, *17*(8), 4056-4059.

groups.¹⁵⁻¹⁶ With such resins, the role of polymer functionality in polymer-induced heteronucleation is probed in the absence of microstructural and topological differences.

Crystallization of acetaminophen from water was investigated because it represents an often employed model system in the crystallization of pharmaceuticals.¹⁷⁻²¹ Heteronuclei used in this study were synthesized via functionalization of Merrifield Resin (see Scheme 2.1).²² Merrifield Resin is a cross-linked poly-chloromethylstyrene resin often used in solid-phase peptide synthesis.²³ Chloromethyl groups on the insoluble polymer can be substituted with functionalized phenols to produce a range of chemistries tethered to the unchanged microstructure of an insoluble network polymer. Successful coupling was verified by Raman spectroscopy, where vibrational bands associated with chloromethyl groups on Merrifield Resin (in particular a stretch at 676 cm⁻¹) were no longer present.²⁴ Furthermore, peaks corresponding to introduced functionalities appear in the Raman spectra of functionalized resins (see Supporting Information, Figure 2.4).



Scheme 2.1 Coupling between Merrifield Resin and phenols to synthesize heteronuclei. The R group indicates the position of functional group variation that was controlled to build the structure-property relationships in this study.

2.2 Methods

Crystallizations were performed in the Technobis CrystalBreeder. Aqueous acetaminophen (0.28 mL, 136 mM) was pipetted into 0.3 mL vials containing a 5 × 2 mm Teflon stir bar and ~0.5 mg polymer heteronuclei. These vials were hermetically sealed and, to ensure dissolution, stirred (1200 rpm) at 60 °C for thirty minutes in the CrystalBreeder. Temperature was then lowered to 30 °C to achieve a supersaturation of 1.19.²⁵ Crystallizations are monitored by measuring the transmissivity of an LED through of each vial. Upon nucleation, crystallites of pharmaceutical

quickly lead to secondary nucleation and crystallization of the bulk sample, resulting in an identifiable drop in transmissivity. This time between supersaturation and a nucleation event is recorded as the induction time. After measuring transmissivity for 300 minutes to allow for nucleation to occur, acetaminophen was dissolved back into solution by reheating the vials to 60 °C for thirty minutes. This dissolution/crystallization cycle was repeated five times with four vials containing the same polymer to give twenty induction time measurements for each sample set. Additionally, the entire process was repeated three times per resin to give a total of 60 induction time values for each chemically distinct heteronucleant. Vials that did not yield any crystallization over the five cycles were removed from statistical analysis (see Supporting Information for full induction time data and discussion).

2.3 Results/Discussion

To quantify the heteronucleation effects of functionalized resins, a probability distribution of induction times was graphed for each resin (Figure 2.1). This plot allows for a direct comparison of how different functionalities act as heteronucleants for acetaminophen crystallization. Data in black represent acetaminophen crystallization without added polymer and colored traces correspond to crystallization in the presence of the polymer heteronuclei depicted below the graph in the same color. The right-hand inset shows the probability of crystallization occurring in the first 25 minutes. A potent heteronucleant is characterized by its ability to reduce the induction time to crystallization. As expected, adding insoluble polymer speeds nucleation rates by heteronuclear seeding. Resins without hydrogen bonding functionalities (PH-MFR and MFR) less quickly nucleate acetaminophen than those that can participate in hydrogen bonding (ACM-MFR, AN-MFR, AP-MFR, MACM-MFR) with the pharmaceutical. Potent heteronuclei display much steeper

slopes early in the crystallization process—meaning many vials are nucleating quickly—and this is reflected in a far lower median induction time (Figure 2.2).

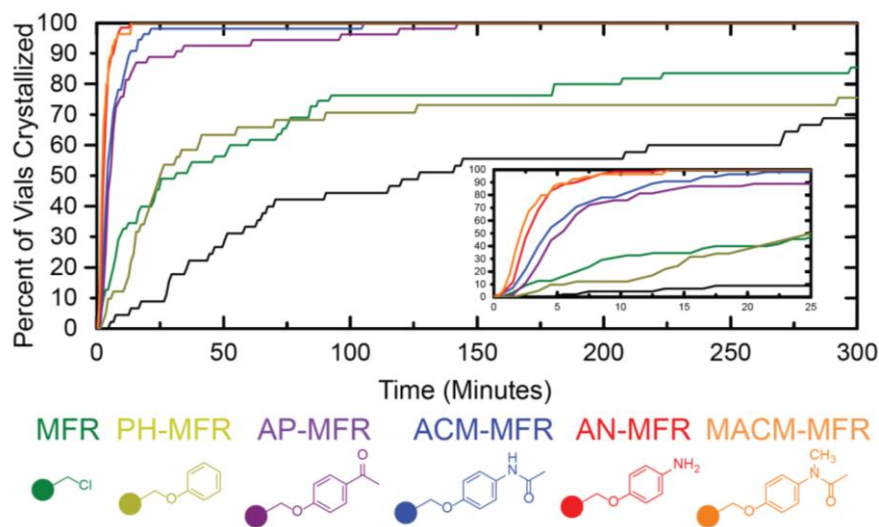


Figure 2.1 Induction time data of polymer induced heteronucleation of acetaminophen crystallization in water (136 mM at 30 °C). The plot in black represents acetaminophen crystallization without added heteronucleant and colored lines depict crystallization in the presence of the functionalized resins (color coded and shown underneath). The inset in the bottom right shows probability of crystallization in the initial 25 minutes.

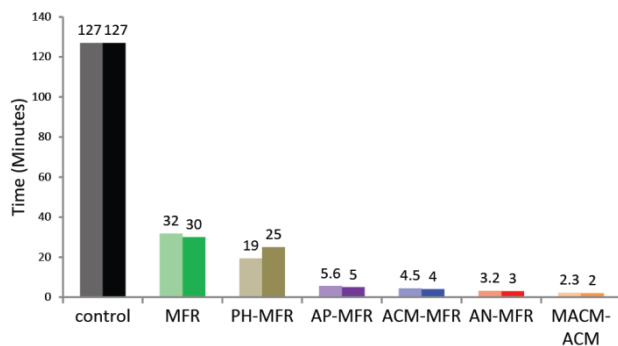


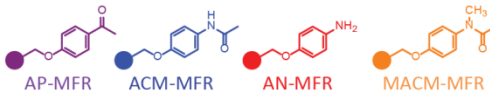
Figure 2.2 Statistical analysis of induction time data for polymer-induced heteronucleation. The median induction time is shown on the left in a lighter color, and the time at which 50% vials have undergone crystallization is shown in a darker color on the right.

Two of the primary factors that dictate the rate of polymer-induced heteronucleation are intermolecular pharmaceutical/heteronuclei interaction strength and solvent effects. In previous

work, insoluble polymers to accelerate nucleation were designed to optimize intermolecular interaction by mimicking drug functionality on heteronuclei.⁹ One method to estimate the interaction energy between two functionalities is by surveying crystalline materials in the Cambridge Structural Database (CSD). The average distance between two functionalities approximates their strength of interaction, where a shorter average bond length indicates a stronger intermolecular interaction between functionalities and longer bonds indicate a weaker interaction. To estimate the affinity of acetaminophen to a given heteronucleant, the average bond length between a phenolic hydroxy group, an analogue for acetaminophen, and hydrogen bond accepting functionalities was calculated (see Supporting Information for motivation to use this particular interaction). Figure 2.3 shows the average bond length between a phenolic hydroxy group and heteronuclei functionalities as found in the CSD. If one only considers the length of the hydroxy/functionality interaction, it is true that mimicking acetaminophen functionality on a resin produces heteronuclei with short intermolecular bonds and presumably strong binding to the pharmaceutical. ACM-MFR and MACM-MFR—resins mimicking acetaminophen—contain the shortest average intermolecular interactions to the phenolic hydroxy group. These resins outperform AP-MFR to accelerate nucleation, which by contrast has the longest average intermolecular bond length to the phenol. If we allow these bond lengths to serve as a gauge for intermolecular interaction energies, it follows that strong binding of acetaminophen to a heteronucleus results in fast heteronucleation. However, for a pharmaceutical to nucleate, it must outcompete water to bind and aggregate on a polymer. This second parameter, competitive binding over solvent, plays an unexplored role in dictating the ability of an insoluble polymer to impact heteronucleation rates. The affinity of water to bind to a functionalized resin can be approximated by the average intermolecular bond distance between a water molecule and the resin functionality;

Figure 2.3 shows the average bond distance between water molecules and the resin functionalities as found in crystalline hydrates. The extent of water solvation to each resin helps to explain the observed ranking of functionalities to accelerate nucleation. Although ACM-MFR contains short intermolecular interactions with phenolic hydroxy groups, it also favorably binds to water, as exemplified by a short water/acetamide bond length ($3.06 \pm 0.02 \text{ \AA}$). The aniline on AN-MFR shows comparatively longer hydrogen bonds to phenolic hydroxy groups, yet very long intermolecular bonds with water ($3.21 \pm 0.001 \text{ \AA}$). Considering these values, we propose acetaminophen outcompetes water to interact with the AN-MFR polymer and undergo rapid nucleation whereas ACM-MFR is slower to heteronucleate due to competitive binding by water molecules. In the case of the methylated MACM-MFR resin, it would seem that the polymer does not substantially bind to acetaminophen over water given the bond length values in Figure 2.3. We might expect the resin to have roughly the same heteronucleation ability as ACM-MFR, contradictory to experimentally measured induction times. However, hydrophobicity plays a crucial role, as steric hindrance prevents water from interacting with the nitrogen atom in the tertiary acetamide of MACM-MFR ($N_{\text{acetamide-O}_{\text{water}}}$ bond length of $3.63 \pm 0.05 \text{ \AA}$) compared to the secondary acetamide in ACM-MFR ($N_{\text{acetamide-O}_{\text{water}}}$ bond length of $3.17 \pm 0.02 \text{ \AA}$). We hypothesize methylation of MACM-MFR decreases intermolecular bond strength between the polymer and water molecules. Without water strongly bound to the acetamide functionality, acetaminophen would be comparatively unhindered to donate into a hydrogen bond with MACM-MFR over ACM-MFR. This model suggests that, rather than a change in intermolecular pharmaceutical/heteronuclei interaction, the increased hydrophobicity of MACM-MFR results in faster heteronucleation compared to ACM-MFR, as evidenced by its lower average induction time. The improvement in heteronucleation rate by MACM-MFR over ACM-MFR highlights the subtle

yet potent effects of solvent on the interplay between dissolved acetaminophen and a heteronucleus. Heteronucleants designed to mimic a target pharmaceutical to crystallize (a homomeric interaction) run the risk of solvation competing with heteronucleation. By imparting hydrophobicity to hydrogen bond acceptors, a heteromeric interaction between acetaminophen and polymer surface has been shown to outperform the previously employed homomeric design for potent heteronuclei.



	AP-MFR	ACM-MFR	AN-MFR	MACM-MFR
Average Induction Time (minutes)	14 ± 3.7	8.0 ± 1.9	3.7 ± 0.3	3.1 ± 0.3
Average bond distance to phenol (Å)	3.32 ± 0.01	3.09 ± 0.03	3.13 ± 0.02	3.05 ± 0.04
Average bond distance to water (Å)	3.09 ± 0.02	3.06 ± 0.02	3.21 ± 0.001	3.04 ± 0.03

Figure 2.3 The average induction time is presented with the standard error of measurement for the four functionalized polymers which induced crystallization in all vials before 300 minutes. Below are the average intermolecular bond distances between a phenolic hydroxy functionality and hydrogen bond accepting functionalities (hydroxy to carbonyl oxygen atom for AP-MFR, ACM-MFR, and MACM-MFR; hydroxy to aniline nitrogen for AN-MFR) as averaged over materials in the Cambridge Structural Database (CSD) containing intermolecular bonds between the relevant functionalities (see Supporting Information for additional details). Also listed is the average bond length to a water molecule from these functionalities as found in crystalline hydrates.

2.4 Conclusion

A versatile methodology has been employed for the uniform synthesis of polymer heteronuclei to compare the ability of various functionalities to reduce induction times for crystallization. A comparison of functionalities acting as heteronuclei, combined with statistical data extracted from the CSD, elucidates the role of solvent effects in the design of potent nucleation accelerators. These updated design requirements for potent heteronuclei can be applied to the accelerated nucleation of large, lipophilic molecules generally slow to nucleate. Further work will investigate the heteronucleation of difficult-to-crystallize pharmaceuticals with the vision that this

heteronucleation technology will aid in the structural determination and processing of molecules resistant to crystallization.

2.5 Supporting Information

2.5.1 Synthesis of functionalized Merrifield Resin

All chemicals were obtained and used without further purification. Merrifield Resin, phenol, and 4-hydroxyacetophenone were purchased from Sigma Aldrich; 4-aminophenol and 4-hydroxyacetophenone were purchased from Acros Organics; acetaminophen was purchased from MP Biomedicals; methyl-acetaminophen was purchased from EnamineStore; and cesium carbonate was purchased from Alfa Aesar.

Merrifield's peptide resin (150 mg) and a phenol (2.5 mmol) were added to a 100 mL round bottom flask containing cesium carbonate (3.5 mmol). Under an inert nitrogen atmosphere, 15 mL dimethylacetamide was then added and the reaction was held at 85 °C overnight. The resulting resin was then thoroughly washed with DMF, DMF:H₂O, H₂O, and methanol and allowed to dry overnight to evaporate any residual solvent.

Although in theory no physical changes should occur upon functionalization, in reality, abrasion due to stirring during functionalization does have a slight effect on resin shape. Because resin swells in organic solvent upon functionalization, it becomes more susceptible to breakage. As a result, smaller pieces of polymer were filtered through a 0.063 mm mesh prior to crystallization experiments.

2.5.2 Raman spectroscopy of functionalized Merrifield Resin

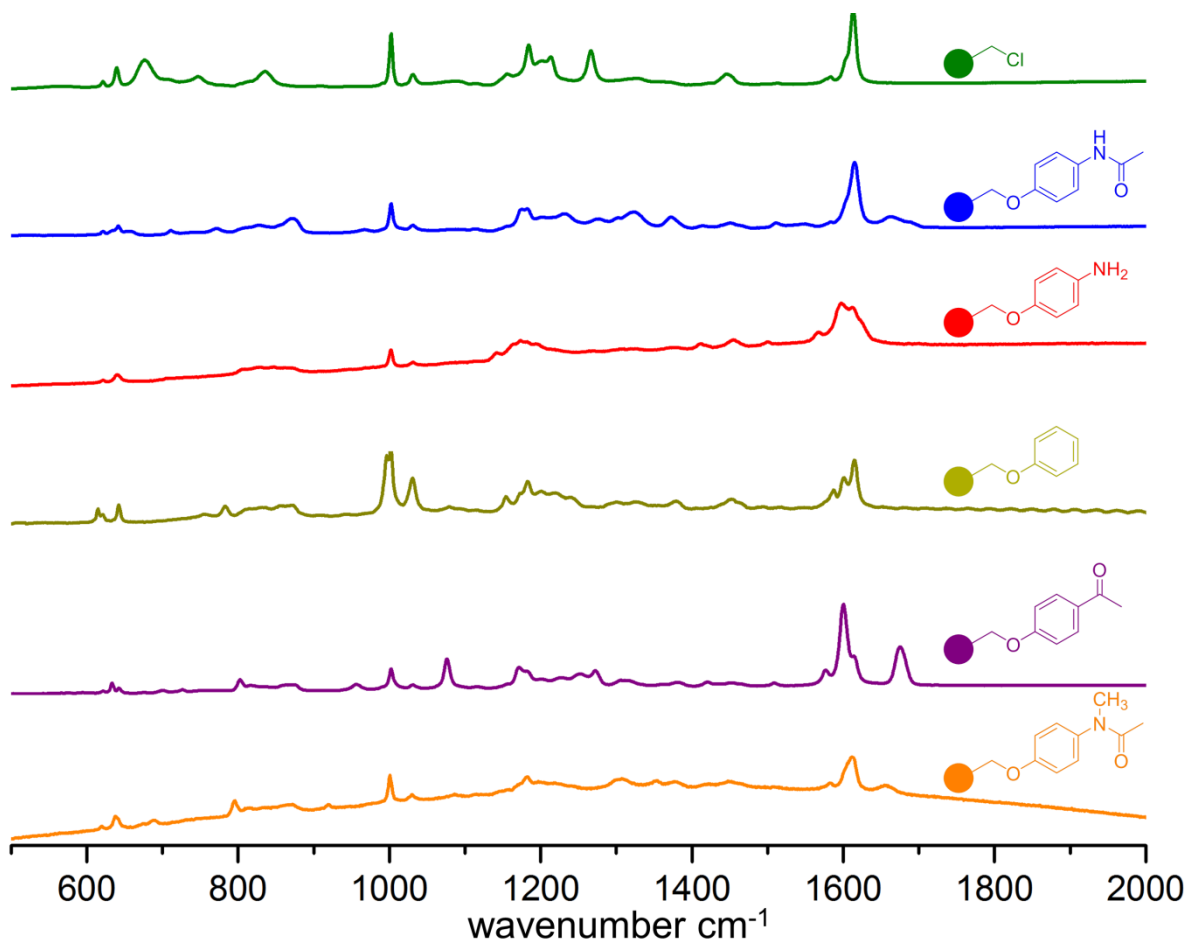


Figure 2.4 Raman spectra of functionalized Merrifield Resins. Each colored plot corresponds with the functionalized resin pictured at the left in the diagram.

Raman spectra was collected on a Renishaw inVia Raman Microscope using a 633 nm laser, 1800 lines/mm grating, 50 μm slit, and a RenCam CCD detector. Spectra was collected from 100-3800 cm^{-1} and analyzed using the WiRE 3.4 software package from Renishaw and OriginPro 9.1. Calibration was performed with a silicon standard.

SI 3. Induction times for acetaminophen crystallization in the presence of polymer heteronuclei

Table 2.1 shows induction time values for acetaminophen crystallization. As mentioned in the manuscript text, vials that did not see crystallization over five heating/cooling cycles were removed from statistical analysis. It is possible that these vials did not yield crystals because of long induction times. However, their anomalous behavior is more likely the result of crystal formation on the closure of the vials lowering supersaturation in solution. In either case discarding these samples may lead to a moderate decrease in reported induction times but without bias. The ranking of heteronuclei in their ability to accelerate nucleation remains the same. The only resin which showed persistent inhibition of crystallization across an entire set of cycles was 4PH-MFR. This resin not only suffers from crystal formation on the closure of vials but also aggregation of highly hydrophobic resins. If heteronucleation occurred within the centers of aggregated polymer beads, such crystals are blocked from secondary nucleation and never cause a strong transmissivity drop. As a result, only 40 crystallization events for acetaminophen containing 4PH-MFR were used for analysis; that being said, even when these induction times are removed in statistical analysis, 4PH-MFR remains the weakest accelerant of heteronucleation.

Table 2.1 Full listing of induction times (in minutes) for acetaminophen crystallization in the presence of insoluble heteronuclei. Values shaded in grey were discarded from statistical analysis—these represent cases where no crystallization occurred over five cycles for an individual vial.

Control	MFR	ACM-MFR	4AM-MFR	4AP-MFR	4PH-MFR	mACM-MFR
58.54	180.65	2.03	0.99	2.46	3.55	2.2
29.08	180.6	2	2.28	3.36	126.69	1.81
286.08	71.97	1.64	2.93	4.3	70.99	1.97
90.72	46.52	1.83	2.66	4.28	41.2	1.47
141.83	84.15	2.23	2.85	61.11	33.83	1.6

44.37	25.81	3.08	3.87	6.72	19.38	2.53
70.64	52.22	4.45	4.35	6.34	26.61	1.92
35.3	23.68	2.53	1.87	96.81	17.68	2.18
36.9	16.67	2.8	4.07	11.24	21.12	2.26
28.41	22.41	3.34	2.41	6.77	13.36	2.59
115.5	37.26	3.97	3.35	119.36	2	1.27
27.56	31.81	2.98	4.67	13.4	4.47	2.67
208.37	36.1	3.4	3.93	11.92	24.82	3.09
28.08	92.93	2.91	5.03	20.28	55.88	2.18
63	75.48	11.3	5.51	11.82	31.86	1.19
17.95	297.79	8.99	6.47	142.81	25.62	2.37
50.83	73.71	4.57	7.56	14.69	15.25	2.57
7.71	60.1	3.99	8.25	8.24	15.86	3.17
217.47	51.37	6.63	4.28	9.73	13.58	0.69
144.92	16.93	4.1	4.36	7.4	6.61	2.77
277.92	8.34	1.75	2.25	4.7	14.59	1.67
65.22	25.97	3.94	2.14	4.06	11.22	1.07
67.7	207.67	12.44	1.91	2.36	20.47	3.04
13.16	87.21	3.27	2.25	4.36	15.02	3.82
270.61	76.23	4.41	2.15	3.5	23.85	0.93
127.09	223.64	13.08	3.39	5.12	292.23	0.82
120.7	84.21	3.58	2.96	4.09	90.79	1.81
46.59	1.47	4.4	3.32	31.24	4.43	4.79

51.07	3.07	5.16	1.74	5.44	12.27	2.05
5.6	2.27	2.67	2.96	7.7	40.35	1.09
271.16	2.05	18.62	2.61	7.44	22.44	1.42
no crystals					no crystals	
observed	2.99	6.95	3	34.66	observed	1.94
no crystals					no crystals	
observed	3.54	5.42	1.72	15.13	observed	2.75
no crystals					no crystals	
observed	1.41	6.58	2.13	4.57	observed	1.82
no crystals					no crystals	
observed	12.39	8.03	2.8	6.83	observed	1.28
no crystals					no crystals	
observed	6.03	4.27	1.96	3.07	observed	3.8
no crystals					no crystals	
observed	7.09	16.77	2.26	4.01	observed	2.52
no crystals					no crystals	
observed	7.83	5.24	2.12	2.57	observed	13.88
no crystals					no crystals	
observed	10.06	7.59	2.37	3.35	observed	5.39
no crystals					no crystals	
observed	23.08	7.89	13.51	4.12	observed	6.09
no crystals					no crystals	
observed	8.39	0.98	2.33	2.39	observed	2.14

no crystals	8.23	12.01	4.63	6.13	no crystals	2.27
observed					observed	
no crystals	17.44	3.04	2.96	3.2	no crystals	1.61
observed					observed	
no crystals	5.82	11.51	2.07	4.15	no crystals	1.93
observed					observed	
no crystals	5.15	6.74	3.36	3.51	no crystals	6.08
observed					observed	
no crystals	6.43	6.05	1.71	3	no crystals	3.5
observed					observed	
no crystals	9.38	4.77	4.75	3.59	no crystals	1.57
observed					observed	
no crystals	no crystals	21.99	3.27	3.98	no crystals	4.72
observed	observed				observed	
no crystals	no crystals	4.42	3.25	2.7	no crystals	3.75
observed	observed				observed	
no crystals	no crystals	10.31	3.29	7.98	no crystals	4.75
observed	observed				observed	
no crystals	no crystals	105.36	3.86	6.44	no crystals	2.07
observed	observed				observed	
no crystals	no crystals	16.04	2.75	5.83	no crystals	8.04
observed	observed				observed	

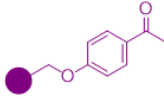
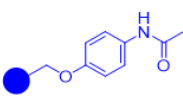
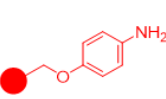
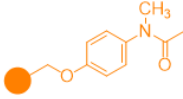
no crystals	no crystals	5.57	4.64	6.98	no crystals	13.82
observed	observed				observed	
no crystals	no crystals	3.95	5.34	5.22	no crystals	7.31
observed	observed				observed	
no crystals	no crystals	10.22	4.83	1.91	no crystals	4.92
observed	observed				observed	
no crystals	no crystals	no crystals	3.59	no crystals	no crystals	no crystals
observed	observed	observed		observed	observed	observed
no crystals	no crystals	no crystals	9.63	no crystals	no crystals	no crystals
observed	observed	observed		observed	observed	observed
no crystals	no crystals	no crystals	7.23	no crystals	no crystals	no crystals
observed	observed	observed		observed	observed	observed
no crystals	no crystals	no crystals	8.03	no crystals	no crystals	no crystals
observed	observed	observed		observed	observed	observed
no crystals	no crystals	no crystals	3.14	no crystals	no crystals	no crystals
observed	observed	observed		observed	observed	observed

SI 4. CSD Search Parameters

To estimate the extent of interaction between acetaminophen and functionalized Merrifield Resins, a CSD search identified materials containing an interaction between a phenolic hydroxy group (as an analogue to acetaminophen) and hydrogen bond accepting functionalities on four of the heteronuclei. The structures were limited to those containing intermolecular bonds ($< 4 \text{ \AA}$) between any phenolic hydroxy (regardless of other aromatic substituents) and each resin functionality as attached to a benzene ring (again, regardless of other substituents). Contacts were defined such that all bonds measured were intermolecular. Table 2.2 summarizes the average and standard error of bond lengths from materials collected in this search.

This interaction—hydroxy donating a hydrogen to the resin functionality—was selected as a model for acetaminophen heteronucleation considering prior work from the Matzger group. In Pfund et al.,⁹ polymer heteronuclei for acetaminophen crystallization were designed to mimic either the acetamide or the phenolic ends of the pharmaceutical. Although these heteronuclei were not controlled for uniform topology, it was found that the acetamide polymer better promoted acetaminophen crystallization compared to the phenolic heteronucleus. In both the monoclinic and orthorhombic packing arrangements of acetaminophen, the acetamide end of the molecule forms a hydrogen bond with the phenolic hydroxy. These observations lead us to believe that acetaminophen aggregates most efficiently on a heteronucleus by way of dimer formation from its phenolic end, and for this reason, the CSD search probed bond distances between a phenolic hydroxy group and hydrogen-bond accepting functionalities on each resin.

Table 2.2 Average intermolecular bond length to resin functionalities, shown with the standard error of measurement and the number of structures included in the averaging. Structures were constrained to those containing intermolecular contacts no more than 4 Å apart.

	 4AP-MFR	 ACM-MFR	 4AM-MFR	 mACM-MFR
Average bond distance to phenol (Å)	3.32 ± 0.01	3.09 ± 0.03	3.13 ± 0.02	3.05 ± 0.04
Number of hits	2515	329	480	156
Average bond distance to water (Å)	3.09 ± 0.02	3.06 ± 0.02	3.21 ± 0.001	3.04 ± 0.03
Number of hits	466	398	310	140
Average bond distance phenol to Nitrogen (Å)		3.37 ± 0.02		3.62 ± 0.03
Number of hits		244		48
Average bond distance water to Nitrogen (Å)		3.17 ± 0.02		3.63 ± 0.05
Number of hits		355		26

2.6 References

1. Mullin, J. W., *Crystallization*. Butterworth-Heinemann: 2001.
2. Nyvlt, J.; Ulrich, J., *Admixtures in Crystallization*. John Wiley & Sons: 2008.
3. Lang, M.; Grzesiak, A. L.; Matzger, A. J., *J. Am. Chem. Soc.* **2002**, *124* (50), 14834-14835.
4. Price, C. P.; Grzesiak, A. L.; Matzger, A. J., *J. Am. Chem. Soc.* **2005**, *127* (15), 5512-5517.
5. Araya-Sibaja, A.; Fandaruff, C.; Campos, C. E.; Soldi, V.; Cardoso, S. G.; Cuffini, S. L., *Scanning* **2013**, *35* (4), 213-221.
6. Sudha, C.; Nandhini, R.; Srinivasan, K., *Cryst. Growth Des.* **2014**, *14* (2), 705-715.
7. Porter III, W. W.; Elie, S. C.; Matzger, A. J., *Cryst. Growth Des.* **2008**, *8* (1), 14-16.
8. Diao, Y.; Myerson, A. S.; Hatton, T. A.; Trout, B. L., *Langmuir* **2011**, *27* (9), 5324-5334.
9. Pfund, L. Y.; Price, C. P.; Frick, J. J.; Matzger, A. J., *J. Am. Chem. Soc.* **2015**, *137* (2), 871-875.
10. Weissbuch, I.; Addadi, L.; Lahav, M.; Leiserowitz, L., *Science* **1991**, *253* (5020), 637-645.
11. Weissbuch, I.; Lahav, M.; Leiserowitz, L., *Cryst. Growth Des.* **2003**, *3* (2), 125-150.

12. López-Mejías, V.; Knight, J. L.; Brooks III, C. L.; Matzger, A. J., *Langmuir* **2011**, *27* (12), 7575-7579.
13. McClelland, A. A.; López-Mejías, V.; Matzger, A. J.; Chen, Z., *Langmuir* **2011**, *27* (6), 2162-2165.
14. Diao, Y.; Helgeson, M. E.; Siam, Z. A.; Doyle, P. S.; Myerson, A. S.; Hatton, T. A.; Trout, B. L., *Cryst. Growth Des.* **2011**, *12* (1), 508-517.
15. Roy, S.; Goud, N. R.; Matzger, A. J., *Chem. Commun.* **2016**, *52* (23), 4389-4392.
16. Roy, S.; Matzger, A. J., *Angew. Chem., Int. Ed.* **2009**, *48* (45), 8505-8508.
17. Hendriksen, B. A.; Grant, D. J., *J. Cryst. Growth* **1995**, *156* (3), 252-260.
18. Liu, X., *J. Phys. Chem. B* **2001**, *105* (47), 11550-11558.
19. Yu, Z. Q.; Chow, P. S.; Tan, R. B., *Org. Process Res. Dev.* **2006**, *10* (4), 717-722.
20. Thomas, L. H.; Wales, C.; Zhao, L.; Wilson, C. C., *Cryst. Growth Des.* **2011**, *11* (5), 1450-1452.
21. Trasi, N. S.; Oucherif, K. A.; Litster, J. D.; Taylor, L. S., *CrystEngComm* **2015**, *17* (6), 1242-1248.
22. Gisin, B., *Helv. Chim. Acta* **1973**, *56* (5), 1476-1482.
23. Merrifield, R. B., *J. Am. Chem. Soc.* **1963**, *85* (14), 2149-2154.
24. Altava, B.; Burguete, M.; Garcia-Verdugo, E.; Luis, S.; Vicent, M., *Tetrahedron* **2001**, *57* (41), 8675-8683.
25. Granberg, R. A.; Rasmuson, Å. C., *J. Chem. Eng. Data* **1999**, *44* (6), 1391-1395.

Chapter 3. Inhibiting or Accelerating Crystallization of Pharmaceuticals by Manipulating Polymer Solubility[†]

3.1 Introduction

The kinetics of crystallization from the supersaturated state are highly dependent on the presence of impurities,¹ and additives are often deliberately included in a crystallization to control crystallization rate.²⁻⁵ Amongst organic crystallizations, there is considerable work on the use of additives to inhibit the precipitation of small-molecule pharmaceuticals.⁶⁻⁸ Inhibiting crystallization is relevant for the processing of pharmaceuticals⁹ and can be necessary to reap the improvements in bioavailability possible using formulation techniques such as amorphous solid dispersions or cocrystals.¹⁰⁻¹² Although water-soluble polymers have shown success as precipitation inhibitors,¹³ assessing the inhibitory ability of a soluble polymer remains a primarily empirical undertaking.¹⁴⁻¹⁵ In this work, we test the hypothesis that functionalities identified as robust heteronucleation promoters of crystallization when tethered to insoluble polymer resins will be potent inhibitors of crystallization when attached to soluble polymer scaffolds.

Discovering the most effective inhibitors of crystallization by direct screening is complicated by the fact that the relevant timescale of crystallization inhibition can be years.¹⁶⁻¹⁷ As a result, the screening of polymers to evaluate their effectiveness often relies on the use of “accelerated

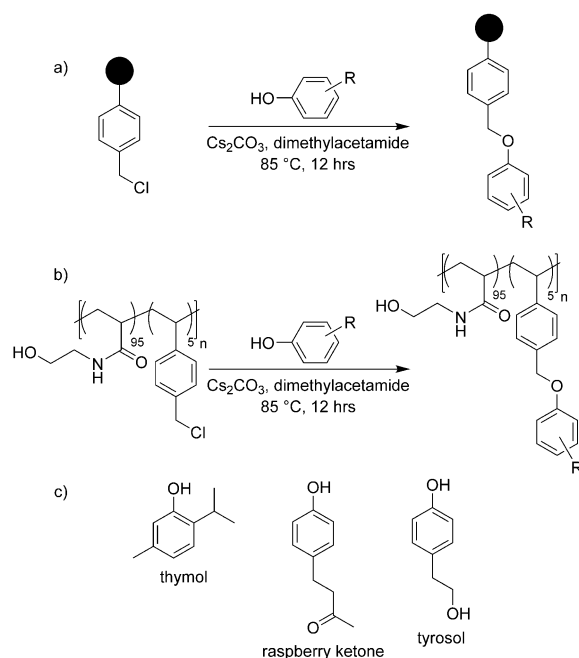
[†] Adapted from Frank, D. S.; Zhu, Q.; Matzger, A. J. *Mol. Pharmaceutics* **2019**, *16*(8), 3720-3725.

stability” testing which does not always reproduce behavior of formulated pharmaceuticals.¹⁸⁻¹⁹ By contrast, heteronucleation rates by crystallization accelerators can be rapidly (minutes to hours) measured to evaluate the ability of a polymer to interact with a crystallizing solute. We propose that the most effective inhibitors of precipitation will contain those functionalities which have been shown to strongly heteronucleate crystallization. Although such a relationship is intuitive when considering the proposed mechanisms for acceleration or inhibition of crystallization by impurities,²⁰⁻²² it has yet to be demonstrated experimentally, and it is not clear if changing aspects of a polymeric additive such as solubility will alter the general relationship between side-chain functionality and the impact of an additive on crystallization. By demonstrating that the same functionalities that promote nucleation on an insoluble polymer will impede crystallization when present in soluble polymer additives, the design of precipitation inhibitors can be informed by insights gained in the study of heteronucleants, and vice versa.²³⁻³¹ This methodology allows for the streamlined assessment of functionalities to determine if they should be included in polymeric precipitation inhibitors for use in amorphous solid dispersions or other supersaturating drug delivery systems.

3.2 Methods

Insoluble polymers to accelerate crystallization were synthesized by functionalizing Merrifield resin (MFR), a crosslinked poly(styrene-*co*-chloromethylstyrene) support typically used for peptide synthesis. Soluble polymers to inhibit crystallization were prepared by post-polymerization functionalization of poly(hydroxyethyl acrylamide-*co*-chloromethylstyrene) (PHEAM). In each of these cases, pendant chloromethyl groups were replaced by substituted

phenols containing a variety of functional groups (Scheme 3.1). This post-polymerization functionalization methodology is advantageous as modifications of polymer chemistry are not accompanied by changes in the morphology, backbone structure, or number-average chain length of polymers; such changes might convolute the effect of functionalizing polymer additives on the kinetics of crystallization. Naturally occurring phenolic compounds tyrosol, thymol, and raspberry ketone were selected as moieties to tether to crystallization additives given their GRAS status (thymol and raspberry ketone)³²⁻³³ or widespread presence in the human diet (tyrosol).³⁴⁻³⁵ These three compounds were chosen in particular because each contains a different functional group (alkyl, ketone, and hydroxyl) to interact with the crystallizing pharmaceutical.



Scheme 3.1 Synthesis of (a) insoluble polymer heteronuclei to accelerate crystallization (black dot represents MFR) and (b) water-soluble polymers to inhibit crystallization. Functionalization with (c) substituted phenols thymol, raspberry ketone, and tyrosol modulates the potency of the polymer to speed or slow crystallization.

Functionalized MFR was synthesized following literature procedures.^{30, 36} Poly(hydroxyethyl acrylamide-*co*-chloromethylstyrene) was synthesized by free radical polymerization in dimethylacetamide and functionalized *in situ* with substituted phenols to give a polymer with a number-average molecular weight of ~3 kDa, or roughly 30 repeat units per polymer ($\bar{D}=2$, see Supporting Information for additional details). The crystallization kinetics of pharmaceuticals pyrazinamide and hydrochlorothiazide (Figure 3.1) were determined using the Technobis CrystalBreeder, where crystallization was monitored by changes in solution turbidity. For each crystallization condition, 80 induction times were measured to compare the effects of different polymer additives (see Supporting Information for details). The resulting crystals were not found to show any dramatic alteration of morphology when grown in the presence of either insoluble heteronuclei or soluble precipitation inhibitors.

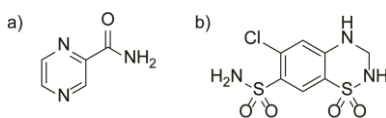


Figure 3.1 Pharmaceuticals (a) pyrazinamide and (b) hydrochlorothiazide were employed to study the effects of additives on crystallization.

3.3 Results and Discussion

Pyrazinamide, a small-molecule antibacterial medication used to treat tuberculosis, was employed as a model compound to investigate the influence of polymeric additives on the kinetics of precipitation. Pyrazinamide crystallization (30 °C, 203 mM in water, giving a supersaturation ratio of 1.3³⁷) in the presence of functionalized MFR and functionalized PHEAM was performed to assess the relative abilities of heteronuclei and water-soluble polymers to alter crystallization

rates. Despite the well-documented ability of polymer heteronuclei to direct the formation of crystalline polymorphs,³⁸ pyrazinamide was consistently found to crystallize in its alpha form throughout all experiments (see Supporting Information). Figure 3.2 shows the percent of the eighty crystallization trails which have undergone precipitation after a given time. The probability of crystallization for any particular trial can be extrapolated from such plots (see Supporting Information for rigorous statistical analysis); however, an empirical comparison of crystallization kinetics is sufficient to compare the relative effects of polymer additives on crystallization rate (where precipitation rates correlate with the length of time for 100% of vials to undergo crystallization). As can be seen in Figure 3.2, polymers functionalized with each substituted phenol alter the kinetics of pyrazinamide precipitation to different extents, and the potency of a polymer to either speed or slow crystallization depends on its pendant functional groups. Previous work on polymer-induced heteronucleation has identified two factors that increase the ability of a polymer to accelerate the precipitation of aqueous solute: interaction strength between solute and polymer and hydrophobicity.^{27-28, 30, 39} Functionalizing MFR with thymol forms an additive (MFR-thymol) without strong hydrogen bonding groups to pyrazinamide, and MFR-thymol does not increase crystallization rates relative to aqueous pyrazinamide within statistical significance. However, functionalizing MFR with phenols that contain hydrogen bond donating or accepting groups, such as raspberry ketone or tyrosol, results in heteronuclei that accelerate pyrazinamide crystallization. Using computed electrostatic potential maps (see Supporting Information), it was found that pyrazinamide contains its most positive region at its amide carbonyl and most negative region at the amide $-NH_2$ group. Thus, it is likely that the ability of these polymers to accelerate

pyrazinamide crystallization stems from favorable hydrogen bonding interactions between the pharmaceutical and polymer, as mediated by hydrogen bonding interactions between the amide on the pharmaceutical with the ketone on MFR-raspberry ketone or the hydroxyl group on MFR-tyrosol. It is apparent that the hydrophobicity of these polymers does not correlate with heteronucleation rates, and that, in this case, crystallization is accelerated by incorporating functionalities that can hydrogen bond with pyrazinamide.

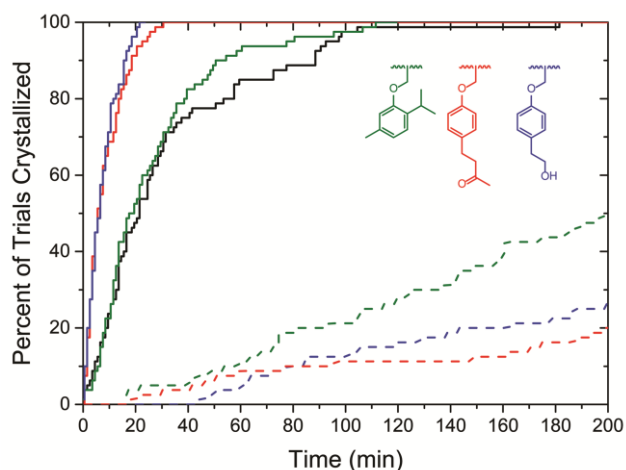


Figure 3.2 Percent of trials crystallized over time of aqueous pyrazinamide (30 °C, 203 mM) containing Merrifield Resin (solid lines) and poly(hydroxyethyl acrylamide-co-chloromethylstyrene) (dashed lines) functionalized with thymol (shown in green), raspberry ketone (red), and tyrosol (blue). Crystallization without additives is shown by the black trace.

Inhibition of crystallization by water-soluble polymers is also a function of polymer-solute interaction strength and hydrophobicity,^{15, 40} where imparting hydrophobicity to water-soluble polymers has been demonstrated to increase their ability to inhibit crystallization.⁴¹⁻⁴³ In the above experiments, small amounts of polymer (1% the weight of pyrazinamide) are used to avoid solubilization of drug and instead to only increase the kinetic barrier to crystallization. Although

increasing the solubility of a pharmaceutical decreases its crystallization propensity, strongly solubilizing additives can lower bioavailability by reducing the concentration of free drug molecules in the gastrointestinal tract.⁴⁴ Stabilizing pharmaceutical in the high-energy supersaturated state provides both a high concentration of free drug and a substantial driving force for absorption across the intestinal barrier.⁴⁵ In the case of the low concentration of PHEAM additives used in this study, no change in the clear point temperature of pyrazinamide was observed, indicating that the inhibitory impact of the polymer stems from increasing the kinetic barrier to crystallization and not the solubility of pyrazinamide.⁴⁶ Furthermore, no evidence of polymer micelle formation was observed via changes in solution turbidity at these concentrations, and although nanoscale micelle formation might not result in changes in solution turbidity detectable by the CrystalBreeder, this would manifest as increased solubility of the API, which is not observed (see Supporting Information). As a result, we hypothesize that soluble polymers inhibit crystallization via adsorption within subcritical nuclei in solution and on the faces of growing crystallites. In general, structure-property relationships are difficult to draw with regard to kinetic barriers to crystallization and the inhibitory ability of polymers is more often rationalized post-hoc rather than predicted prior to experiment. Following the general hypothesis proposed above, we would anticipate that PHEAM-tyrosol and PHEAM-raspberry ketone will be superior inhibitors of pyrazinamide crystallization compared to PHEAM-thymol, given that MFR-tyrosol and MFR-raspberry ketone outperform MFR-thymol to accelerate pyrazinamide crystallization. As shown in Figure 3.2, this prediction is verified by experiment. Despite the difference in their effects on crystallization, the functional group trends seen for acceleration by functionalized MFR

are reflected in the ranking of PHEAM polymers to inhibit pyrazinamide crystallization, even though such an effect originates from only 5% of side-chain functionalities on the water-soluble polymer (higher ratios of chloromethylstyrene render the copolymer insoluble in water). This example demonstrates the ability of using the relative heteronucleation rates of a pharmaceutical to inform the design of water-soluble inhibitors of precipitation.

The effect of small-molecules on the crystallization kinetics of pyrazinamide was also investigated. It was also found that 1 mol% of the small-molecule phenolic compounds, not attached to a polymer, were able to inhibit pyrazinamide crystallization (see Supporting Information); however, they show a far weaker effect to inhibit precipitation when compared to soluble polymers. This limited effect of the phenolic compounds when compared to the effect of soluble polymer is remarkable given the low ratio of chloromethylstyrene units in the PHEAM copolymer. There is roughly 20 times the concentration of thymol, tyrosol, or raspberry ketone functionalities in crystallizations containing small molecule additives as compared to those containing functionalized PHEAM. Although there is growing interest in using small molecules as nucleation inhibitors both in solution and in coamorphous forms,⁴⁷⁻⁵¹ there is an unambiguous advantage (at least in this system) to using soluble polymers as opposed to soluble small molecules to inhibit precipitation, both in the magnitude of crystallization inhibition and in the ability to control precipitation rates.

To further probe this connection between insoluble heteronucleants and polymer inhibitors of crystallization, and to test the robustness of our hypothesis that relative heteronucleation rates will predict the ability of functionalized polymers to inhibit precipitation, the crystallization of

hydrochlorothiazide from water was investigated. Figure 3.3 shows the percent of vials of supersaturated solutions of hydrochlorothiazide that undergo crystallization over time (see Supporting Information for statistical analysis). These data show the same general trend as found in pyrazinamide crystallizations, being that the ranking of functionalized MFR to accelerate crystallization (MFR-raspberry ketone is the most effective hydrochlorothiazide heteronucleant, followed by MFR-tyrosol and MFR-thymol) matches the ranking of functionalized PHEAM to inhibit crystallization (PHEAM-raspberry ketone is the most effective inhibitor of hydrochlorothiazide crystallization, followed by PHEAM-tyrosol, and finally PHEAM-thymol). As discussed above, the potency of a crystallization additive depends on its interaction strength with both solute and solvent. The interaction strength between polymer and solvent was approximated using interaction distances from crystal structures in the Cambridge Structural Database, and it was found that alcohol functionalities have a shorter median intermolecular bond distance to water molecules as compared to ketone functionalities (see Supporting Information). One interpretation for why polymer functionalized with raspberry ketone outperforms those functionalized with tyrosol is that they are less strongly solvated by water. Another possibility is that hydrochlorothiazide forms stronger hydrogen bonds to polymers functionalized with raspberry ketone over those functionalized with tyrosol. Given the propensity of sulfonamide functionalities to act as hydrogen bond donors,⁵² it is possible that the observed ranking of polymer effectiveness to impact crystallization stems from the stronger hydrogen bond accepting character of ketones (on PHEAM-raspberry ketone) compared to alcohols (PHEAM-tyrosol) or alkyl (PHEAM-thymol) substituents.⁵³ This theory is supported by an analysis using electrostatic potential maps

(see Supporting Information), where it was found that hydrochlorothiazide contains a strongly positive region between its cyclic amide and sulfonamide functionalities which might mediate strong interactions with the partially negative ketone functionality on PHEAM-raspberry ketone. Overall, the factors that determine the impact of a crystallization additive are complex and depend on many parameters including the identity of crystallizing solute. The power of polymer-induced heteronucleation as a predictive technology is that there is no need to make assumptions about the relative contributions of hydrophobicity or noncovalent interactions between polymer and solute when developing crystallization inhibitors.

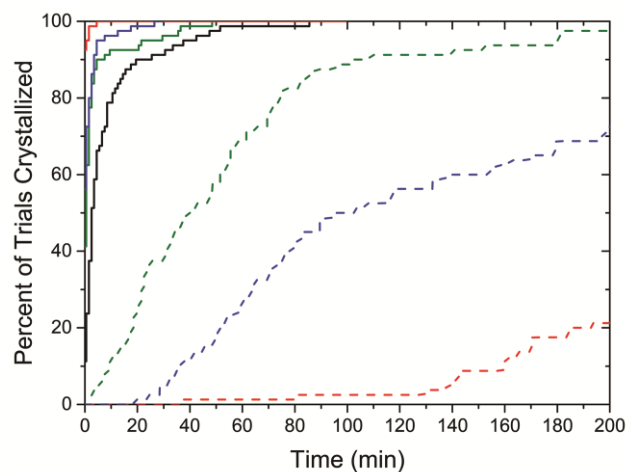


Figure 3.3 Percent of trials crystallized of aqueous hydrochlorothiazide (30 °C, 7.05 mM, giving a supersaturation ratio of 2.554) with Merrifield Resin (solid lines) and poly(hydroxyethyl acrylamide-co-chloromethylstyrene) (dashed lines) additives functionalized with thymol (shown in green), raspberry ketone (red), and tyrosol (blue). Crystallization without additives is shown in black.

Although there are substantial differences between the ability of each PHEAM to maintain supersaturation of hydrochlorothiazide, differences between the ability of each MFR to heteronucleate are less dramatic. One interpretation of this asymmetry is that water-soluble

polymers can inhibit both nucleation and crystal growth of hydrochlorothiazide, whereas insoluble polymers only promote nucleation. Thus, it is possible that functional group changes on water-soluble polymers have a larger effect on the kinetics of crystallization than functional group changes of insoluble resins because water-soluble additives have a dual action to slow both nucleation and crystal growth. This difference between the effects of PHEAM and MFR is particularly considerable considering that PHEAM contains a much lower percent of functionalized groups (~5%) compared to MFR (~67%). The ability of water-soluble polymers to inhibit crystal growth may also explain why PHEAM outperforms low concentrations of small-molecule phenols to inhibit pyrazinamide crystallization. Low concentrations of small-molecule additives have been proposed to delay precipitation by interrupting the formation of nucleation clusters in solution.⁵¹ Polymers may inhibit precipitation in part by this same mechanism, yet also have been shown to delay the growth of crystallites as well.⁴⁰ In tandem, these effects render polymer more able to sustain a high concentration of pharmaceutical during administration as opposed to small-molecule nucleation inhibitors (see Supporting Information for comparison for pyrazinamide crystallization). Additionally, despite the clear correlation between the inhibitory effect of PHEAM and the accelerating effect of MFR containing the same functionalities, it should be noted that functionalities tethered to a hydrophobic polymer versus a hydrophilic polymer exist in very different chemical environments. In the examples explored above, the chemical microenvironment around a functionality seems to not be crucial in dictating its intermolecular interaction strength with solute. However, a wider range of both soluble polymer chemistry and

insoluble resin chemistry is required to investigate the applicability of these concepts across other systems.

A general relationship between accelerators and inhibitors of pyrazinamide and hydrochlorothiazide crystallization has been identified. The ability of an insoluble polymer to heteronucleate crystallization or a water-soluble additive to inhibit crystallization can be optimized by post-polymerization functionalization. It was found that the same functional groups that promote heteronucleation on an insoluble polymer also promote crystallization inhibition by a soluble polymer additive; however, the ability of water-soluble polymers to inhibit crystallization is far more sensitive to functional group chemistry than the ability of insoluble polymers to accelerate crystallization. These findings imply that similar interactions between polymer and pharmaceutical occur during heteronucleation by insoluble polymers and during crystallization inhibition by soluble polymers; from a practical standpoint the observation that each of these crystallization technologies can inform the other when designing polymers to control the crystallization rate of pharmaceuticals offers a pathway to more efficient discovery of new polymers to control pharmaceutical crystallization.

3.4 Supporting Information

3.4.1 Synthesis of Functionalized Merrifield Resin

MFR-Thymol

Merrifield resin (100.1 mg, Aldrich, 1% cross-linked, 200-400 mesh, 4.38 mmol Cl⁻/g) was swollen in 10 mL dimethylacetamide containing 2-isopropyl-5-methylphenol (0.67 mmol, Acros

99%) and cesium carbonate (0.67 mmol, Alfa 99%). The reaction was stirred at 85 °C overnight and product was filtered and washed with acetone, dimethylformamide, dimethylformamide/water, water, and methanol and dried overnight on the benchtop prior to use in crystallization experiments.

MFR-Raspberry Ketone

Merrifield resin (105.1 mg, Aldrich, 1% cross-linked, 200-400 mesh, 4.38 mmol Cl⁻/g) was swollen in 10 mL dimethylacetamide containing raspberry ketone 4-(4-hydroxyphenyl)-2-butanone (0.72 mmol, Aldrich 99%) and cesium carbonate (0.70 mmol, Alfa 99%). The reaction was stirred at 85 °C overnight and product was filtered and washed with acetone, dimethylformamide, dimethylformamide/water, water, and methanol and dried overnight on the benchtop prior to use in crystallization experiments.

MFR-Tyrosol

Merrifield resin (109.8 mg, Aldrich, 1% cross-linked, 200-400 mesh, 4.38 mmol Cl⁻/g) was swollen in 10 mL dimethylacetamide containing 2-(4-hydroxyphenyl)ethanol (0.86 mmol, TCI >98.0%) and cesium carbonate (0.72 mmol, Alfa 99%). The reaction was stirred at 85 °C overnight and product was filtered and washed with acetone, dimethylformamide, dimethylformamide/water, water, and methanol and dried overnight on the benchtop prior to use in crystallization experiments.

Functionalization was verified using Raman spectroscopy on a Renishaw inVia Raman microscope equipped with a RenCam CCD detector, a 785 nm diode laser, 1200 lines/mm grating, and a 65 μm slit. Spectra were analyzed using the WiRE 3.4 software package and calibrated using

a silicon standard. As can be seen in Figure 3.4, Merrifield Resin functionalized with substituted phenols does not show a broad chloromethyl stretch at 676 cm^{-1} . FT-IR spectra of these materials are shown in Figure 3.5, collected on a Nicolet iS50 FT-IR using a diamond ATR accessory. Although there are only a few differences in the Raman spectra between each functionalized MFR, many differences between these materials can be seen by FT-IR spectroscopy, including a broad stretch at 3400 cm^{-1} in Figure 3.5a corresponding to the hydroxy functionality on MFR-tyrosol as well as a sharp peak at 1711 cm^{-1} in Figure 3.5b corresponding to the ketone functionality on MFR-raspberry ketone.

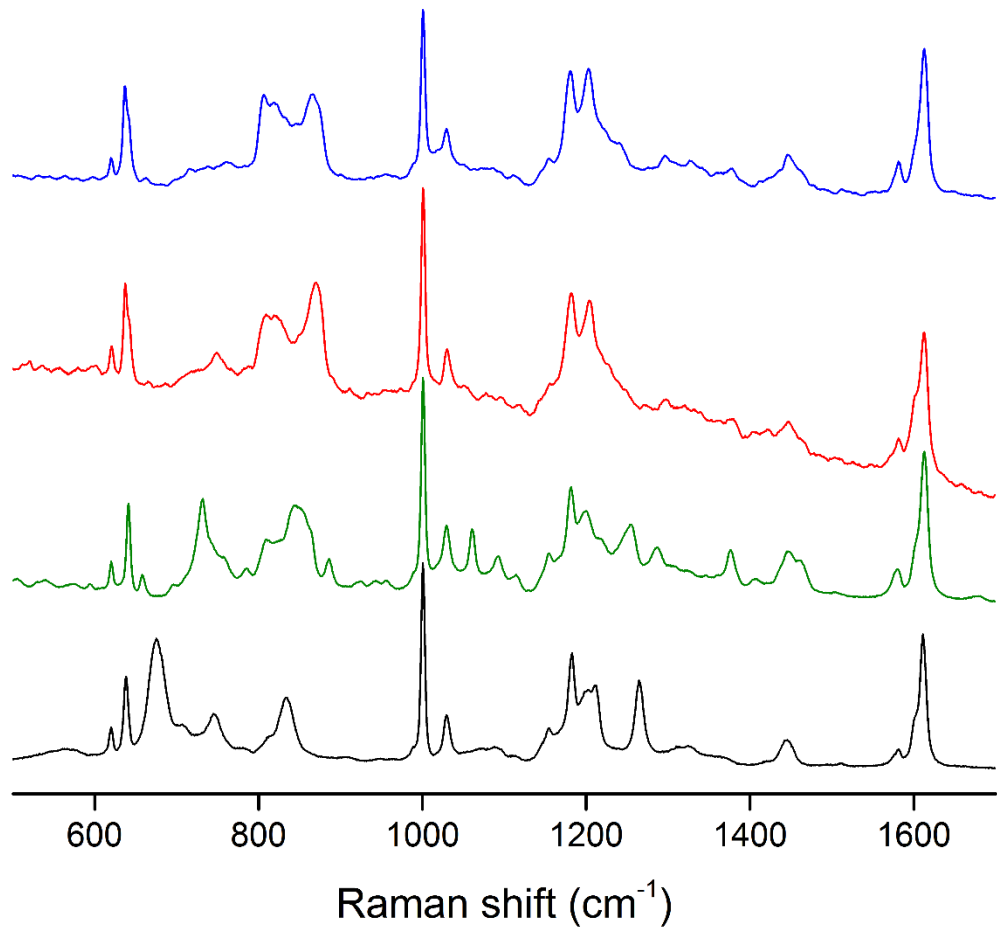


Figure 3.4. Raman spectroscopy of functionalized Merrifield Resins with substituted phenols. Chloromethyl substitution confirmed by the loss of the band at 676 cm⁻¹ in the unfunctionalized MFR.

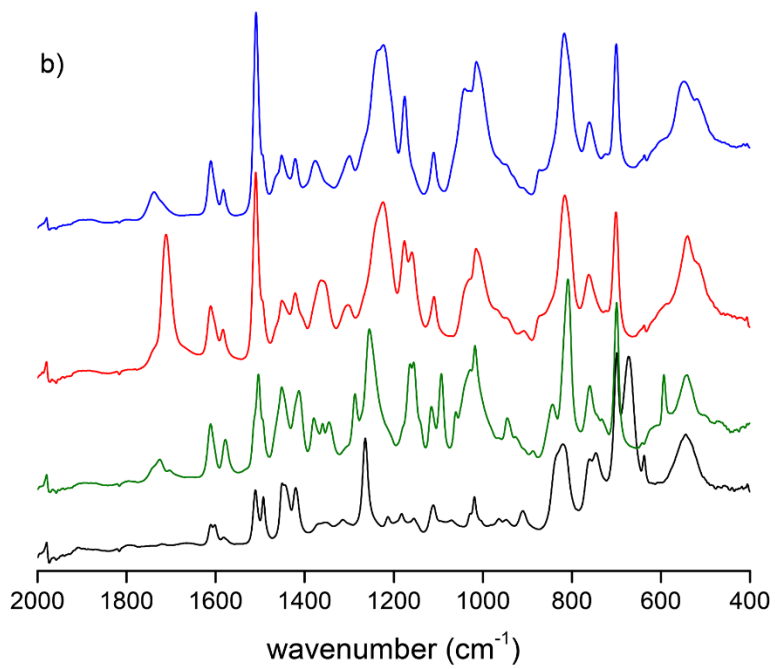
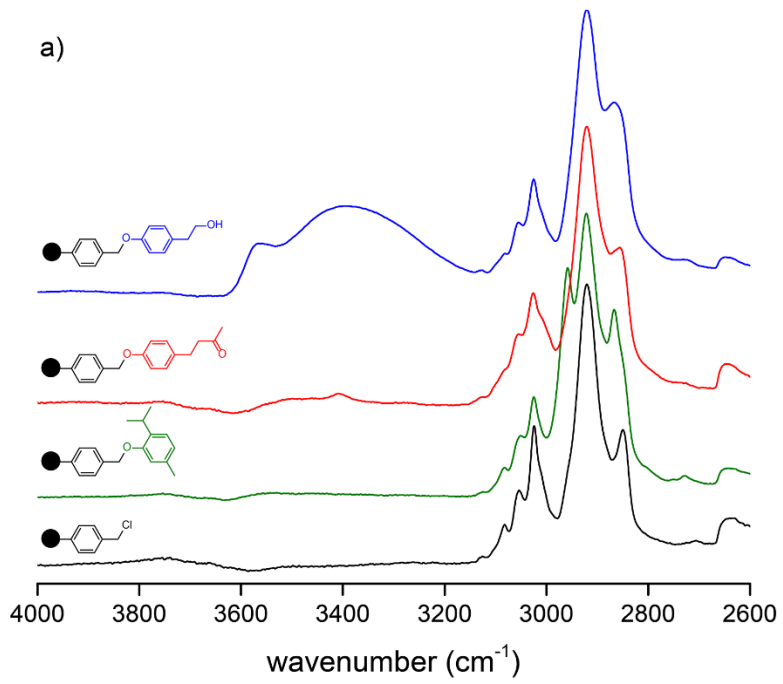


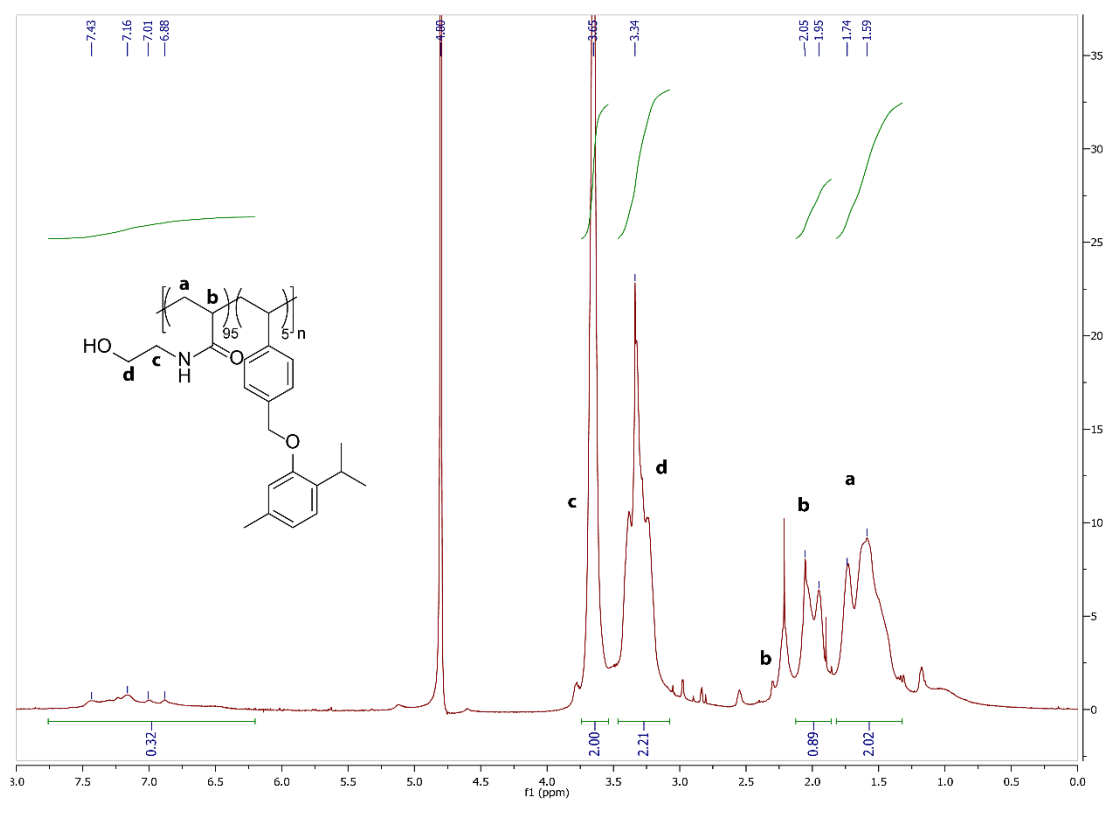
Figure 3.5. FT-IR spectra of functionalized Merrifield Resin between (a) 2600-4000 cm^{-1} and between (b) 400-2000 cm^{-1} . Each colored trace in (b) corresponds to the compounds drawn in the same color on the left in (a).

3.4.2 Synthesis of Water-Soluble Copolymers

Poly(N-hydroxyethyl acrylamide-*co*-chlorostyrene) polymers were synthesized by free radical polymerization in dimethylacetamide. N-hydroxyethyl acrylamide monomer (Aldrich, 97%) was purified through an MEHQ removal column and 4-vinylbenzyl chloride (Aldrich, 90%) was purified through a *tert*-butylcatechol removal column prior to polymerization. N-hydroxyethyl acrylamide (29 mmol), chloromethylstyrene (1.2 mmol), and 2,2'-Azobis(2-methylpropionitrile) (0.13 mmol, Aldrich, 98%) were dissolved in 10 mL dimethylacetamide and heated at 65 °C under a nitrogen atmosphere for 12 hours to allow for polymerization. After polymerization, product was separated into three 10 mL aliquots for post-polymerization functionalization. At this stage, polymer was not purified, as removal of solvent lead to an insoluble polymer, possibly caused by interchain crosslinking. Functionalization was verified using $^1\text{H-NMR}$ spectroscopy; data were collected in D_2O at 500 MHz on a Varian INOVA-500 spectrometer.

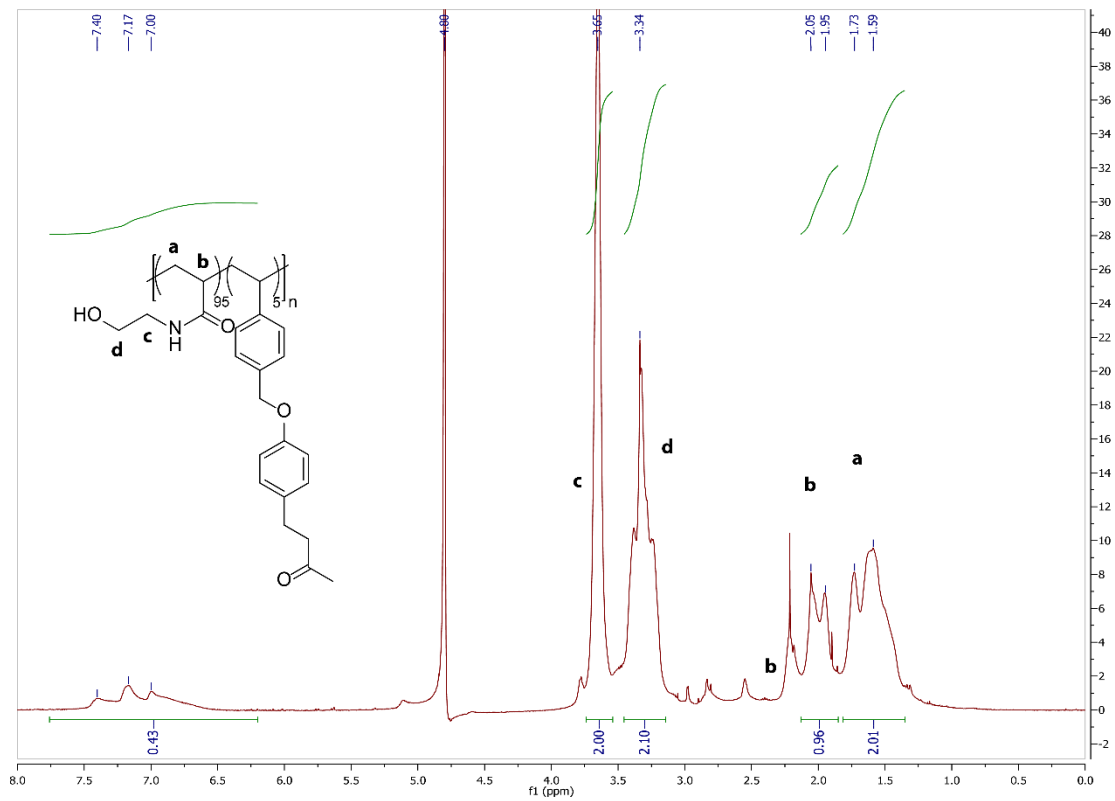
PHEAM-Thymol

2-Isopropyl-5-methylphenol (1.05 mmol, Acros 99%) and cesium carbonate (1.03 mmol, Alfa 99%) were added to poly(N-hydroxyethyl acrylamide-*co*-chlorostyrene) dissolved in 10 mL dimethylacetamide. The mixture was heated at 85 °C under a nitrogen atmosphere for 12 hours and precipitated in a mixture of acetone and hexane (3:1 by volume) and dried *in vacuo* at 60 °C for 2 hours to remove excess solvent. The polymer was then dissolved in methanol, precipitated in diethyl ether, dried *in vacuo* at 60 °C for 2 hours, and stored in a desiccator prior to use. Yield: 1.031 g. $M_n = 2950$ Da, $M_w = 7044$ Da, $\bar{D} = 2.39$. Integration of aromatic protons relative to the methylene at 3.65 ppm indicates complete functionalization of chloromethylstyrene moieties on the polymer, given complete incorporation of chloromethylstyrene during polymerization.



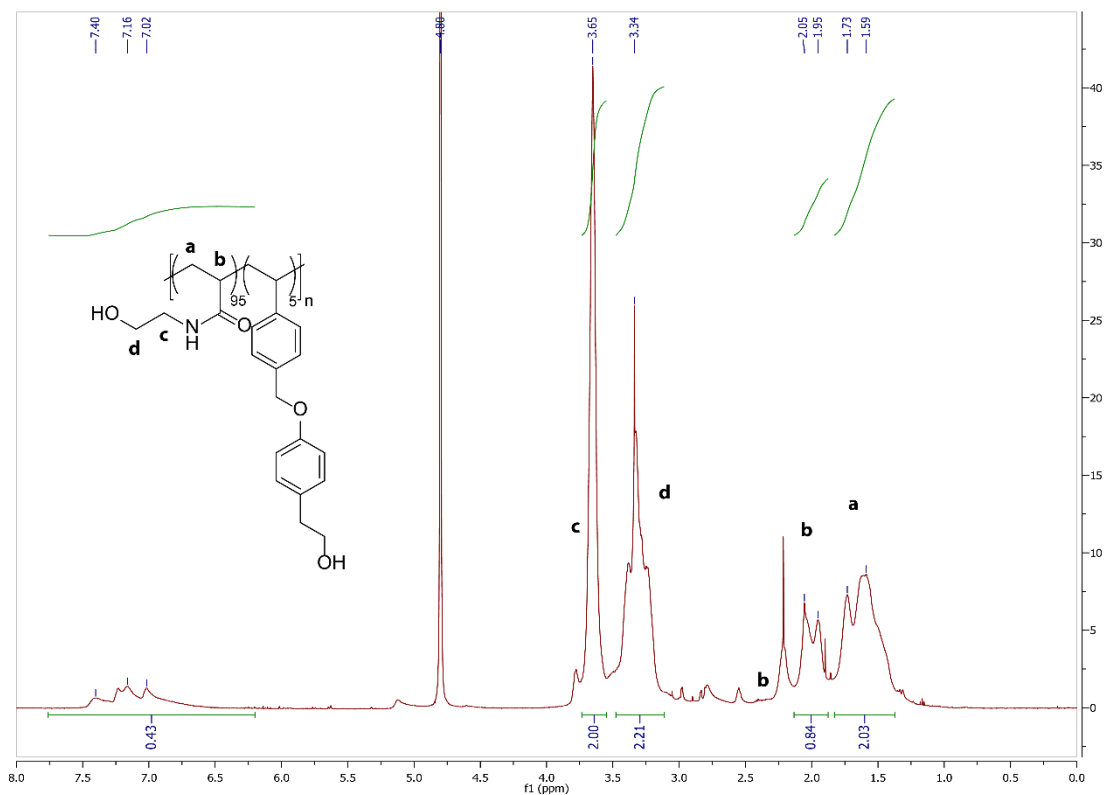
PHEAM-Raspberry Ketone

4-(4-hydroxyphenyl)-2-butanone (0.99 mmol, Aldrich 99%) and cesium carbonate (1.01 mmol, Alfa 99%) were added to poly(N-hydroxyethyl acrylamide-*co*-chlorostyrene) dissolved in 10 mL dimethylacetamide. The mixture was heated at 85 °C under a nitrogen atmosphere for 12 hours and precipitated in a mixture of acetone and hexane (3:1 by volume) and dried *in vacuo* at 60 °C for 2 hours to remove excess solvent. The polymer was then dissolved in methanol, precipitated in diethyl ether, dried *in vacuo* at 60 °C for 2 hours, and stored in a desiccator prior to use. Yield: 823 mg. $M_n = 3729$ Da, $M_w = 8398$ Da, $\bar{D} = 2.25$. Integration of aromatic protons relative to the methylene at 3.65 ppm indicates complete functionalization of chloromethylstyrene moieties on the polymer.



PHEAM-Tyrosol

2-(4-hydroxyphenyl)ethanol (1.01 mmol, TCI >98.0%) and cesium carbonate (1.02 mmol, Alfa 99%) were added to poly(N-hydroxyethyl acrylamide-*co*-chlorostyrene) dissolved in 10 mL dimethylacetamide. The mixture was heated at 85 °C under a nitrogen atmosphere for 12 hours and precipitated in a mixture of acetone and hexane (3:1 by volume) and dried *in vacuo* at 60 °C for 2 hours to remove excess solvent. The polymer was then dissolved in methanol, precipitated in diethyl ether, dried *in vacuo* at 60 °C for 2 hours, and stored in a desiccator prior to use. Yield: 854 mg. $M_n = 3772$ Da, $M_w = 8811$ Da, $\bar{D} = 2.34$. Integration of aromatic protons relative to the methylene at 3.65 ppm indicates complete functionalization of chloromethylstyrene moieties on the polymer.



3.4.3 Gel Permeation Chromatography of PHEAM Polymers

PHEAM molecular weights were determined using aqueous gel permeation chromatography. The retention time of PHEAM-thymol, PHEAM-raspberry ketone, and PHEAM-tyrosol on a Waters 1515 Isocratic HPLC Pump through Ultra HydroGel Columns was determined in aqueous solution containing 0.1 M sodium nitrate at 40 °C at a 1 mL/minute flow rate. Polymer was detected using changes in refractive index and molecular weights were determined relative to poly(ethylene glycol) standards (Figure 3.6). Differences in apparent molecular weight of these

polymers is ascribed to changes in their hydrodynamic volume rather than differences in number-average chain length; all polymers were functionalized from the same parent batch of poly(N-hydroxyethyl acrylamide-*co*-chloromethylstyrene).

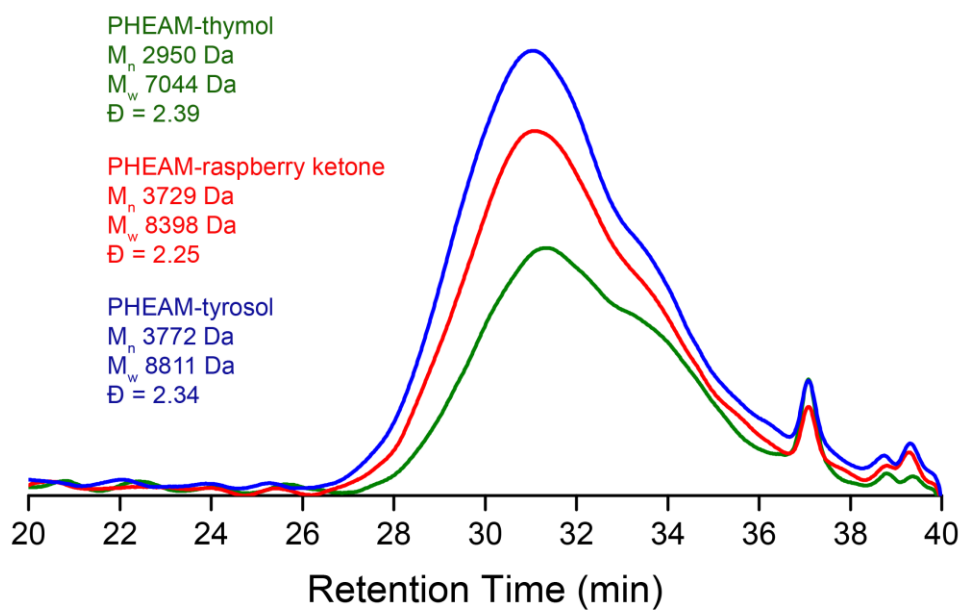


Figure 3.6. GPC of functionalized PHEAM polymers.

3.4.4 Induction Times to Crystallization of Pyrazinamide and Hydrochlorothiazide containing Functionalized Polymeric Materials

In the Technobis CrystalBreeder, aqueous solutions of pyrazinamide (0.28 mL, 203 mM) were heated at 65 °C for half an hour and brought to 30 °C to achieve a supersaturation of roughly 1.3.³⁷ Crystallization was identified as the moment when transmissivity began to drop for stirred solution vials (stirred at 1200 rpm with a Teflon stir bar). Approximately 0.5-1.0 mg of MFR was added to crystallizations as a heteronucleant to speed crystallization and 0.25 mg/mL PHEAM (1 wt% of pyrazinamide) was added to crystallizations to inhibit pyrazinamide crystallization. Crystallizations were repeated five times for sixteen vials to give a total of 80 inductions times to crystallization.

Aqueous hydrochlorothiazide (0.28 mL, 7.05 mM) was heated at 65 °C for half an hour and brought to 30 °C to achieve a supersaturation of roughly 2.5.⁵⁴ Solution transmissivity was monitored while stirred with a Teflon stir bar (1200 rpm) and the induction time to crystallization was identified at the point when transmissivity began to drop. Approximately 0.25-0.5 mg of functionalized MFR was added as a crystallization heteronucleant and 0.021 mg/mL PHEAM (1 wt% of hydrochlorothiazide) was added to crystallizations as a crystallization inhibitor. Crystallizations were repeated five times for sixteen vials to give a total of 80 inductions times to crystallization.

Induction Times to Crystallization

A complete list of the 80 induction times to crystallization for pyrazinamide (203 mM, 30 °C) are shown in Table 3.1 (graphed in the manuscript as Figure 3.2).

Table 3.1. Induction times (minutes) to crystallization of aqueous pyrazinamide with heteronuclei and water-soluble polymer additives.

control	MFR- thymol	MFR- raspberry ketone	MFR- tyrosol	PHEAM-thymol	PHEAM-raspberry ketone	PHEAM-tyrosol
1.36	0.78	1.07	0.92	17.26	18.04	44.81
1.39	1.67	1.23	1.01	17.3	21.64	47.5
1.9	1.81	1.34	1.23	17.96	30.15	51.42
2.79	4.15	1.4	1.25	22.59	42.72	60.24
3.76	4.94	1.81	1.28	41.03	47.66	62.83
4.61	5.69	1.85	1.3	43.48	51.3	64.28
4.88	5.9	2.04	1.9	48.3	60.97	72.4
5.13	6.87	2.17	1.97	54.78	76.31	78.38
5.48	7.3	2.25	2.31	60.1	96.05	85.56
6.19	7.62	2.3	2.35	64.71	149.31	86.35
7.07	7.69	2.31	2.36	67	162.28	102.07
7.07	7.77	2.43	2.48	72.76	171.08	106.45
7.88	8.6	2.69	2.54	73.41	175.24	120.34
8.1	8.73	2.87	2.69	75.81	188.06	129.78
9.61	8.79	3.15	2.78	75.91	195.85	139.94
9.78	9.04	3.32	2.9	81.29	198.34	143.82

10.23	9.07	3.63	3.05	94.26	227.83	163.5
10.38	9.45	3.64	3.32	103.52	238.38	178.78
10.58	11.29	3.68	3.44	106.3	239.04	186.92
11.69	11.51	3.7	3.47	106.54	251.24	187.83
11.97	11.98	3.93	3.56	115.55	271.56	200.69
12.87	12.1	3.95	3.6	120.05	276.47	204.41
13.17	12.16	4.02	4.06	123.35	285.06	221.79
13.3	12.41	4.17	4.09	126.13	288.19	234.29
14.14	12.62	4.3	4.35	138.66	293.28	238.08
14.19	12.82	4.36	4.86	142.42	326.18	252.55
14.39	13.52	4.4	4.86	143.8	329.82	252.74
14.46	13.63	4.59	4.95	145.58	336.39	280.27
14.6	13.91	4.88	5.03	150.84	no crystallization observed	294.26
14.91	14.02	4.88	5.09	158.84	no crystallization observed	320.79
15.86	14.22	4.9	5.36	160.36	no crystallization observed	352.94
16.08	14.34	5.08	5.52	161.07	no crystallization observed	354.09
17.2	14.5	5.13	5.77	161.33	no crystallization observed	no crystallization observed
17.36	14.63	5.19	5.94	161.61	no crystallization observed	no crystallization observed

17.53	16.67	5.49	5.96	175.34	no crystallization observed	no crystallization observed
17.77	16.94	5.88	5.97	184.77	no crystallization observed	no crystallization observed
19.86	17.06	6.04	6.71	188.84	no crystallization observed	no crystallization observed
20.53	17.58	6.07	6.75	190.21	no crystallization observed	no crystallization observed
21.92	17.88	6.29	6.8	195.51	no crystallization observed	no crystallization observed
22.01	18.45	6.33	7.1	199.1	no crystallization observed	no crystallization observed
22.04	20.51	6.78	7.46	201.5	no crystallization observed	no crystallization observed
22.13	20.91	7.11	7.51	202.02	no crystallization observed	no crystallization observed
22.38	21.09	7.52	7.53	202.05	no crystallization observed	no crystallization observed
25.43	22.01	7.63	7.65	204.4	no crystallization observed	no crystallization observed
25.57	22.37	8.05	7.84	206.2	no crystallization observed	no crystallization observed
25.64	22.55	8.12	7.86	207.51	no crystallization observed	no crystallization observed

25.68	23.3	8.2	8.13	210.05	no crystallization observed	no crystallization observed
26.34	23.71	8.24	8.45	212.27	no crystallization observed	no crystallization observed
27.68	25.14	8.42	8.97	215.96	no crystallization observed	no crystallization observed
27.87	26.66	8.47	9.25	216.46	no crystallization observed	no crystallization observed
29.15	27.64	9.1	9.26	226.1	no crystallization observed	no crystallization observed
29.22	28.83	9.41	9.3	227.96	no crystallization observed	no crystallization observed
30.65	29.14	10.25	9.9	229.89	no crystallization observed	no crystallization observed
31.4	29.49	10.49	9.92	243.67	no crystallization observed	no crystallization observed
31.85	30.3	10.77	10.06	243.93	no crystallization observed	no crystallization observed
32.61	31.03	12.01	10.25	244.14	no crystallization observed	no crystallization observed
32.87	31.26	12.36	10.47	249.4	no crystallization observed	no crystallization observed
35.91	33.01	13.06	11.16	250.01	no crystallization observed	no crystallization observed

36.95	34.43	13.37	11.5	267.56	no crystallization observed	no crystallization observed
38.09	34.44	13.47	11.71	268.61	no crystallization observed	no crystallization observed
41.76	35.32	13.57	11.79	272.97	no crystallization observed	no crystallization observed
42.34	36.09	14.17	11.87	286.13	no crystallization observed	no crystallization observed
51.68	36.58	14.27	11.97	290.32	no crystallization observed	no crystallization observed
54.05	39.7	14.28	12.12	309.84	no crystallization observed	no crystallization observed
58.32	40.2	15.12	13.45	no crystallization observed	no crystallization observed	no crystallization observed
58.56	40.78	15.52	14.15	no crystallization observed	no crystallization observed	no crystallization observed
58.9	43.78	16.75	14.44	no crystallization observed	no crystallization observed	no crystallization observed
60.92	46.89	17.82	16.46	no crystallization observed	no crystallization observed	no crystallization observed
73.44	48.67	17.87	16.52	no crystallization observed	no crystallization observed	no crystallization observed
73.99	49.66	18.47	16.68	no crystallization observed	no crystallization observed	no crystallization observed

78.27	50.61	19.43	16.78	no crystallization observed	no crystallization observed	no crystallization observed
89.19	51.4	19.78	16.99	no crystallization observed	no crystallization observed	no crystallization observed
89.38	55.98	19.87	17.92	no crystallization observed	no crystallization observed	no crystallization observed
89.62	59.45	21.08	17.96	no crystallization observed	no crystallization observed	no crystallization observed
91.47	61.38	21.22	18.02	no crystallization observed	no crystallization observed	no crystallization observed
93.12	78.27	23.04	19.21	no crystallization observed	no crystallization observed	no crystallization observed
98.23	81.98	25.55	19.69	no crystallization observed	no crystallization observed	no crystallization observed
99.26	96.25	26.66	21.83	no crystallization observed	no crystallization observed	no crystallization observed
105.82	107.59	28.75	21.91	no crystallization observed	no crystallization observed	no crystallization observed
182.53	112.25	31.61	22.85	no crystallization observed	no crystallization observed	no crystallization observed

To analyze the statistical significance of these relative crystallization rates of pyrazinamide, data are plotted as a Kaplan-Meier survival function (where survival represents the ability of a supersaturated solution to avoid precipitation) with 95% confidence intervals in Figure 3.7.

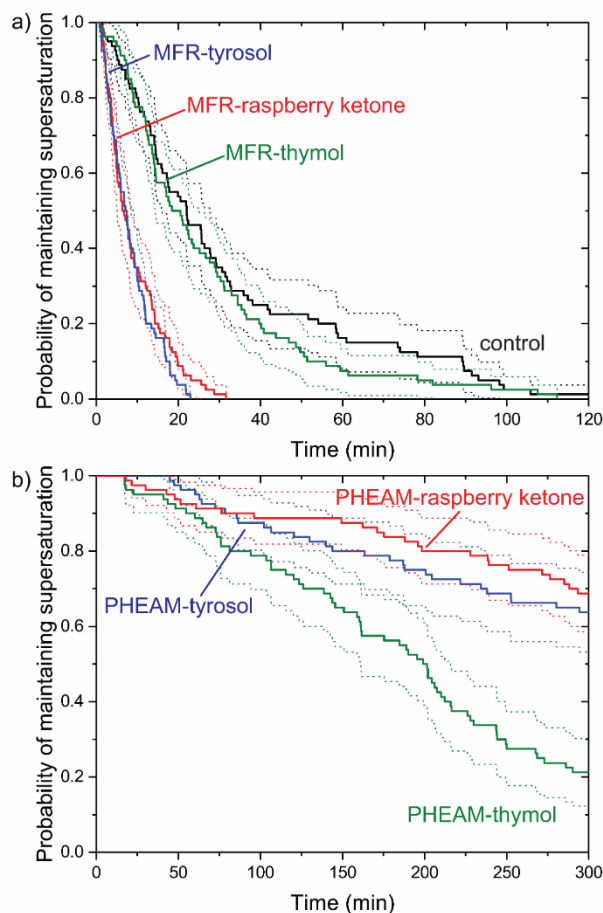


Figure 3.7. Survival plots for pyrazinamide crystallization, where survival represents the ability of a supersaturated solution to maintain supersaturation without crystallization, drawn with 95% confidence intervals, comparing a) control (neat) pyrazinamide crystallization and crystallization with added MFR, and b) pyrazinamide crystallizations with 1 wt% functionalized PHEAM polymers.

Comparing induction times for neat pyrazinamide and crystallizations containing polymer heteronuclei using the Fisher test ($P < 0.05$) reflects the analysis shown using confidence intervals (MFR-thymol is slower than MFR-raspberry ketone and MFR-tyrosol, which have similar effects to speed pyrazinamide crystallization). However, comparing crystallizations which contain PHEAM polymer additives is not possible using these traditional statistical methods due to the

many vials which did not crystallize within 6 hours. Analysis using 95% confidence intervals generated using Greenwood's formula⁵⁵ captures statistical differences between these trials.

Table 3.2 shows a complete list of the measured induction times to crystallization for hydrochlorothiazide (7.05 mM, 30 °C), as shown in the manuscript as Figure 3.3. Crystallizations that occurred before vials had equilibrated to a temperature of 30 °C are given an induction time of 0 minutes.

Table 3.2. Induction times (minutes) to crystallization of aqueous hydrochlorothiazide (7.05 mM, 30 °C) with heteronuclei and water-soluble polymer additives.

control	MFR-thymol	MFR-raspberry ketone	MFR-tyrosol	PHEAM-thymol	PHEAM-raspberry ketone	PHEAM-tyrosol
0	0	0	0	3.33	37.51	19.25
0	0	0	0	3.39	81.65	24.67
0	0	0	0	4.77	130.97	29.47
0.19	0	0	0	5.34	138.36	29.91
0.32	0	0	0	7.09	141.94	32.22
0.66	0	0	0	7.71	143.04	34.37
0.79	0	0	0	8.76	143.81	35.22
0.9	0	0	0	10.65	160.57	36.72
0.99	0	0	0	10.92	160.91	37.07
1	0	0	0	11.93	162.58	41.94
1.03	0	0	0	13.91	165.47	42.33
1.05	0.04	0	0	14.69	170.72	46.25
1.13	0.13	0	0	16.11	171.48	49.16
1.46	0.17	0	0	17	171.87	50.09
1.52	0.18	0	0	17.24	184.08	51.76
1.53	0.23	0	0	18.73	186.1	52.14
1.61	0.25	0	0	19.02	194.13	53.16
1.74	0.27	0	0	19.37	208.85	54.14

1.8	0.35	0	0	19.57	222.49	57.56
2.02	0.38	0	0	21.32	223.16	59.5
2.1	0.4	0	0.01	21.32	224.05	60.87
2.13	0.44	0	0.19	22.45	227.83	61.7
2.31	0.55	0	0.23	22.66	228.95	63.47
2.36	0.73	0	0.23	22.83	239.14	64.02
2.43	0.84	0	0.27	23.14	275.98	64.6
2.44	0.87	0	0.29	23.3	307.41	65
2.56	0.88	0	0.39	23.31	310	70.77
2.72	0.89	0	0.4	24.21	no crystallization observed	71.87
2.72	0.91	0	0.4	24.96	no crystallization observed	72.75
2.75	0.95	0	0.41	25.56	no crystallization observed	75.56
3.1	0.95	0	0.45	31.46	no crystallization observed	76
3.23	0.96	0	0.48	32.4	no crystallization observed	77.68
3.25	0.96	0	0.55	32.6	no crystallization observed	80.67
3.27	1.02	0	0.59	33.18	no crystallization observed	81.89
3.35	1.03	0	0.64	34.14	no crystallization observed	83.52
3.48	1.14	0	0.74	34.29	no crystallization observed	83.92
3.74	1.18	0	0.79	36.31	no crystallization observed	90.06
3.8	1.2	0	0.81	37.53	no crystallization observed	90.99
3.88	1.21	0	0.83	38.32	no crystallization observed	92.19
3.96	1.21	0	0.88	39.44	no crystallization observed	96.66
3.99	1.23	0	0.88	41.49	no crystallization observed	104.54
4.05	1.3	0	0.9	43.84	no crystallization observed	107.22
4.14	1.31	0	0.9	47.57	no crystallization observed	115.57
4.5	1.39	0	0.96	48.56	no crystallization observed	117.45

4.61	1.47	0	0.97	49.55	no crystallization observed	118.61
4.83	1.51	0	1.04	49.94	no crystallization observed	133.45
4.99	1.63	0	1.17	52.3	no crystallization observed	133.59
5.25	1.67	0	1.19	52.67	no crystallization observed	138.39
5.33	1.68	0	1.24	53.73	no crystallization observed	155.4
5.4	1.89	0	1.26	54.65	no crystallization observed	157.29
5.59	2.27	0	1.3	55.59	no crystallization observed	162.46
5.77	2.36	0	1.31	56.21	no crystallization observed	170.2
5.79	2.36	0	1.56	56.25	no crystallization observed	179.2
6.21	2.4	0	1.59	57.12	no crystallization observed	180.63
7.26	2.47	0	1.63	59.55	no crystallization observed	180.88
7.4	2.48	0	1.67	62.14	no crystallization observed	197.05
7.8	2.63	0	1.88	62.89	no crystallization observed	199.1
8.5	2.65	0	1.93	65.22	no crystallization observed	199.66
9.14	2.69	0	2.01	70.18	no crystallization observed	207.34
9.19	2.69	0	2.01	70.37	no crystallization observed	215.51
9.2	2.7	0.09	2.04	70.75	no crystallization observed	223.58
9.32	2.82	0.1	2.43	72.94	no crystallization observed	263.92
9.98	3	0.13	2.44	74.04	no crystallization observed	265.68
11.11	3	0.16	2.81	74.56	no crystallization observed	310.7
11.42	3.22	0.22	3.11	75.85	no crystallization observed	no crystallization observed
12.99	3.42	0.23	3.18	76.8	no crystallization observed	no crystallization observed
13.58	3.52	0.24	3.33	82.87	no crystallization observed	no crystallization observed
14.04	4.28	0.25	3.57	84.24	no crystallization observed	no crystallization observed

15.91	4.6	0.28	3.68	86.2	no crystallization observed	no crystallization observed
16.02	4.96	0.33	4.03	88.05	no crystallization observed	no crystallization observed
18.2	5.01	0.46	4.44	96.15	no crystallization observed	no crystallization observed
20.85	5.93	0.47	4.47	102.17	no crystallization observed	no crystallization observed
26.25	8.11	0.59	4.55	109.75	no crystallization observed	no crystallization observed
31.17	10.4	0.64	5.1	140.96	no crystallization observed	no crystallization observed
34.83	21.03	1.21	5.5	153.6	no crystallization observed	no crystallization observed
38.51	22.24	1.39	5.5	180.12	no crystallization observed	no crystallization observed
43.53	30.48	2.32	8.22	181.75	no crystallization observed	no crystallization observed
48.29	36.75	2.57	13.21	182.38	no crystallization observed	no crystallization observed
52.23	37.71	2.63	18.43	203.18	no crystallization observed	no crystallization observed
86.23	49.15	5.05	27.47	no crystallization observed	no crystallization observed	no crystallization observed

Kaplan-Meier survival curves of the ability for each polymer to maintain supersaturation are shown in Figure 3.8 with 95% confidence intervals. Here, the effects of functionalized heteronuclei (Figure 3.8a) and water-soluble polymer inhibitors (Figure 3.8b) on crystallization can be compared for statistical significance. There are statistically significant differences between each of the crystallizations containing PHEAM polymer using a 95% confidence interval analysis. However, although crystallizations containing with MFR are statistically faster than control crystallizations by the Fisher test ($P < 0.05$), the only statistical difference amongst crystallizations containing MFR was found between MFR-raspberry ketone and MFR-thymol. Potential reasons for these results are discussed in the manuscript text.

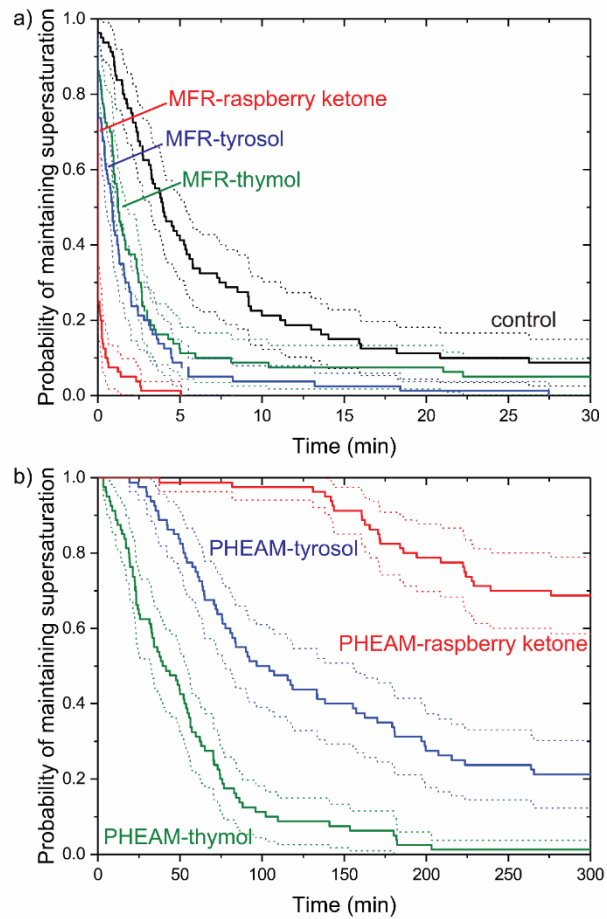


Figure 3.8. Survival plots for hydrochlorothiazide crystallization, where survival represents the ability of a supersaturated solution to maintain supersaturation without crystallization, drawn with 95% confidence intervals, comparing a) control (neat) hydrochlorothiazide crystallization and crystallization with added MFR, and b) crystallizations with 1 wt% functionalized PHEAM polymers.

3.4.5 Induction Times to Crystallization of Pyrazinamide and Hydrochlorothiazide containing Small-Molecule Additives

Pyrazinamide crystallization in the presence of 1 mol% phenolic additives was also performed to investigate the impact of small-molecules on the kinetics of pyrazinamide precipitation. As shown in Figure 3.9, although these compounds act as inhibitors of precipitation, there is not a dramatic difference between their abilities to maintain pyrazinamide supersaturation, and they are far weaker inhibitors of crystallization compared to functionalized PHEAM.

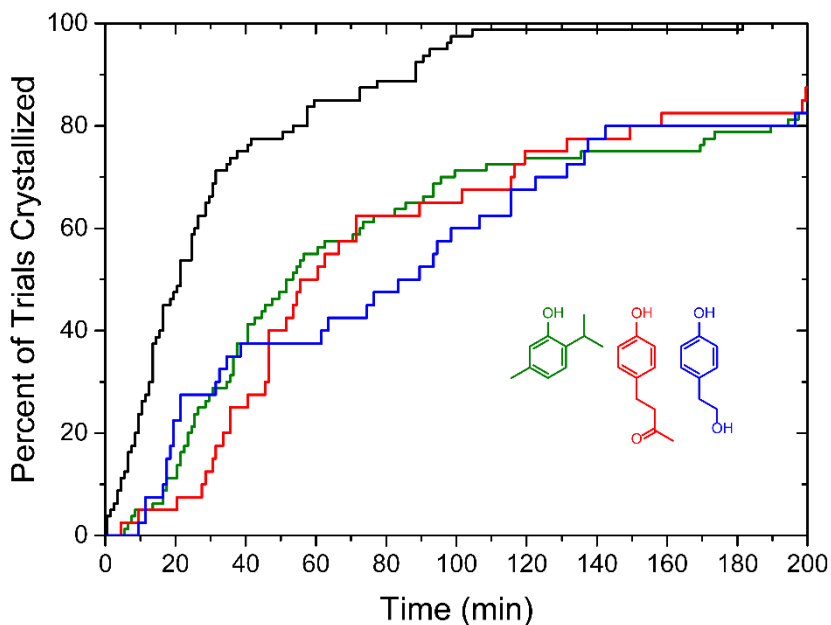


Figure 3.9. Aqueous crystallization kinetics of pyrazinamide (shown in black, 203 mM, 30 °C) in the presence of 1 mol% small-molecule additives thymol (green), raspberry ketone (red), and tyrosol (blue), pictured in the lower right of the figure.

3.4.6 Solubility of Pharmaceutical Solutes in Presence of PHEAM Polymers

Solubility differences for pyrazinamide and hydrochlorothiazide in aqueous solution containing each polymer additive were evaluated by comparing the clear point temperature of each solute during dissolution. Clear points were measured at a heating rate of 5 °C/minute. As can be seen in Figure 3.10, there are no substantial differences between the clear point temperatures for solutions containing each soluble polymer additive.

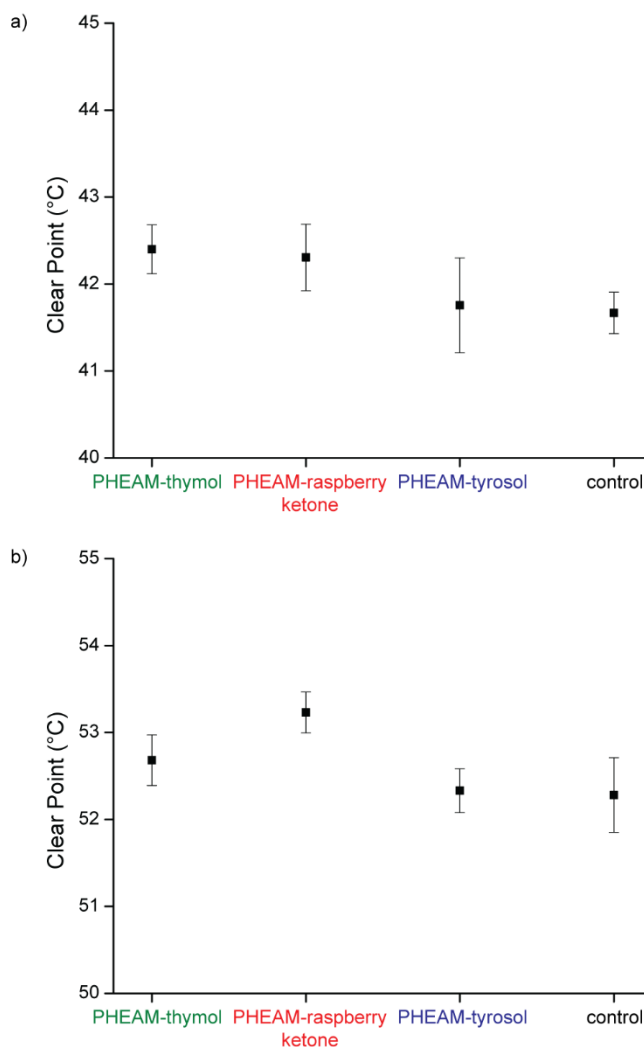


Figure 3.10. Clear point temperature (with standard error) upon heating of a) pyrazinamide (25 mg/mL) and b) hydrochlorothiazide (2.1 mg/mL) in the presence of 1 wt% soluble polymer (denoted under the x-axis on the plot) and in aqueous solution (denoted as control group).

3.4.7 Polymorphic Phase of Pharmaceutical Solutes

Using Raman spectroscopy, the polymorphic phase of crystallized pharmaceutical was determined in the crystallization conditions described in the manuscript (see Figure 3.11). Pyrazinamide was found to crystallize in the alpha form from water, regardless of the presence of dissolved polymer or polymer heteronuclei. Hydrochlorothiazide was found to crystallize in Form I (see Figure 3.12) regardless of the presence of insoluble or soluble polymer additives.

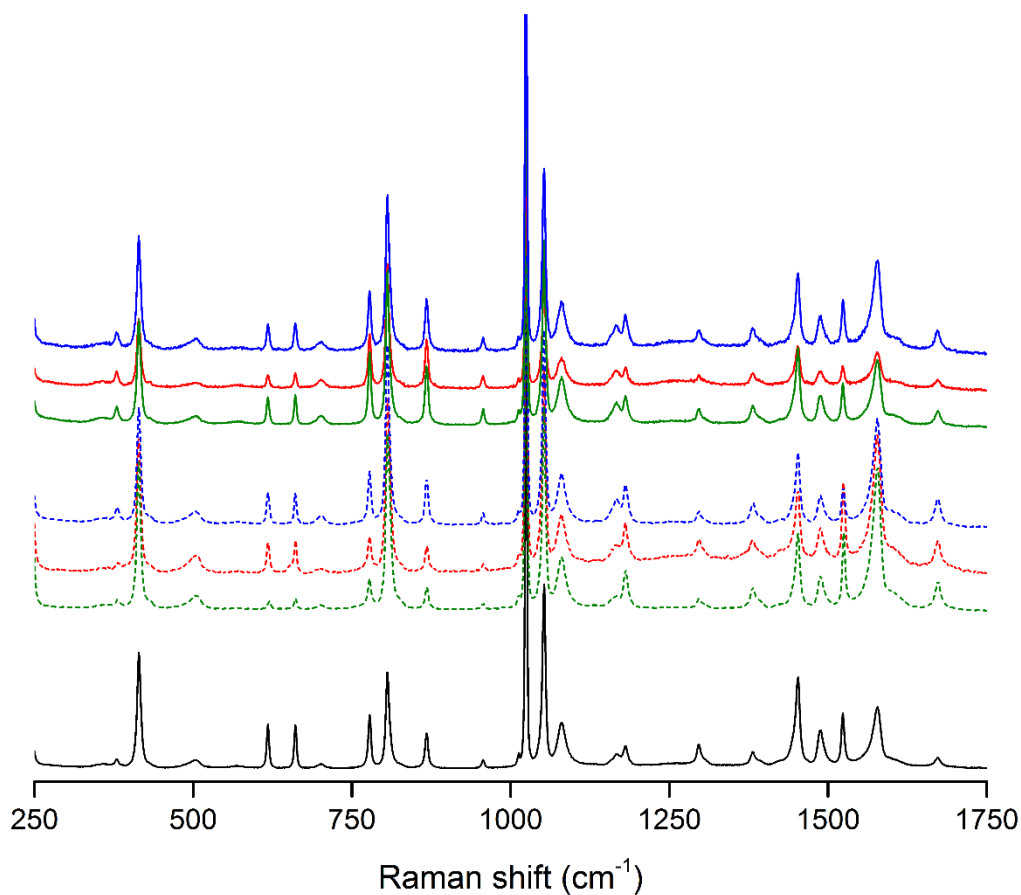


Figure 3.11. Raman spectroscopy of pyrazinamide crystallized from aqueous solution (black trace), aqueous solution with PHEAM (dotted colored traces, following the coloring scheme for functionalized polymers used throughout the manuscript), and aqueous solution with PHEAM (solid colored traces). All crystals were found to be alpha pyrazinamide.

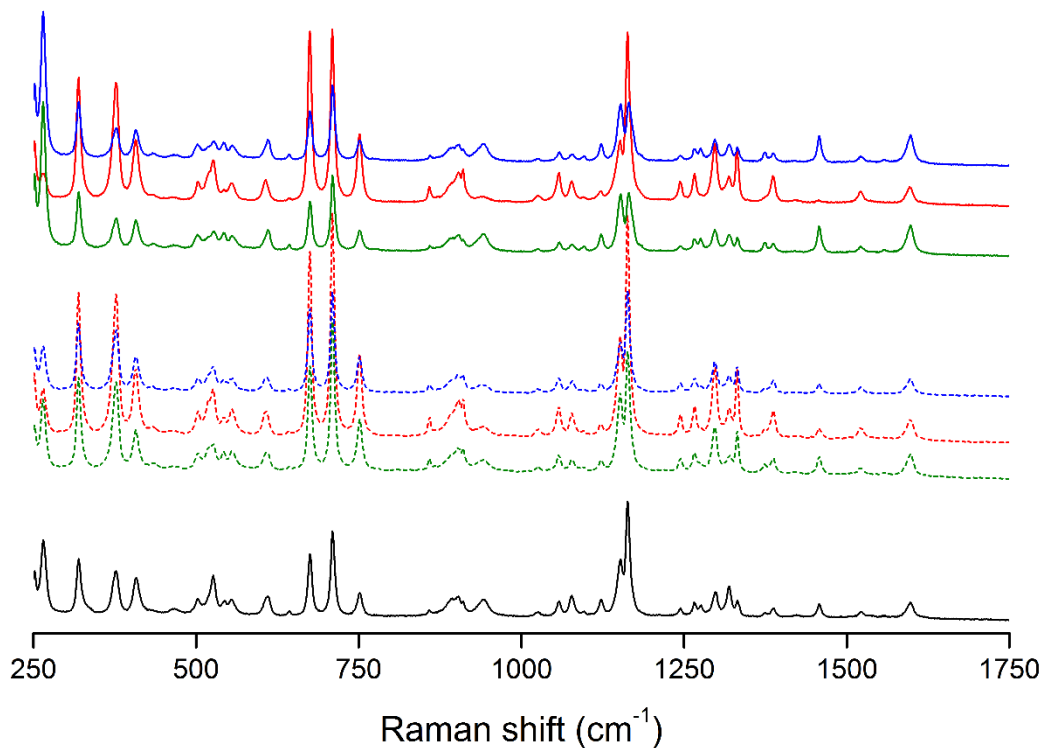


Figure 3.12. Raman spectroscopy of hydrochlorothiazide crystallized from aqueous solution (black trace), aqueous solution with PHEAM (dotted colored traces, following the coloring scheme for functionalized polymers used throughout the manuscript), and aqueous solution with PHEAM (solid colored traces). All crystals were found to be hydrochlorothiazide Form I.

3.4.8 Average Intermolecular Bond Lengths from the Cambridge Structural Database

The average intermolecular bond length between water and alcohol or ketone functionalities was computed from crystal structures in the Cambridge Structural Database (CSD version 5.40, November 2018, 3D coordinates determined, no ions, only organics) for intermolecular bond distances between 2.5 and 3.5 Å (following procedures in Frank, *et al*⁴³) to estimate the interaction strength between water and functionalities on raspberry ketone and tyrosol. The average bond distance between water and a ketone functionality is 2.920 ± 0.004 Å (median of 2.857 Å, mode of 2.828 Å) and the average intermolecular bond distance between water and an aliphatic hydroxy functionality is 2.866 ± 0.003 Å (median of 2.795 Å, mode of 2.736 Å), compared in Figure 3.13.

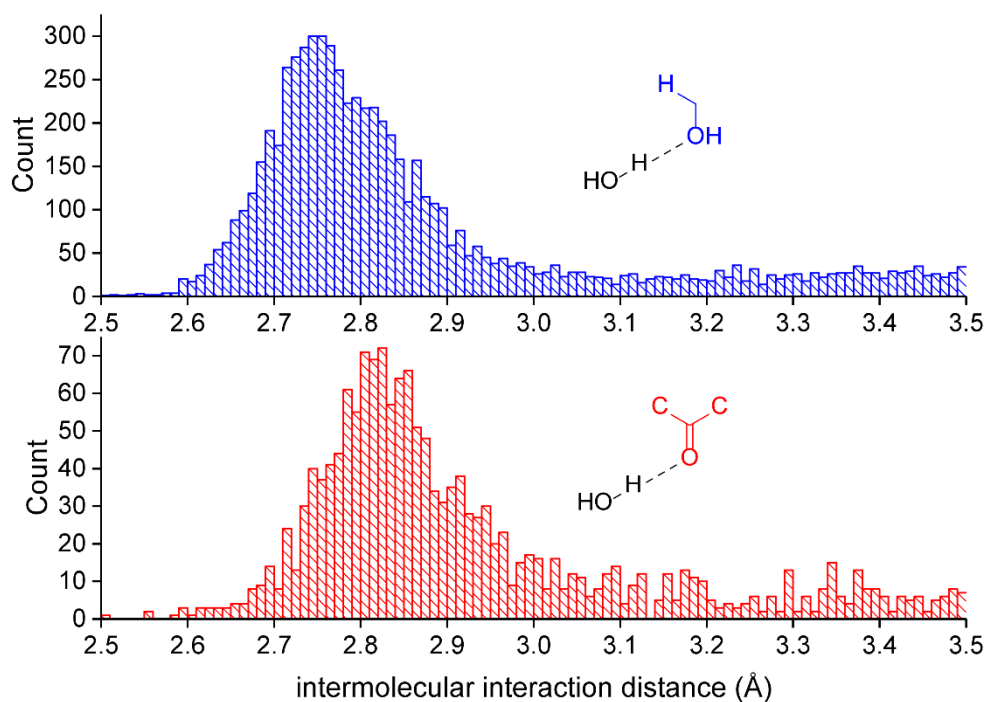


Figure 3.13. Histogram of interaction distances between aliphatic hydroxyl group and water (shown in upper panel in blue) and ketone functionality and water (shown in lower panel in red).

3.4.9 Electrostatic Potential Surfaces of APIs and Polymer Functionalities

Electrostatic potential maps represent the charge distribution around a molecule and visualize potential donor and acceptor sites. Shown below in Figure 3.14, electrostatic potential maps for both APIs and each polymer functionality reveal potential sites of interaction between the pharmaceutical and either soluble or insoluble polymers.

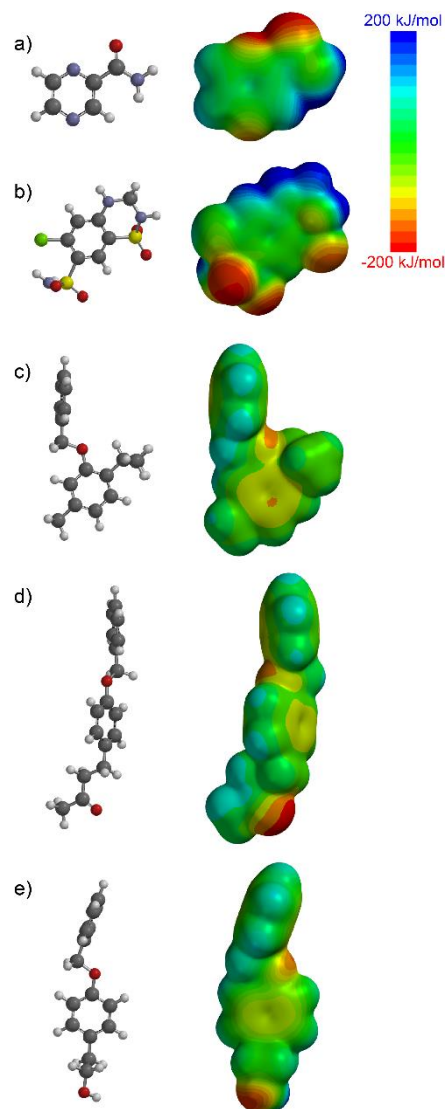


Figure 3.14. Electrostatic potential maps of a) pyrazinamide, b) hydrochlorothiazide, and polymers functionalized with c) thymol, d) raspberry ketone, and e) tyrosol (functionalization is represented by replacement of the phenol with a benzyl ether) calculated using density functional theory at the B3LYP/6-31+G** level of theory (regions of negative potential represented by red, positive potential presented by blue, and neutral represented by green).

Pyrazinamide contains its most positive and negative potentials at the ketone and -NH_2 regions on its primary amide. Thus, we hypothesize that the pharmaceutical interacts with polymer

functionalities via its primary amide rather than its pyridine nitrogen atoms. Hydrochlorothiazide was found to interact more strongly with polymers functionalized with raspberry ketone as compared to those functionalized with tyrosol. The pharmaceutical shows a large region of positive potential around its cyclic amide and sulfonamide sites. Therefore, we hypothesize that this positive region favorably interacts with the positive node on raspberry ketone to facilitate the inhibition or acceleration of crystallization in solution.

3.5 References

1. Mullin, J. W., *Crystallization*. Elsevier: 2001.
2. Song, R.-Q.; Cölfen, H., Additive controlled crystallization. *CrystEngComm* **2011**, *13* (5), 1249-1276
3. Perez, L. A.; Chou, K. W.; Love, J. A.; Van Der Poll, T. S.; Smilgies, D. M.; Nguyen, T. Q.; Kramer, E. J.; Amassian, A.; Bazan, G. C., Solvent additive effects on small molecule crystallization in bulk heterojunction solar cells probed during spin casting. *Adv. Mater.* **2013**, *25* (44), 6380-6384.
4. Hendriksen, B. A.; Grant, D. J., The effect of structurally related substances on the nucleation kinetics of paracetamol (acetaminophen). *J. Cryst. Growth* **1995**, *156* (3), 252-260.
5. Hekmat, D.; Hebel, D.; Joswig, S.; Schmidt, M.; Weuster-Botz, D., Advanced protein crystallization using water-soluble ionic liquids as crystallization additives. *Biotechnol. Lett* **2007**, *29* (11), 1703-1711.
6. Variankaval, N.; Cote, A. S.; Doherty, M. F., From form to function: Crystallization of active pharmaceutical ingredients. *AIChE J.* **2008**, *54* (7), 1682-1688.
7. Chen, J.; Sarma, B.; Evans, J. M.; Myerson, A. S., Pharmaceutical crystallization. *Cryst. Growth Des.* **2011**, *11* (4), 887-895.
8. Shekunov, B. Y.; York, P., Crystallization processes in pharmaceutical technology and drug delivery design. *J. Cryst. Growth* **2000**, *211* (1-4), 122-136.
9. Raghavan, S.; Trividic, A.; Davis, A.; Hadgraft, J., Crystallization of hydrocortisone acetate: influence of polymers. *Int. J. Pharm.* **2001**, *212* (2), 213-221.
10. Ullah, M.; Hussain, I.; Sun, C. C., The development of carbamazepine-succinic acid cocrystal tablet formulations with improved in vitro and in vivo performance. *Drug Dev. Ind. Pharm.* **2016**, *42* (6), 969-976
11. Rodríguez-hornedo, N.; Murphy, D., Significance of controlling crystallization mechanisms and kinetics in pharmaceutical systems. *J. Pharm. Sci.* **1999**, *88* (7), 651-660

12. Wilson, V.; Lou, X.; Osterling, D. J.; Stolarik, D. F.; Jenkins, G.; Gao, W.; Zhang, G. G.; Taylor, L. S., Relationship between amorphous solid dispersion In Vivo absorption and In Vitro dissolution: phase behavior during dissolution, speciation, and membrane mass transport. *J. Controlled Release* **2018**, *292*, 172-182.
13. Warren, D. B.; Benameur, H.; Porter, C. J.; Pouton, C. W., Using polymeric precipitation inhibitors to improve the absorption of poorly water-soluble drugs: A mechanistic basis for utility. *J. Drug Targeting* **2010**, *18* (10), 704-731.
14. Baghel, S.; Cathcart, H.; O'Reilly, N. J., Polymeric amorphous solid dispersions: a review of amorphization, crystallization, stabilization, solid-state characterization, and aqueous solubilization of biopharmaceutical classification system class II drugs. *J. Pharm. Sci.* **2016**, *105* (9), 2527-2544
15. Ilevbare, G. A.; Liu, H.; Edgar, K. J.; Taylor, L. S., Maintaining supersaturation in aqueous drug solutions: impact of different polymers on induction times. *Cryst. Growth Des.* **2012**, *13* (2), 740-751.
16. Theil, F.; Anantharaman, S.; Kyeremateng, S. O.; van Lishaut, H.; Dreis-Kühne, S. H.; Rosenberg, J. r.; Mägerlein, M.; Woehrl, G. H., Frozen in time: kinetically stabilized amorphous solid dispersions of nifedipine stable after a quarter century of storage. *Mol. Pharmaceutics* **2016**, *14* (1), 183-192
17. Theil, F.; Milsmann, J.; Kyeremateng, S. O.; Anantharaman, S.; Rosenberg, J. r.; van Lishaut, H., Extraordinary Long-Term-Stability in Kinetically Stabilized Amorphous Solid Dispersions of Fenofibrate. *Mol. Pharmaceutics* **2017**, *14* (12), 4636-4647.
18. Law, D.; Krill, S. L.; Schmitt, E. A.; Fort, J. J.; Qiu, Y.; Wang, W.; Porter, W. R., Physicochemical considerations in the preparation of amorphous ritonavir–poly (ethylene glycol) 8000 solid dispersions. *J. Pharm. Sci.* **2001**, *90* (8), 1015-1025.
19. Guo, Y.; Shalaev, E.; Smith, S., Physical stability of pharmaceutical formulations: solid-state characterization of amorphous dispersions. *Trends Anal. Chem.* **2013**, *49*, 137-144.
20. Givargizov, E. I., *Oriented crystallization on amorphous substrates*. Springer Science & Business Media: 2013.
21. Suryanarayanan, R.; Duggirala, N. K.; Li, J.; Gopinath, T., Supramolecular Synthon Approach to Design Amorphous Solid Dispersions with Exceptional Physical Stability. *Chem. Commun.* **2019**.
22. Van Eerdenbrugh, B.; Taylor, L. S., An ab initio polymer selection methodology to prevent crystallization in amorphous solid dispersions by application of crystal engineering principles. *CrystEngComm* **2011**, *13* (20), 6171-6178.
23. Chadwick, K.; Chen, J.; Myerson, A. S.; Trout, B. L., Toward the rational design of crystalline surfaces for heteroepitaxy: role of molecular functionality. *Cryst. Growth Des.* **2012**, *12* (3), 1159-1166.
24. Curcio, E.; López-Mejías, V.; Di Profio, G.; Fontananova, E.; Drioli, E.; Trout, B. L.; Myerson, A. S., Regulating nucleation kinetics through molecular interactions at the polymer–solute interface. *Cryst. Growth Des.* **2014**, *14* (2), 678-686.

25. Diao, Y.; Helgeson, M. E.; Siam, Z. A.; Doyle, P. S.; Myerson, A. S.; Hatton, T. A.; Trout, B. L., Nucleation under soft confinement: role of polymer–solute interactions. *Cryst. Growth Des.* **2011**, *12* (1), 508-517.
26. Diao, Y.; Myerson, A. S.; Hatton, T. A.; Trout, B. L., Surface design for controlled crystallization: The role of surface chemistry and nanoscale pores in heterogeneous nucleation. *Langmuir* **2011**, *27* (9), 5324-5334.
27. López-Mejías, V.; Knight, J. L.; Brooks III, C. L.; Matzger, A. J., On the mechanism of crystalline polymorph selection by polymer heteronuclei. *Langmuir* **2011**, *27* (12), 7575-7579.
28. McClelland, A. A.; López-Mejías, V.; Matzger, A. J.; Chen, Z., Peering at a Buried Polymer– Crystal Interface: Probing Heterogeneous Nucleation by Sum Frequency Generation Vibrational Spectroscopy. *Langmuir* **2011**, *27* (6), 2162-2165.
29. Artusio, F.; Pisano, R., Surface-induced crystallization of pharmaceuticals and biopharmaceuticals: a review. *Int. J. Pharm.* **2018**, *547* (1-2), 190-208.
30. Frank, D. S.; Matzger, A. J., Influence of chemical functionality on the rate of polymer-induced heteronucleation. *Cryst. Growth Des.* **2017**, *17* (8), 4056-4059.
31. Hamm, L. M.; Giuffre, A. J.; Han, N.; Tao, J.; Wang, D.; De Yoreo, J. J.; Dove, P. M., Reconciling disparate views of template-directed nucleation through measurement of calcite nucleation kinetics and binding energies. *PNAS* **2014**, *111* (4), 1304-1309.
32. Opdyke, D., 4-(p-Hydroxyphenyl)-2-butanone. *Food. Cosmet. Toxicol* **1978**, *16* (781782), 4.
33. Heath, H. B., *Source Book of Flavors:(AVI Sourcebook and Handbook Series)*. Springer Science & Business Media: 1981; Vol. 2.
34. Galanakis, C. M., *Food waste recovery: processing technologies and industrial techniques*. Academic Press: 2015.
35. Tripoli, E.; Giammanco, M.; Tabacchi, G.; Di Majo, D.; Giammanco, S.; La Guardia, M., The phenolic compounds of olive oil: structure, biological activity and beneficial effects on human health. *Nut. Res. Rev.* **2005**, *18* (1), 98-112.
36. Gisin, B., The preparation of Merrifield-resins through total esterification with cesium salts. *Helv. Chim. Acta* **1973**, *56* (5), 1476-1482.
37. Zhang, K.; Shen, H.; Xu, S.; Zhang, H.; Zhu, M.; Shi, P.; Fu, X.; Yang, Y.; Gong, J., Thermodynamic study of solubility for pyrazinamide in ten solvents from T=(283.15 to 323.15) K. *J. Chem. Thermodyn.* **2017**, *112*, 204-212.
38. Price, C. P.; Grzesiak, A. L.; Matzger, A. J., Crystalline polymorph selection and discovery with polymer heteronuclei. *J. Am. Chem. Soc.* **2005**, *127* (15), 5512-5517.
39. Pfund, L. Y.; Price, C. P.; Frick, J. J.; Matzger, A. J., Controlling pharmaceutical crystallization with designed polymeric heteronuclei. *J. Am. Chem. Soc.* **2015**, *137* (2), 871-875.
40. Ilevbare, G. A.; Liu, H.; Edgar, K. J.; Taylor, L. S., Impact of polymers on crystal growth rate of structurally diverse compounds from aqueous solution. *Mol. Pharmaceutics* **2013**, *10* (6), 2381-2393.
41. Mosquera-Giraldo, L. I.; Borca, C. H.; Parker, A. S.; Dong, Y.; Edgar, K. J.; Beaudoin, S. P.; Slipchenko, L. V.; Taylor, L. S., Crystallization Inhibition Properties of Cellulose Esters and

- Ethers for a Group of Chemically Diverse Drugs-Experimental and Computational Insight. *Biomacromolecules* **2018**, *19* (12), 4593-4606.
42. Yin, L.; Hillmyer, M. A., Preparation and performance of hydroxypropyl methylcellulose esters of substituted succinates for in vitro supersaturation of a crystalline hydrophobic drug. *Mol. Pharmaceutics* **2013**, *11* (1), 175-185.
43. Frank, D. S.; Matzger, A. J., Effect of Polymer Hydrophobicity on the Stability of Amorphous Solid Dispersions and Supersaturated Solutions of a Hydrophobic Pharmaceutical. *Mol. Pharmaceutics* **2019**, *16* (2), 682-688.
44. Poelma, F.; Breäs, R.; Tukker, J.; Crommelin, D., Intestinal absorption of drugs. The influence of mixed micelles on the disappearance kinetics of drugs from the small intestine of the rat. *J. Pharm. Pharmacol.* **1991**, *43* (5), 317-324.
45. Brouwers, J.; Brewster, M. E.; Augustijns, P., Supersaturating drug delivery systems: the answer to solubility-limited oral bioavailability? *J. Pharm. Sci.* **2009**, *98* (8), 2549-2572.
46. Jackson, M. J.; Kestur, U. S.; Hussain, M. A.; Taylor, L. S., Characterization of supersaturated Danazol solutions—impact of polymers on solution properties and phase transitions. *Pharm. Res.* **2016**, *33* (5), 1276-1288.
47. Dengale, S. J.; Grohgan, H.; Rades, T.; Löbmann, K., Recent advances in co-amorphous drug formulations. *Adv. Drug Delivery Rev.* **2016**, *100*, 116-125
48. Suresh, K.; Mannava, M. C.; Nangia, A., A novel curcumin–artemisinin coamorphous solid: physical properties and pharmacokinetic profile. *RSC Adv.* **2014**, *4* (102), 58357-58361
49. Heffernan, C.; Ukrainczyk, M.; Zeglinski, J.; Hodnett, B. K.; Rasmuson, A. C., The Influence of Structurally-Related Impurities on the Crystal Nucleation of Curcumin. *Cryst. Growth Des.* **2018**, *18* (8), 4715-4723.
50. Pons Siepermann, C. A.; Huang, S.; Myerson, A. S., Nucleation inhibition of benzoic acid through solution complexation. *Cryst. Growth Des.* **2017**, *17* (5), 2646-2653
51. Pons Siepermann, C. A.; Myerson, A. S., Inhibition of nucleation using a dilute, weakly hydrogen-bonding molecular additive. *Cryst. Growth Des.* **2018**, *18* (6), 3584-3595.
52. Johnston, A.; Florence, A. J.; Shankland, N.; Kennedy, A. R.; Shankland, K.; Price, S. L., Crystallization and crystal energy landscape of hydrochlorothiazide. *Cryst. Growth Des.* **2007**, *7* (4), 705-712.
53. Steiner, T., The hydrogen bond in the solid state. *Angew. Chem. Int. Ed.* **2002**, *41* (1), 48-76.
54. Ammar, H.; Ibrahim, S.; El-Faham, T., Interaction of chlorothiazide and hydrochlorothiazide with certain amides, imides and xanthenes. *Pharmazeutische Industrie* **1981**, *43*, 292-295.

Chapter 4. Effect of Polymer Hydrophobicity on the Stability of Amorphous Solid Dispersions and Supersaturated Solutions of a Hydrophobic Pharmaceutical[†]

4.1 Introduction

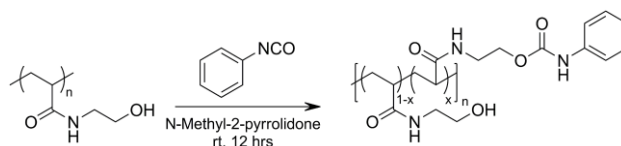
The dissolution rate of pharmaceuticals can be enhanced by delivery from an amorphous phase,¹ leading to increased apparent oral bioavailability for many hydrophobic drugs.² As a result, there is substantial interest in formulating poorly-soluble drugs in amorphous solid dispersions, a mixture of amorphous drug and stabilizing excipients.³ However, there are two mechanisms by which the theoretical solubility advantage can fail to be delivered experimentally: crystallization of pharmaceutical within an amorphous solid dispersion during storage and crystallization of pharmaceutical from the supersaturated solution generated upon dissolution of the amorphous phase.³⁻⁵ Polymers are particularly well-positioned for use as stabilizers of amorphous drug given their ability to inhibit crystallization when intimately mixed with pharmaceutical in amorphous solid dispersions⁶ and when dissolved in solution.⁷⁻⁸ However, the fundamental structure-function relationships that dictate the stability of amorphous solid dispersions and polymer-stabilized supersaturated solutions are often difficult to deconvolute from effects rising from changes in physical properties of polymers such as differing chain lengths/topology. In this work, a post-polymerization functionalization strategy is used to probe the effect of polymer hydrophobicity on stability without

[†] Adapted from Frank, D. S.; Matzger, A. J. *Mol. Pharmaceutics* **2019**, *16*(2), 682-688.

altering other physical parameters of the polymers. The influence of polymer hydrophobicity on precipitation inhibition in supersaturated solutions and crystallization inhibition in amorphous solid dispersions is determined using a set of functionalized polymers for the same model pharmaceutical. There are few studies that correlate the stability of amorphous solid dispersions and the supersaturated state for a given combination of pharmaceutical and polymeric excipient;⁹⁻¹² however, effective formulation additives in amorphous solid dispersions must inhibit crystallization in both of these contexts. By controlling for physical differences amongst polymer and the chemical identity of crystallizing drug, the relationship between polymer hydrophobicity and stability can be understood in order to optimize the properties of polymer for long-term stability of amorphous solid dispersions.

The influence of polymer hydrophobicity on the ability of a class of poly(N-hydroxyethyl acrylamide) (PHEAM) polymers to inhibit crystallization of ethenzamide was examined in both aqueous solution and in the amorphous phase. Ethenzamide is BCS Class II analgesic drug (solubility of 8.8 mM in deionized water¹³) commonly co-administered with NSAIDs such as acetaminophen or aspirin.¹⁴⁻¹⁵ Delivery of ethenzamide in its amorphous phase will increase solubility; however, polymer stabilizers are necessary to prevent precipitation in aqueous media at elevated supersaturation.⁷ It has been observed in other systems that polymers of moderate hydrophobicity are more potent inhibitors of crystallization from aqueous solution than hydrophobic or hydrophilic polymers.^{8, 16-20} Completely hydrophilic polymers more favorably interact with solvent over solute, yet fully hydrophobic polymers form insoluble globules in aqueous solution.⁸ Partially hydrophobic polymers maintain water solubility while driving strong interactions with dissolved pharmaceutical and tend to be the most effective inhibitors of crystallization from supersaturated solutions.²⁰⁻²¹ To rigorously investigate the effect of increasing

hydrophobicity of a water-soluble polymer on the inhibition of precipitation, PHEAM polymers were treated with phenyl isocyanate to transform hydrophilic hydroxy groups on the polymer to hydrophobic phenyl carbamate moieties (see Scheme 1). A single batch of PHEAM was functionalized to ensure that only changes in side-chain functionality, rather than polymer chain length, were probed across crystallization experiments. The induction time to crystallization of supersaturated ethenzamide was measured with equivalent weight loading of this polymer series to determine the effect of hydrophobicity on supersaturation maintenance for a hydrophobic drug.



Scheme 4.1 Functionalization of poly(N-hydroxyethyl acrylamide) to tether hydrophobic phenyl groups to side chains on the polymer.

The effect of functionalization and increasing hydrophobicity of polymer on the ability of PHEAM to stabilize amorphous solid dispersions of ethenzamide was also investigated. Ethenzamide is particularly apt for this study given its lack of degradation upon melting and its strong crystallization propensity during quench cooling (see Supporting Information). To inhibit recrystallization of its amorphous phase, it is necessary to add stabilizing additives.²²⁻²⁷ However, there is less consensus on the factors which dictate stability in amorphous solid dispersions, and a diverse set of polymer parameters have been shown to influence stability in amorphous solid dispersions of drugs, such as weight percent loading of polymeric stabilizer,²⁸ molecular weight of polymer,²⁹⁻³⁰ hydrogen bonding between polymer and dispersed pharmaceutical,³¹ and the solubility of polymer in amorphous pharmaceutical.³²⁻³³ Empirical screening for stable amorphous solid dispersions has a long history,⁵ yet design strategies for polymers to ensure long-term stability are still emerging in the field.³⁴⁻³⁵ By partially functionalizing hydroxy groups in PHEAM

polymers, the effect of hydrophobic residues on amorphous stability was probed and compared to the effect on inhibition in aqueous precipitation to address the overall impact of polymer hydrophobicity to stabilize against solution and amorphous phase crystallization.

4.2 Experimental

Poly(hydroxyethyl acrylamide) (PHEAM) was synthesized by free-radical polymerization in dimethylformamide to give a polymer with a number-average molecular weight of 38 kDa ($\bar{M}_n=1.5$, molecular weights calculated relative to polystyrene standards). Functionalization was achieved using phenyl isocyanate to form polymers where a portion of backbone chain hydroxy groups are capped with phenyl groups via carbamate linkages (3% and 10% by NMR spectroscopy, here after referred to as PHEAM-3% and PHEAM-10% respectively) following literature procedures.³⁶ PHEAM with 20% side-chain functionalization was not soluble in water and thus not used in this study.

Precipitation kinetics were measured in the Technobis CrystalBreeder. Ethenzamide (0.28 mL, 18 mM) dissolved in an aqueous solution containing 300 $\mu\text{g/mL}$ polymer additive (10% the weight of ethenzamide) was pipetted into 0.3 mL vials containing a 5 \times 2 mm Teflon stir bar. While stirred at 1200 rpm, vials were heated to 65 $^\circ\text{C}$ to allow for complete dissolution of drug, then cooled (5 $^\circ\text{C}/\text{min}$) to 30 $^\circ\text{C}$, where the induction time to crystallization was monitored by changes in solution turbidity. Experiments were repeated five times for 24 vials to give a total of 120 induction times to crystallization.

Amorphous solid dispersions of ethenzamide with PHEAM polymers were prepared by quench cooling. Ethenzamide (10 wt%) and polymer (90 wt%) were dissolved (5 mg overall per mL, ratio of \sim 13 repeat units of polymer per molecule of ethenzamide) in methylene chloride/methanol (1:1

by volume) and 0.3 mL of solution was distributed onto six regions on a glass slide. The material was heated to 140 °C for one minute then quench cooled to room temperature to form amorphous dispersions, resulting in a monophasic material with a single glass transition temperature (see Supporting Information for additional details). Dispersions were stored at ambient humidity and temperature and were analyzed by powder X-ray diffraction daily to determine the crystallization propensity of each dispersion over time.

4.3 Results/Discussion

Inhibition of Crystallization from Supersaturated Solution

Functionalizing hydroxy side chains with hydrophobic phenyl groups improves the ability of PHEAM polymers to inhibit crystallization from aqueous solution. As shown in Figure 4.1, the number of side-chain phenyl groups on a polymer additive correlates with the induction time to precipitation of ethenzamide. For 18 mM ethenzamide at 30 °C without polymer additives, the average induction time to precipitation is 3.1 ± 0.8 minutes. Adding 300 $\mu\text{g/mL}$ unfunctionalized PHEAM (10% the weight of dissolved ethenzamide) only weakly inhibits crystallization, extending the induction time to 4.7 ± 0.7 minutes. However, PHEAM variants functionalized with phenyl isocyanate perform better with increasing degrees of functionalization, with PHEAM-3% lengthening the average induction time to 8.9 ± 1.5 minutes and PHEAM-10% inhibiting crystallization to 16.1 ± 1.8 minutes (see Supporting Information for details on statistical significance). This relationship between hydrophobic content on polymers and stability against precipitation is in line with previous work using linear polymers of varying backbone chain chemistry and for polymeric micelles.^{8, 17, 21} Furthermore, by using a set of otherwise equivalent polymers, this result can be said to be robust in relating the hydrophobicity of dissolved polymers and

their ability to inhibit aqueous ethenzamide crystallization without the influence of other possibly confounding parameters of polymer additives.

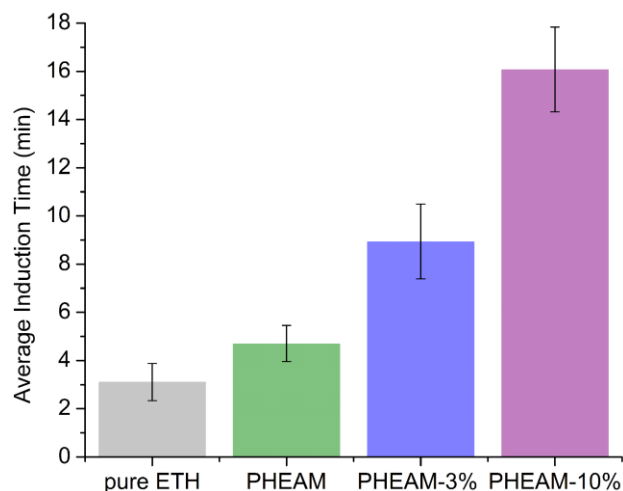


Figure 4.1 Average induction time of aqueous ethenzamide (3 mg/mL, 18 mM) crystallization at 30 °C (shown with standard error) with 300 µg/mL poly(hydroxyethyl acrylamide) polymers as crystallization additives.

Inhibition of Crystallization from Amorphous Solid Dispersions

The stability of amorphous solid dispersions of ethenzamide in PHEAM polymers (90 wt% polymer, 10 wt% drug) at ambient temperature and humidity was also quantified. It was found that dispersions containing PHEAM-10% stabilized the amorphous phase far more effectively than either PHEAM-3% or unfunctionalized PHEAM. Changes in the crystalline content of amorphous solid dispersions over time are shown in Figure 4.2. Similar to trends seen in solution, the addition of phenyl moieties on PHEAM increases stability against crystallization. Dispersions containing unfunctionalized PHEAM undergo devitrification within 2 ± 0.5 days (see Supporting Information for full set of crystallization experiments). Partially functionalizing PHEAM to PHEAM-3% does not result in longer stability for amorphous dispersions. However, at 10% functionalization,

PHEAM-10% strongly inhibits ethenzamide crystallization in amorphous dispersions. Throughout all trials, ethenzamide dispersed in PHEAM-10% did not undergo crystallization within a week of preparation, and even up to four weeks after preparation, dispersions still lacked any crystalline peaks by PXRD. In some regards, this stability ranking of these dispersions is contrary to an expected result—masking hydroxy functionalities on PHEAM might remove hydrogen bonding sites between polymer and amorphous drug. However, there is reason to expect that replacing hydroxy groups on the dispersed polymer with carbamate functionalities would increase the interaction strength between polymer and ethenzamide. A survey of structures in the Cambridge Structural Database (CSD) containing amide functionalities (the hydrogen bond donor in ethenzamide) interacting with oxygen atoms shows that the average intermolecular bond distance between amide groups and carbamate functionalities ($N_{\text{amide}}-O_{\text{carbamate}}$) is shorter than that between amide groups and hydroxy oxygens ($N_{\text{amide}}-O_{\text{alcohol}}$, see Supporting Information for additional details). This shorter average intermolecular bond distance would imply a greater interaction strength between ethenzamide and carbamate moieties as compared to ethenzamide and free hydroxy groups, which might account for the improved stability of PHEAM-10% dispersions.

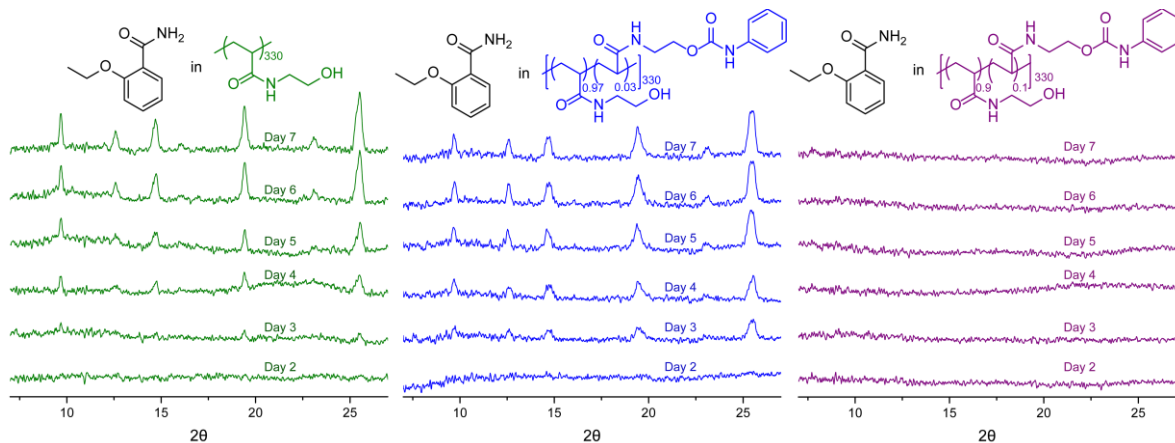


Figure 4.2 Powder X-ray diffraction data of amorphous solid dispersions over time. Crystalline content of a dispersion containing 10 wt% ethenzamide in PHEAM over one week is shown on the left (in green), as

compared to ethenzamide in PHEAM-3% (blue) and ethenzamide in PHEAM-10% (in purple). Diffraction patterns have been background subtracted and baseline corrected to remove signal from amorphous polymer and glass substrate.

In addition to intermolecular interaction strength, hygroscopicity of amorphous solid dispersions plays a central role in dictating their stability against crystallization. Water absorbed by amorphous materials acts as a plasticizer to increase molecular mobility and crystallization rates, as well as can lead to phase separation in otherwise miscible dispersions.³⁷⁻⁴³ In fact, this effect of humidity induced crystallization has been observed in the case of amorphous ethenzamide dispersed in microcrystalline cellulose.²⁵⁻²⁶ As a result, amorphous solid dispersions containing hygroscopic polymers tend to be less resistant to crystallization in the presence of moisture than those containing less hygroscopic polymers,⁴⁴ and the improved stability of dispersions containing PHEAM-10% over PHEAM-3% or PHEAM may result from the lower hygroscopicity of host polymer. For this series of PHEAM polymers, capping hydrophilic hydroxy groups with hydrophobic phenyl moieties leads to less ambient water absorbed by amorphous solid dispersions. As shown in Table 1, thermogravimetric analysis (TGA) of amorphous dispersions indicates that over four times the weight percent of water is absorbed at ambient humidity by unfunctionalized PHEAM as compared to PHEAM-10%. Such differences are reflected in the water vapor sorption isotherms at 25 °C of pure polymer (Figure 4.3), which show that at 60% RH, PHEAM-10% takes up significantly less water by weight percent (5.8%) as compared to PHEAM-3% (10.0%) or PHEAM (13.2%). Other physical properties of these polymers such as average chain length or glass transition temperatures (shown in Table 1) cannot explain the dramatic differences in their stabilizing ability. We propose that water absorbed in the amorphous dispersions containing hydrophilic polymer increases molecular mobility of drug which leads to crystallization. To test this hypothesis, amorphous solid dispersions containing unmodified PHEAM were prepared and stored both in ambient conditions and under dry conditions (in a desiccator). Ethenzamide

dispersed in PHEAM under ambient conditions is unstable and undergoes devitrification in ~2 days after preparation. However, dispersions stored under dry conditions show much longer physical stability and do not crystallize within a week of preparation (see Supporting Information). In the absence of atmospheric water, amorphous solid dispersions of ethenzamide in PHEAM are dramatically stabilized, and as a result, the improved stability of PHEAM-10% dispersions can be attributed to their low hygroscopicity. Imparting hydrophobicity through post-polymerization modification restricts PHEAM-10% from absorbing water from the atmosphere and thus dispersions with this polymer are less prone to water-induced plasticization and devitrification during storage.

Table 4.1 Glass transition temperatures of pure PHEAM polymers and amorphous solid dispersions of polymer and ethenzamide (10 wt% drug) as measured by inflection points by modulated DSC (see Supporting Information for additional details, each value the average of two measured transition temperatures). Water content was measured as total weight loss by TGA below 125 °C for amorphous dispersions stored at ambient temperature and humidity for 24 hours. Dispersions were verified to be amorphous prior to TGA by polarized light microscopy.

	PHEAM	PHEAM-3%	PHEAM-10%
T _g of pure polymer (°C)	121.5 ± 0.8	123.7 ± 1.3	120.0 ± 0.7
T _g of amorphous dispersion (°C)	98.5 ± 0.8	96.5 ± 0.2	90.9 ± 2.5
Water content by TGA (%)	5.6 ± 0.1	3.9 ± 1.2	1.2 ± 0.2

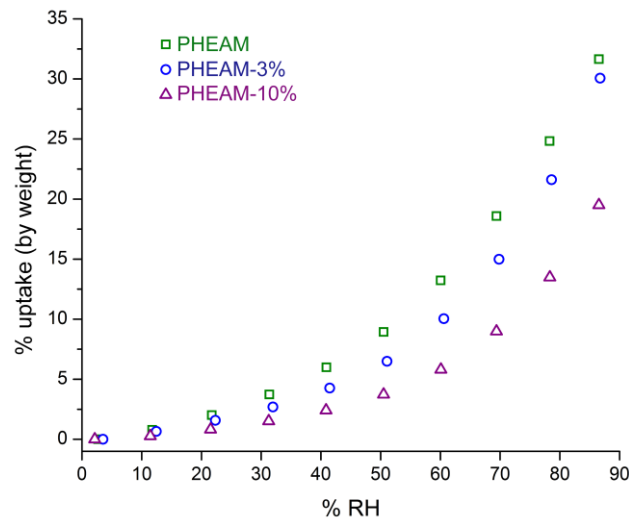


Figure 4.3 Percent uptake of water vapor by pure polymeric materials. PHEAM is shown with green squares, PHEAM-3% is shown with blue circles, and PHEAM-10% is shown with purple triangles.

Another possible effect of post-polymerization modification, independent of the amount of water absorbed by these polymers, is that the interactions between ethenzamide and carbamate functionalities on PHEAM-10% are more stable to disruption by water than ethenzamide interactions with hydroxy groups on PHEAM. This secondary effect is likely the origin of the superior ability of PHEAM-10% to inhibit aqueous precipitation of ethenzamide over unfunctionalized PHEAM (Figure 4.1); however, it may also play a role to dictate the stability ranking of amorphous solid dispersions. To examine this hypothesis, the relative strength of interactions between polymer and either pharmaceutical or water were approximated by the average intermolecular bond distance between relevant functionalities from a survey of structures in the CSD. The average intermolecular bond distance between primary amide functionalities (representing ethenzamide) or water and primary alcohol or carbamate groups (representing unfunctionalized and functionalized polymer, respectively) are shown in Figure 4.4 (see Supporting Information for additional details). The average intermolecular bond distance between

water and carbamate functionalities ($O_{\text{water}}\text{---}O_{\text{carbonyl}}$, $2.91 \pm 0.01 \text{ \AA}$) is slightly less than that from amide to carbamate groups ($N_{\text{amide}}\text{---}O_{\text{carbonyl}}$, $2.99 \pm 0.02 \text{ \AA}$), or roughly equal when accounting for differences in the van der Waals radii of oxygen (1.58 \AA) and nitrogen (1.64 \AA).⁴⁵ However, the average intermolecular distance between water and alcohol groups ($O_{\text{water}}\text{---}O_{\text{alcohol}}$, $2.85 \pm 0.004 \text{ \AA}$) is far shorter than that from amide to hydroxy functionalities ($N_{\text{amide}}\text{---}O_{\text{alcohol}}$, $3.04 \pm 0.02 \text{ \AA}$). If one uses these average intermolecular bond distances as a proxy for interaction strength, it follows that water has the potential to easily outcompete ethenzamide to interact with pendant hydroxy functionalities on PHEAM, leading to dispersions and solution complexes with labile interactions with drug and limited stability against crystallization. However, water forms only slightly shorter bonds than primary amides to carbamate groups, which might indicate that the amide-carbamate interaction between ethenzamide and PHEAM-10% is less likely to be disrupted by absorbed water in the amorphous solid dispersion or free water in a solution complex as compared to hydrogen bonding interactions between ethenzamide and the free hydroxy groups in PHEAM. Furthermore, such an effect of protecting polymer-pharmaceutical interactions from ambient water is likely promoted by hydrophobic phenyl groups attached to carbamate functionalities on PHEAM-10%. This general principle of water outcompeting pharmaceutical to bind with polymer functionalities has been observed in the relative kinetics of solution crystallization using polymer additives;^{8, 46-47} however, such an effect is rarely evoked to explain the relative kinetics of devitrification for amorphous solid dispersions. In the case of amorphous solid dispersions of ethenzamide and functionalized PHEAM polymers, the superior stability of PHEAM-10% over PHEAM-3% may stem from improved resilience to molecular interaction by water. Although pure PHEAM-3% absorbs less water than unfunctionalized PHEAM, dispersions containing PHEAM-3% do not display improved stability relative to amorphous solid dispersions

in PHEAM. This instability may be because drug-polymer interactions in amorphous solid dispersions containing PHEAM-3% can be easily interrupted by atmospheric water, and despite a decrease in polymer hygroscopicity, such dispersions do not show an improvement in physical stability against crystallization. PHEAM-10% not only is a less hygroscopic polymer than PHEAM-3%, but its intermolecular interactions with ethenzamide are relatively more stable to disruption from atmospheric water (Figure 4.4). The same chemical factors that dictate the stability of polymer-pharmaceutical solution aggregates (in the case of precipitation inhibition) might also dictate stability of amorphous solid dispersions given that in both situations, intermolecular interaction between water (either as a solvent or from the atmosphere) and polymer has the effect of displacing pharmaceutical which leads to crystallization. As a result, the complex polymeric materials which have been developed to maintain supersaturation of hydrophobic drugs may also serve well to stabilize amorphous solid dispersions in the case of crystallizations accelerated by water absorption in hygroscopic dispersions. However, it should be noted that increasing the hydrophobicity of amorphous solid dispersions may also impact their kinetics of dissolution and drug release, which in turn could influence the degree to which polymers can stabilize supersaturated solutions.⁴⁸⁻⁴⁹ Further studies will be necessary to test the validity of the above crystallization assays in predicting the *in vivo* stability of these amorphous solid dispersions during administration.

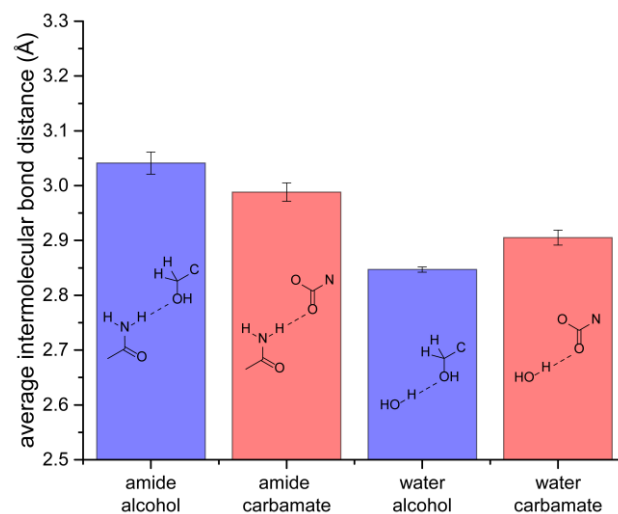


Figure 4.4 Average intermolecular bond distance between amide or water groups and carbamate and primary alcohol groups as determined by an arithmetic average of bond distances from crystal structures from the CSD, shown with standard error. Interaction distances with alcohol functionalities are shown in blue and interaction distances with carbamate functionalities are shown in red.

4.4 Conclusion

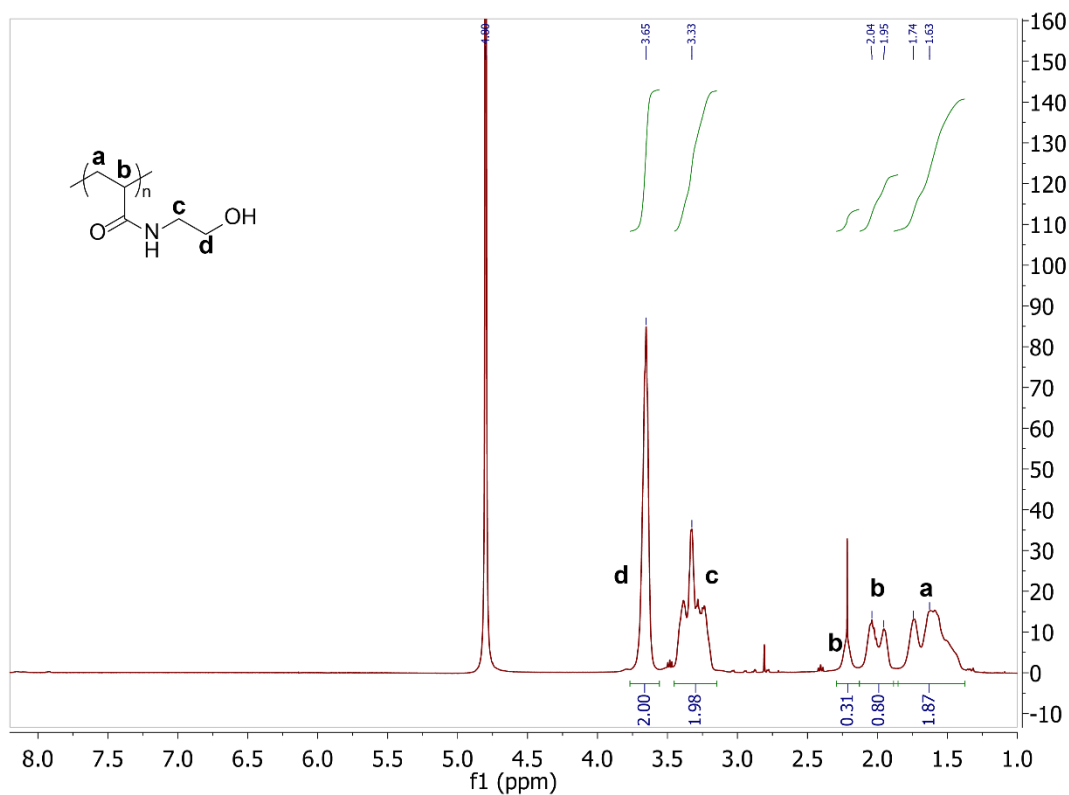
In this study, we provide evidence that introducing hydrophobic functionalities on water-soluble polymers via post-polymerization modification improves the stability of amorphous solid dispersions and supersaturated solutions of pharmaceutical. Optimizing polymer design for amorphous solid dispersions is essential to prevent recrystallization from the amorphous phase and from solution.⁵⁰⁻⁵¹ Imparting hydrophobicity to water-soluble polymers has a dual effect of optimizing the performance of amorphous solid dispersions. In the amorphous phase, hydrophobic residues decrease hygroscopicity and protect interactions between polymer and pharmaceutical from interruption by atmospheric water. In aqueous solution, hydrogen bonding between polymer and bulk water competes with bonding between drug and polymer, and tethering hydrophobic functionalities on a water-soluble polymer can preferentially interact to stabilize supersaturated drug from precipitation.²¹ A central finding to this study is that many of the same interactions govern stability of solution polymer-pharmaceutical complexes and amorphous solid dispersions

in the presence of humidity. This generalization allows for the application of polymers optimized to maintain aqueous supersaturation in amorphous solid dispersions, where strong polymer-drug interactions serve to protect dispersions from atmospheric humidity. Future work will investigate functionalization methodologies to impart hydrophobicity to a broad range of water-soluble polymers and improve their ability to stabilize amorphous and supersaturated phases for efficacious oral delivery.

4.5 Supporting Information

4.5.1 Synthesis and characterization of poly(N-hydroxyethyl acrylamide)

N-hydroxyethyl acrylamide monomer (Aldrich, 97%) was purified through an MEHQ removal column. N-hydroxyethyl acrylamide (11.9 mmol) was dissolved in dimethylformamide (5 mL) containing 2,2'-Azobis(2-methylpropionitrile) (0.07 mmol, Aldrich, 98%) and heated at 65 °C under a nitrogen atmosphere for 12 hours to allow for polymerization. The resulting poly(N-hydroxyethyl acrylamide) was precipitated in acetone and heated in vacuo to remove excess solvent, then dissolved in ethanol and precipitated in hexanes, washed with acetone, and dried in vacuo at 85 °C. Yield: 1.225 g. T_g : 125.7 ± 0.3 °C. $^1\text{H-NMR}$ data were collected in D_2O at 400 MHz.



Molecular weights were determined by gel permeation chromatography in tetrahydrofuran. Due to insolubility of PHEAM in tetrahydrofuran, PHEAM was reacted with excess trifluoroacetic anhydride in CH_2Cl_2 to form a soluble variant.⁵² This soluble variant was dissolved in tetrahydrofuran (1 mg/mL) and a 50 μL injection volume was passed through a Shimadzu GPC with UV-vis and RI detection with 3 columns connected in series: a Waters Styragel HT-4 (7.8 x 300 mm, 10 μm particles), a Waters Styragel HT-3 (7.8 x 300 mm, 10 μm particles), and a 100 Å PSS GRAM (8 x 300 mm, 10 μm particles). Molecular weights were calculated relative to polystyrene standards using UV-vis detection at 264 nm with a flow rate of 1 mL/min.

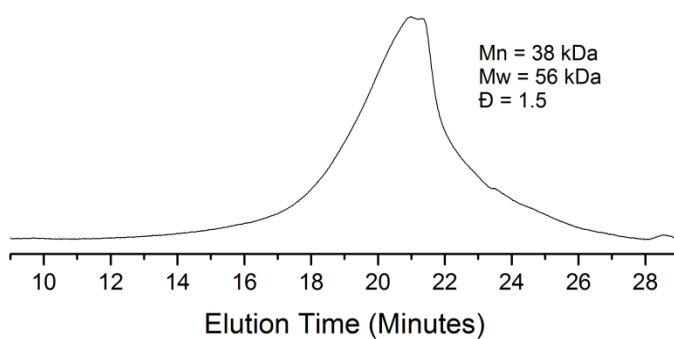


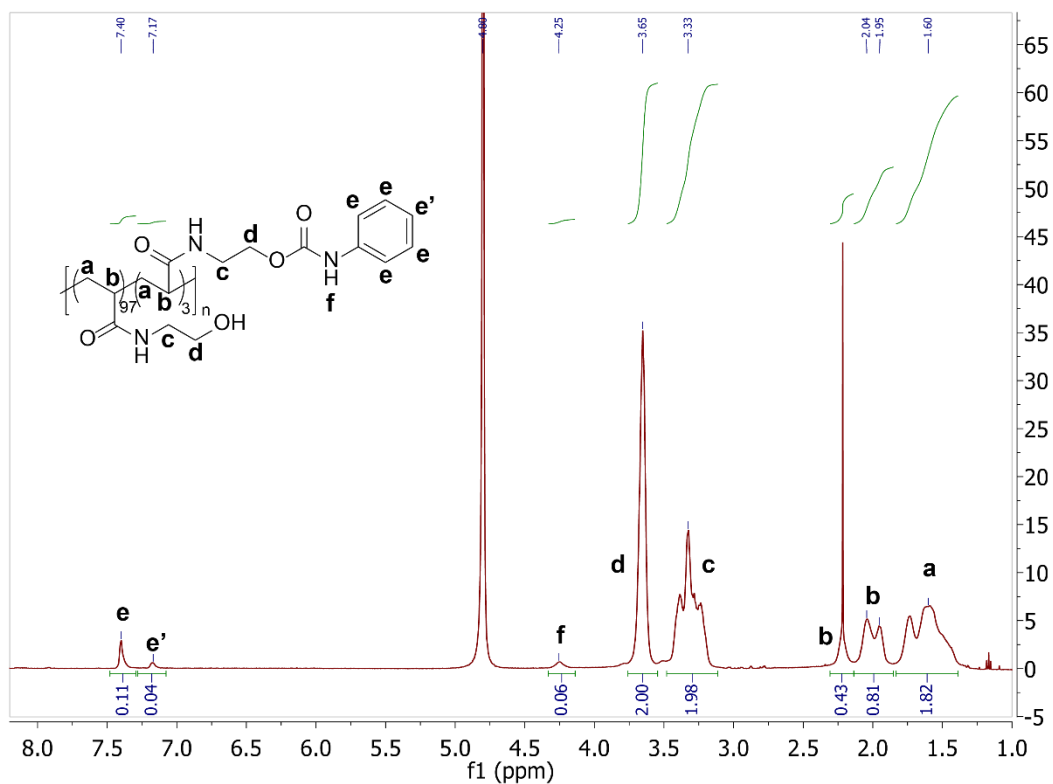
Figure 4.5. Elution time of PHEAM in tetrahydrofuran through GPC column with a flow rate of 1 mL/min. Molecular weights were calculated relative to polystyrene standards in tetrahydrofuran using UV-vis detection at 264 nm.

4.5.2 Functionalization of PHEAM polymers

Following procedures in Biedermann, et al, pendant hydroxy functionalities on PHEAM were functionalized using phenyl isocyanate.³⁶

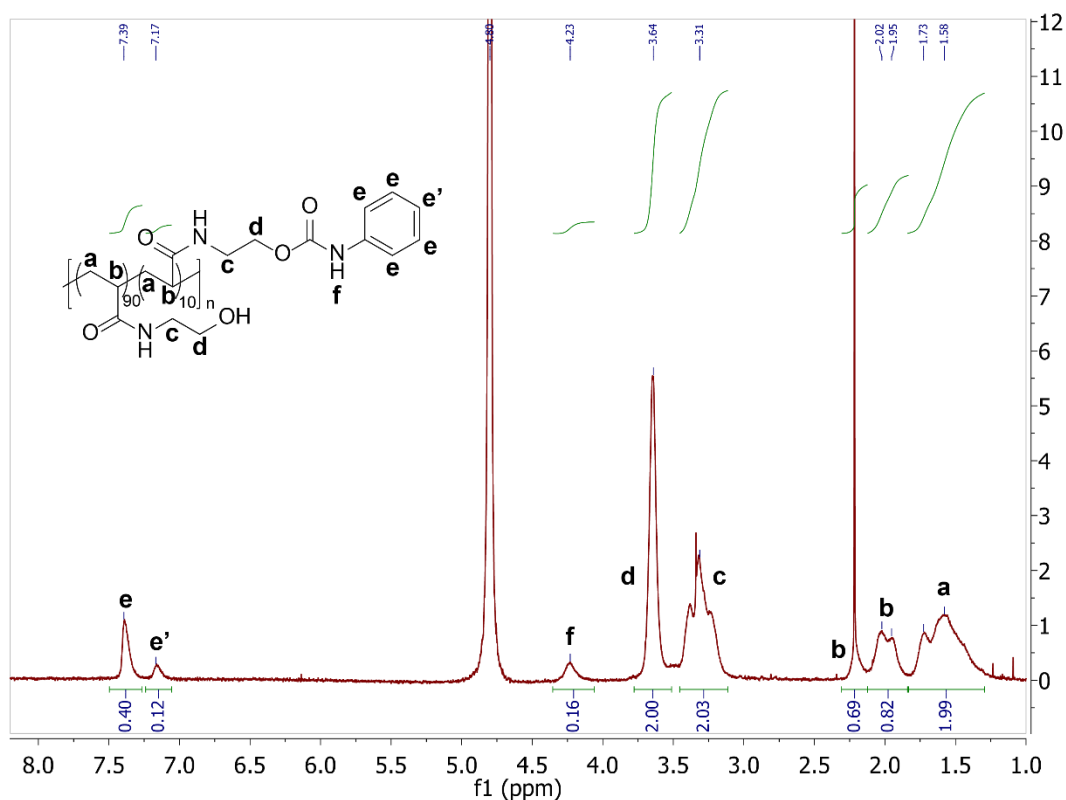
PHEAM-3%

Poly(N-hydroxyethyl acrylamide) (181.4 mg, 1.57 mmol -OH groups) was dissolved in NMP (6 mL). Under a nitrogen atmosphere, phenyl isocyanate (10 μ L, 0.092 mmol, Aldrich, \geq 98%) was added and the reaction mixture was stirred at room temperature for 12 hours. The resulting polymer was precipitated in hexanes, dissolved in ethanol, re-precipitated in hexanes, and dried in vacuo at 85 $^{\circ}$ C. Yield: 148.8 mg. 3% functionalization by 1 H-NMR. T_g : 128.0 ± 0.1 $^{\circ}$ C. 1 H-NMR data were collected in D_2O at 400 MHz.



PHEAM-10%

Poly(N-hydroxyethyl acrylamide) (184.0 mg, 1.6 mmol -OH groups) was dissolved in NMP (6 mL). Under a nitrogen atmosphere, phenyl isocyanate (20 μ L, 0.184 mmol, Aldrich, \geq 98%) was added and the reaction mixture was stirred at room temperature for 12 hours. The resulting polymer was precipitated in hexanes, dissolved in ethanol, re-precipitated in hexanes, and dried in vacuo at 85 $^{\circ}$ C. Yield: 142 mg. 10% functionalization by 1 H-NMR. T_g : 127.4 ± 0.2 $^{\circ}$ C. 1 H-NMR data were collected in D_2O at 400 MHz.



4.5.3 Thermal analysis of ethenzamide, pure polymers, and amorphous solid dispersions

Recrystallization of pure ethenzamide from the amorphous phase does not show characteristic melting point depression associated with degradation upon three heat/melt cycles (see Figure 4.6) and recrystallizes during cooling, whereas amorphous solid dispersions containing PHEAM polymers are stable at ambient temperature (<25 °C). These criteria make ethenzamide an ideal model compound to formulate in an amorphous solid dispersion by melt-quenching and study its devitrification rates.

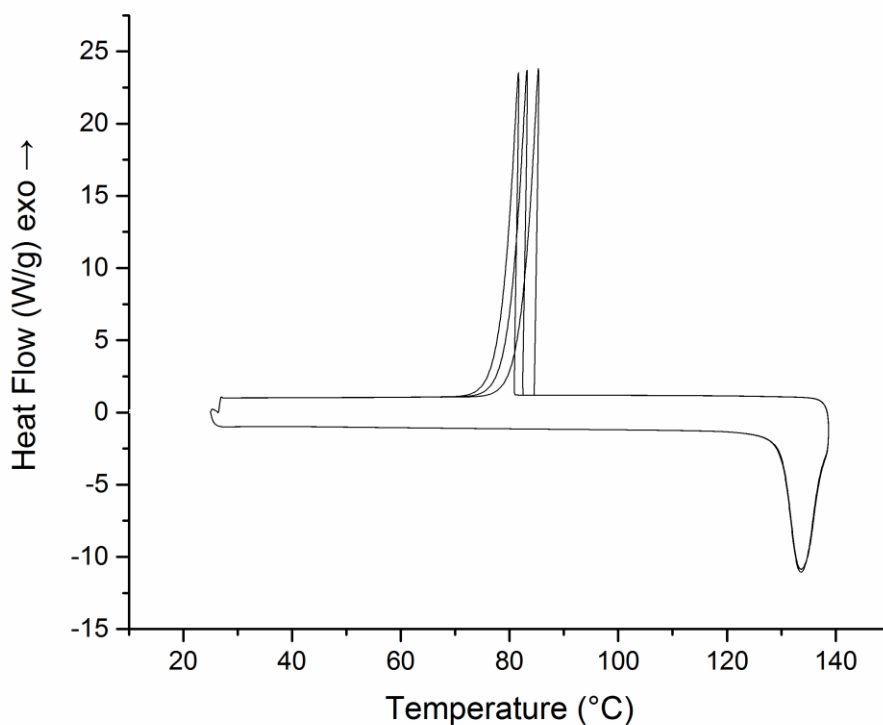


Figure 4.6. DSC thermogram of 0.9 mg pure ethenzamide melting and recrystallization at a 20 °C/minute scanning rate.

Glass transition temperatures for pure polymers were measured by MDSC in a Q20 DSC by heating at 3 °C/minute in aluminum pans containing pinholes with ± 1.25 °C modulation every 40 seconds. T_g were taken as the inflection point along the glass transition as determined by TA

Universal Analysis software; glass transition temperatures shown in the manuscript text are the average of two heatings. Figures 4.7 and 4.8 show examples of thermal traces for the measured glass transition temperatures for pure polymer (Figure 4.7) and dispersions of polymer and ethenzamide (Figure 4.8) respectively. Amorphous solid dispersions of ethenzamide were vitrified at 140 °C directly prior to measurement and thus should not contain absorbed water. Furthermore, immediately after quench cooling, dispersions show only a single glass transition temperature, implying the existence of a single phase containing drug and polymer.

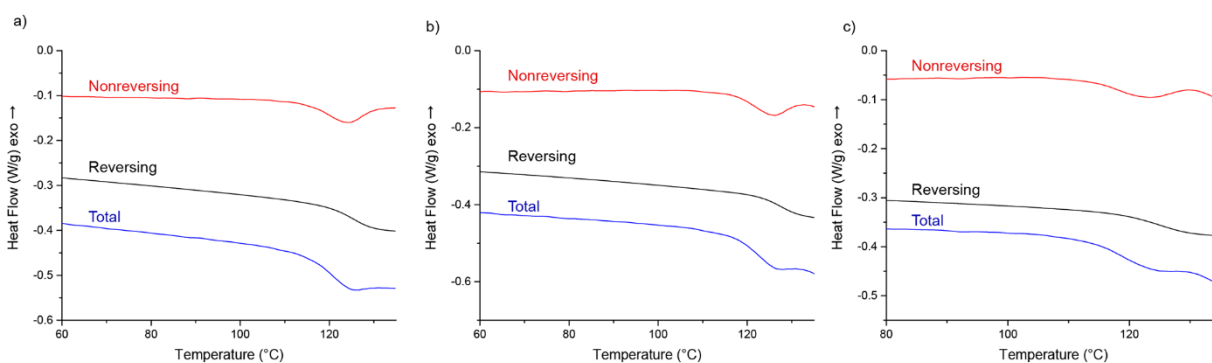


Figure 4.7. Glass transition temperatures of a) PHEAM, b) PHEAM-3%, and c) PHEAM-10% as measured by MDSC.

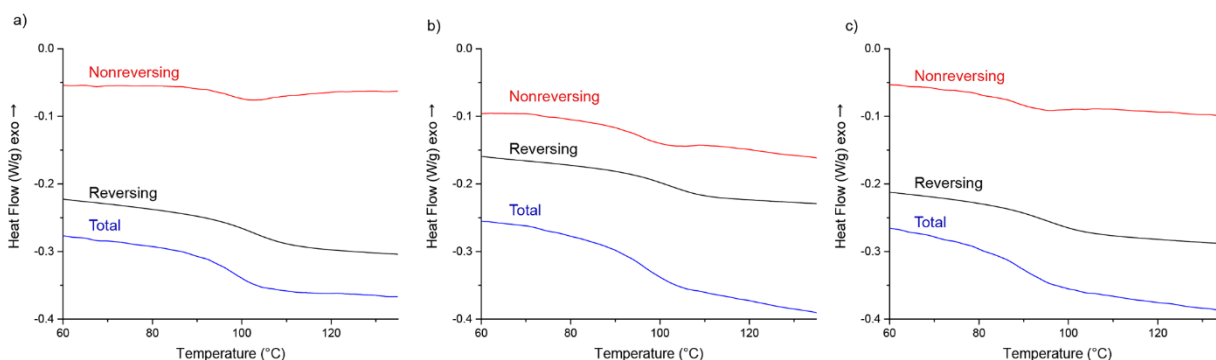


Figure 4.8. Glass transition temperatures of dispersions of ethenzamide with a) 90 wt% PHEAM, b) 90 wt% PHEAM-3%, and c) 90 wt% PHEAM-10% as measured by MDSC after vitrification at 140 °C.

Thermogravimetric analysis was performed on a Q50 TGA from TA instruments. Water content in ~1 mg amorphous solid dispersions was determined by measuring mass loss up to 125 °C after storage at ambient humidity for 24 hours using nitrogen as the inlet gas.

4.5.4 Theoretical solubility of amorphous ethenzamide

The theoretical solubility ratio of amorphous ethenzamide was determined by equating expressions for the difference in free energy between the amorphous and crystalline forms, $\Delta G_{a \rightarrow c}$,²⁻³ following the procedures described by Hillmyer and coworkers.¹⁸ Using a $\Delta H_{fus} = 28.9$ kJ/mol and $T_m = 133.6$ °C determined from melting thermogram in Figure 4.6, the solubility ratio $S_{amorphous}/S_{crystalline}$ was determined at a range of temperatures and is shown below in Figure 4.9. Supersaturation maintenance at 30 °C is clearly relevant to administration of amorphous ethenzamide, as the amorphous pharmaceutical is predicted to have a solubility over 8 times that of crystalline ethenzamide.

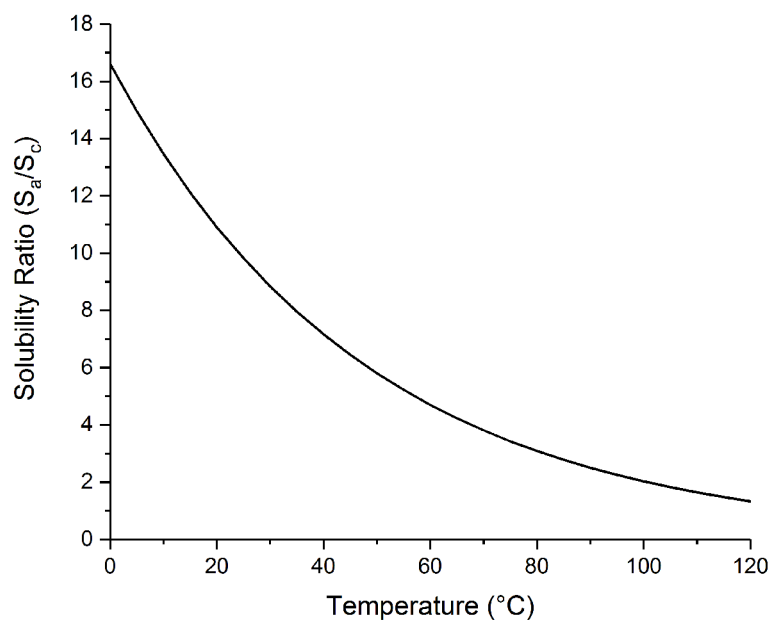


Figure 4.9. Theoretical amorphous solubility of ethenzamide determined by equating expressions for $\Delta G_{a \rightarrow c}$.

4.5.5 Statistical analysis of precipitation kinetics of ethenzamide

Induction times to precipitation of ethenzamide in water containing PHEAM polymer additives were compared for statistical significance using one-way ANOVA with Fisher LSD and Tukey HSD tests at the 0.05 level (Table 4.2). Nonsignificant difference was found between crystallizations of pure ethenzamide and those containing unfunctionalized PHEAM in both tests and between those containing PHEAM and PHEAM-3% using the Tukey test.

Table 4.2. ANOVA with Fisher LSD and Tukey HSD tests to determine statistical significance between mean induction times at the 0.05 level. Differences which were judged to be statistically significant (probability of null hypothesis > 0.05) are colored in green and differences which are not are shown in red.

	Mean Difference	Fisher LSD Probability of Null Hypothesis	Tukey HSD Probability of Null Hypothesis
PHEAM pure ETH	1.60267	0.37992	0.81584
PHEAM-3% pure ETH	5.83108	0.00148	0.00803
PHEAM-3% PHEAM	4.22842	0.02083	0.09521
PHEAM-10% pure ETH	12.97083	4.20E-12	0
PHEAM-10% PHEAM	11.36817	1.00E-09	0
PHEAM-10% PHEAM-3%	7.13975	1.04E-04	5.98E-04

Furthermore, there is a clear proportionality between percent functionalization of PHEAM polymers and the induction time to ethenzamide crystallization, as demonstrated by a box plot comparing median induction times (Figure 4.10).

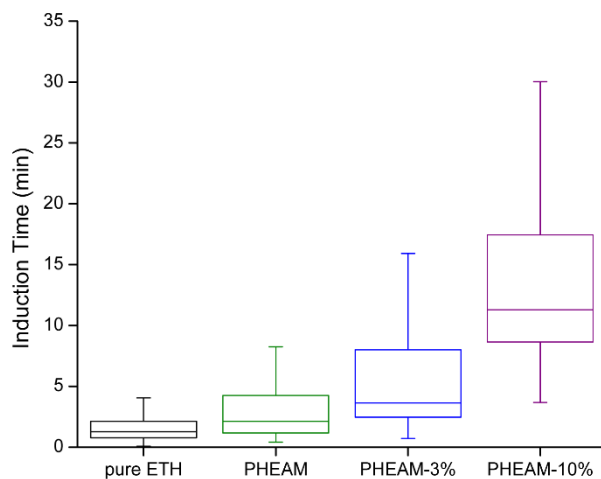
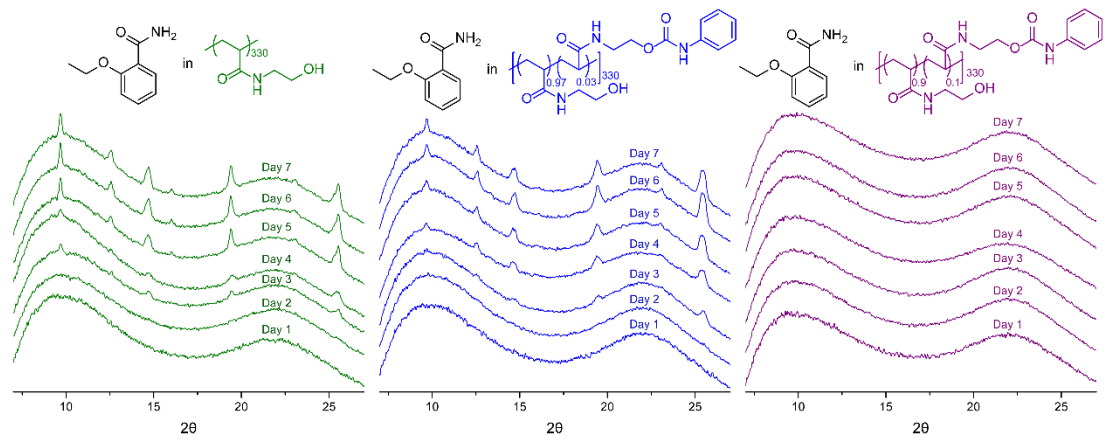
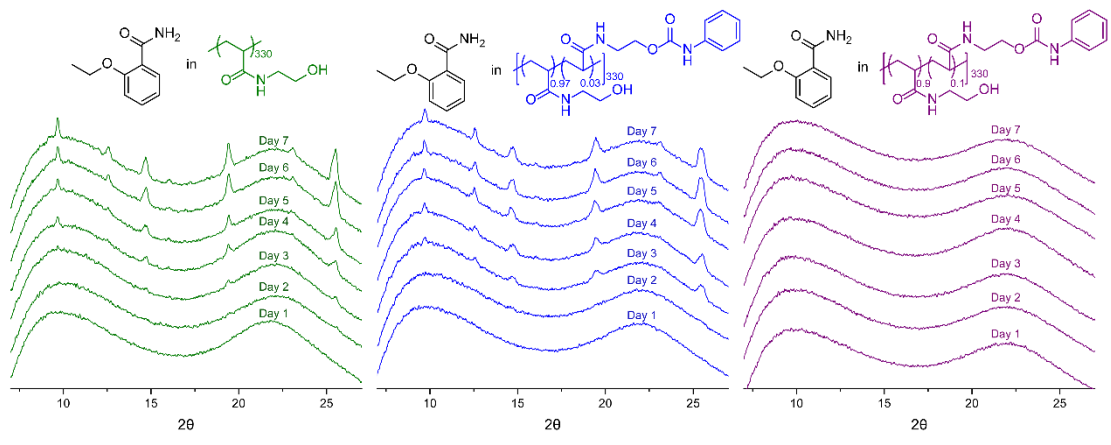


Figure 4.10. Box plot showing median, 25-75th percentile range (limits to the box), and 5-95th percentile ranges (denoted by error bars) of the induction time to crystallization of aqueous ethenzamide in the presence of polymer additives.

4.5.6 Powder X-ray diffraction of ethenzamide amorphous solid dispersions

Amorphous solid dispersions containing 90 wt% PHEAM, PHEAM-3%, and PHEAM-10% were stored at ambient temperature and humidity (~22 °C, ~50% RH) and monitored daily by PXRD for the appearance of crystalline peaks associated with ethenzamide. PXRD data were collected on a Rigaku SmartLab X-ray diffractometer at 40 kV, 44 mA using CuK α radiation ($\lambda = 1.54187 \text{ \AA}$) from 5° to 40° 2 θ with a scan speed of 0.4 s/step and a step size of 0.01°.

Patterns in the manuscript text are presented with background subtraction. For this process, the PXRD pattern collected on Day 1 (prior to crystallization) was subtracted from subsequent PXRD patterns and baseline corrected such that changes in crystallinity over time are isolated from amorphous background from dispersed polymer and the glass substrate. Raw PXRD patterns are presented here in the Supporting Information (Figure 4.11).



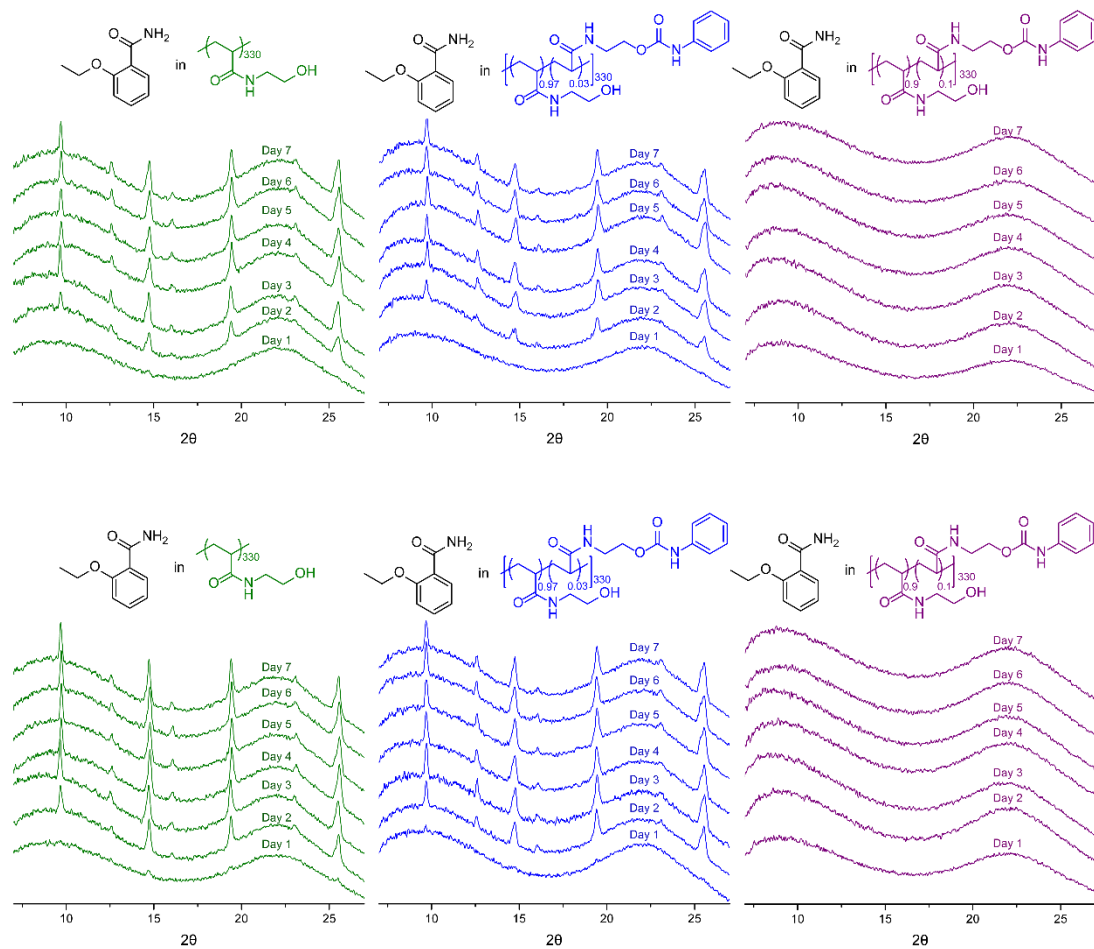


Figure 4.11. PXRD patterns of amorphous dispersions of ethenzamide and PHEAM polymers (90 wt%) over time. Each amorphous solid dispersion contains the polymer shown above each set of powder patterns. Samples stored during the same time period are compared across the x-axis.

Crystallization kinetics of amorphous solid dispersions of PHEAM and ethenzamide (90 wt% polymer) were also performed in parallel in a desiccator and under ambient conditions. Uncorrected PXRD patterns are shown in Figure 4.12; although ethenzamide dispersions in PHEAM (90 wt% polymer) undergo crystallization within a day of storage, under dry conditions, devitrification was not observed within a week of preparation.

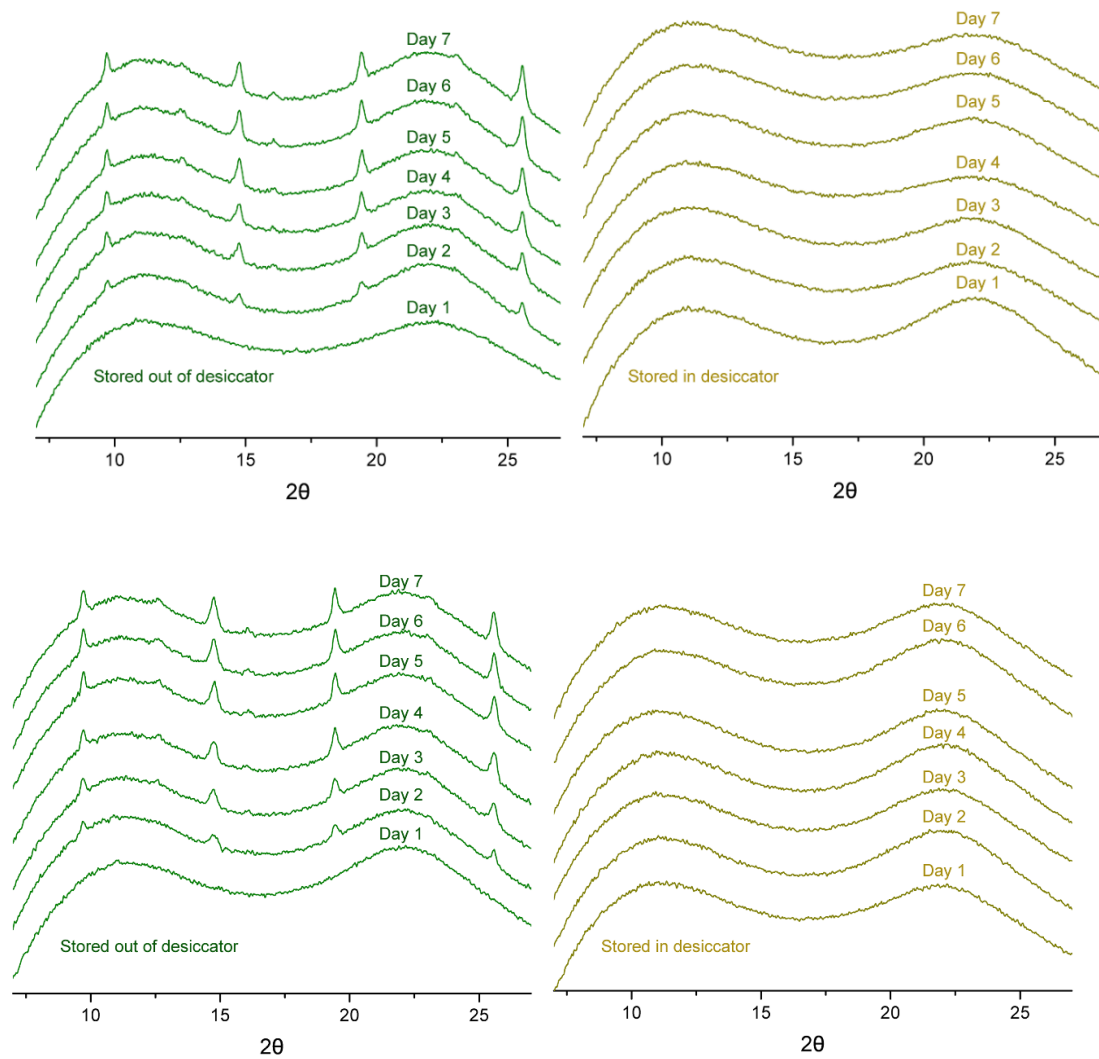


Figure 4.12. PXRD patterns of PHEAM ethenzamide dispersions (90 wt% polymer) stored under ambient conditions (green on the left) and stored in desiccator (shown in yellow on the right).

4.5.7 Dynamic vapor sorption of pure PHEAM polymers

Dynamic vapor sorption was performed using a Q5000 SA Dynamic Vapor Sorption Analyzer. Sample mass was determined from 0-90% RH at steps of 10% RH with 20 minutes allowed for equilibration starting from an initial mass of ~4 mg.

4.5.8 CSD Interaction Survey

Average intermolecular bond lengths were calculated from structures in the Cambridge Structural Database. Figure 4.13 shows a histogram of interaction distances between primary amide groups (representing ethenzamide) or water molecules and carbamate or alcohol functionalities. Structures were restricted to those with intermolecular contacts between 0 to 5 Å, 3D coordinates determined, no ions, and only organic structures using CSD version 5.38 (updated May 2016).

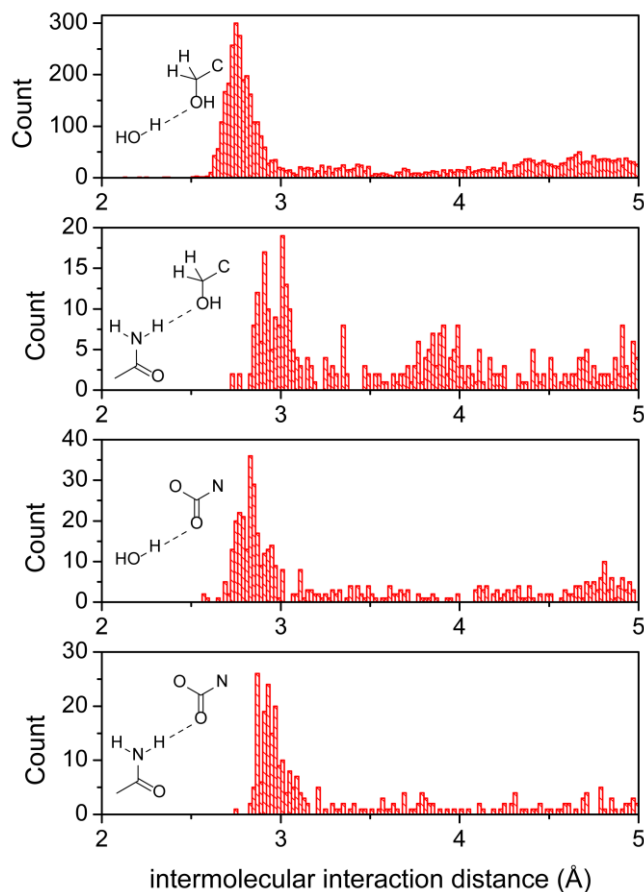


Figure 4.13. Histogram of interaction distances between functional groups as shown above. Hydrogen bonding in the crystal structures was found predominately in the regions between 2.5 and 3.5 Å.

Upon inspection of these selected crystal structures, it was found that hydrogen bonding interactions do not occur across all distance ranges between 0 and 5 Å, but instead are primarily confined around 3 Å. As a result, the computed average intermolecular bond distances in the manuscript text were calculated only using values between 2.5 and 3.5 Å to best represent the intermolecular interaction strength between functionalities in a hydrogen bond. Those average distances are shown below in Figure 4.14, uncorrected for differences in the van der Waals radii of oxygen (1.58 Å) and nitrogen (1.64 Å).⁵⁴ If one uses the median intermolecular interaction distance to represent interaction strength (rather than the mean), the same effects of functionalizing PHEAM are reflected by changes of interaction distance to ethenzamide and water (shorter median interaction distance between polymer and ethenzamide upon functionalization, longer median

interaction distance between polymer and water upon functionalization). Interactions where amide functionalities act as hydrogen bond acceptors are also shown in Figure 4.14 and very likely exist between ethenzamide and PHEAM; however, comparing the strengths of these interactions ($O_{\text{amide}}-O_{\text{hydroxy}}$ and $O_{\text{amide}}-N_{\text{carbamate}}$) is complicated by differences in van der Waals radii between oxygen and nitrogen.

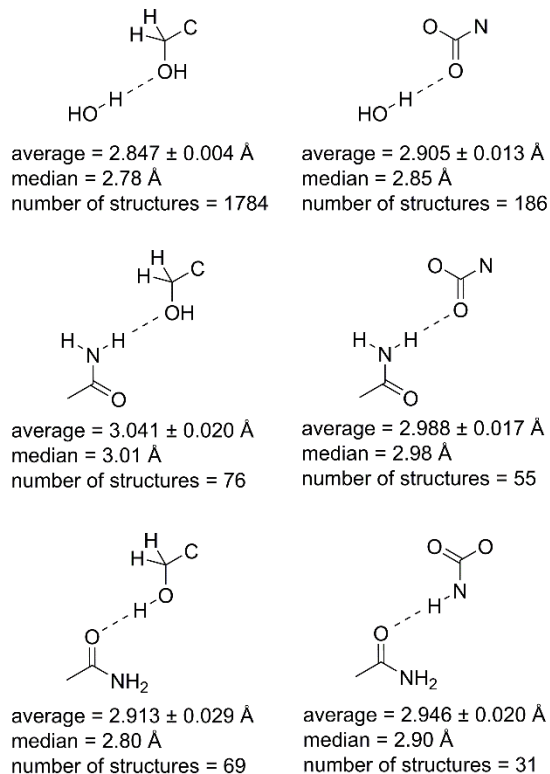


Figure 4.14. Average intermolecular bond distances between amide groups or water molecules and primary alcohol or carbamate groups as determined from averaging interaction distances from a survey of known crystal structures. Structures were restricted to those with intermolecular contacts between 2.5 to 3.5 Å, 3D coordinates determined, no ions, and only organic structures using CSD version 5.38 (updated May 2016).

4.6 References

- Hancock, B. C.; Parks, M., What is the true solubility advantage for amorphous pharmaceuticals? *Pharm. Res.* **2000**, *17* (4), 397-404.
- Amidon, G. L.; Lennernäs, H.; Shah, V. P.; Crison, J. R., A theoretical basis for a biopharmaceutical drug classification: the correlation of in vitro drug product dissolution and in vivo bioavailability. *Pharm. Res.* **1995**, *12* (3), 413-420.
- Serajuddin, A., Solid dispersion of poorly water-soluble drugs: Early promises, subsequent problems, and recent breakthroughs. *J. Pharm. Sci.* **1999**, *88* (10), 1058-1066.
- Rodríguez-hornedo, N.; Murphy, D., Significance of controlling crystallization mechanisms and kinetics in pharmaceutical systems. *J. Pharm. Sci.* **1999**, *88* (7), 651-660.
- Chiou, W. L.; Riegelman, S., Pharmaceutical applications of solid dispersion systems. *J. Pharm. Sci.* **1971**, *60* (9), 1281-1302.
- Yu, L., Amorphous pharmaceutical solids: preparation, characterization and stabilization. *Adv. Drug Delivery Rev.* **2001**, *48* (1), 27-42.
- Raghavan, S.; Trividic, A.; Davis, A.; Hadgraft, J., Crystallization of hydrocortisone acetate: influence of polymers. *Int. J. Pharm.* **2001**, *212* (2), 213-221.

8. Ilevbare, G. A.; Liu, H.; Edgar, K. J.; Taylor, L. S., Maintaining supersaturation in aqueous drug solutions: Impact of different polymers on induction times. *Cryst. Growth Des.* **2012**, *13* (2), 740-751.
9. Chauhan, H.; Kuldipkumar, A.; Barder, T.; Medek, A.; Gu, C.-H.; Atef, E., Correlation of inhibitory effects of polymers on indomethacin precipitation in solution and amorphous solid crystallization based on molecular interaction. *Pharm. Res.* **2014**, *31* (2), 500-515.
10. Chauhan, H.; Hui-Gu, C.; Atef, E., Correlating the behavior of polymers in solution as precipitation inhibitor to its amorphous stabilization ability in solid dispersions. *J. Pharm. Sci.* **2013**, *102* (6), 1924-1935.
11. Blaabjerg, L. I.; Lindenberg, E.; Löbmann, K.; Grohganz, H.; Rades, T., Is there a correlation between the glass forming ability of a drug and its supersaturation propensity? *Int. J. Pharm.* **2018**, *538* (1-2), 243-249
12. Van Eerdenbrugh, B.; Baird, J. A.; Taylor, L. S., Crystallization tendency of active pharmaceutical ingredients following rapid solvent evaporation—classification and comparison with crystallization tendency from undercooled melts. *J. Pharm. Sci.* **2010**, *99* (9), 3826-3838.
13. Sarmah, K. K.; Boro, K.; Arhangelskis, M.; Thakuria, R., Crystal structure landscape of ethenzamide: a physicochemical property study. *CrystEngComm* **2017**, *19* (5), 826-833.
14. Kawano, O.; Sawabe, T.; Misaki, N.; Fukawa, K., Studies on Combination Dosing (III) Aspirin And Ethenzamide. *Jpn. J. Pharmacol.* **1978**, *28* (6), 829-835.
15. Khatioda, R.; Saikia, B.; Das, P. J.; Sarma, B., Solubility and in vitro drug permeation behavior of ethenzamide cocrystals regulated in physiological pH environments. *CrystEngComm* **2017**, *19* (46), 6992-7000.
16. Ting, J. M.; Navale, T. S.; Bates, F. S.; Reineke, T. M., Design of tunable multicomponent polymers as modular vehicles to solubilize highly lipophilic drugs. *Macromolecules* **2014**, *47* (19), 6554-6565.
17. Johnson, L. M.; Li, Z.; LaBelle, A. J.; Bates, F. S.; Lodge, T. P.; Hillmyer, M. A., Impact of polymer excipient molar mass and end groups on hydrophobic drug solubility enhancement. *Macromolecules* **2017**, *50* (3), 1102-1112.
18. Yin, L.; Hillmyer, M. A., Preparation and performance of hydroxypropyl methylcellulose esters of substituted succinates for in vitro supersaturation of a crystalline hydrophobic drug. *Mol. Pharmaceutics* **2013**, *11* (1), 175-185.
19. Xu, S.; Dai, W.-G., Drug precipitation inhibitors in supersaturable formulations. *Int. J. Pharm.* **2013**, *453* (1), 36-43.
20. Tale, S.; Purchel, A. A.; Dalsin, M. C.; Reineke, T. M., Diblock Terpolymers Are Tunable and pH Responsive Vehicles To Increase Hydrophobic Drug Solubility for Oral Administration. *Mol. Pharmaceutics* **2017**, *14* (11), 4121-4127.
21. Mosquera-Giraldo, L. I.; Borca, C. H.; Meng, X.; Edgar, K. J.; Slipchenko, L. V.; Taylor, L. S., Mechanistic design of chemically diverse polymers with applications in oral drug delivery. *Biomacromolecules* **2016**, *17* (11), 3659-3671.
22. Danjo, K.; Nakata, T.; Otsuka, A., Preparation and dissolution behavior of ethenzamide solid dispersions using various sugars as dispersion carriers. *Chem. Pharm. Bull.* **1997**, *45* (11), 1840-1844.
23. Hanawa, T.; Ikoma, R.; Watanabe, A.; Hidaka, M.; Sugihara, M., Preparation and characterization of sealed heated mixture of ethenzamide and porous calcium silicate. *Chem. Pharm. Bull.* **1996**, *44* (7), 1367-1371.

24. Hirasawa, N.; Okamoto, H.; Danjo, K., Lactose as a low molecular weight carrier of solid dispersions for carbamazepine and ethenzamide. *Chem. Pharm. Bull.* **1999**, *47* (3), 417-420.
25. Matsumoto, K.; Nakai, Y.; Yonemochi, E.; Oguchi, T.; Yamamoto, K., Physicochemical characteristics of porous crystalline cellulose and formation of an amorphous state of ethenzamide by mixing. *Int. J. Pharm.* **1994**, *108* (3), 167-172.
26. Matsumoto, K.; Nakai, Y.; Yonemochi, E.; Oguchi, T.; Yamamoto, K., Effect of pore size on the gaseous adsorption of ethenzamide on porous crystalline cellulose and the physicochemical stability of ethenzamide after storage. *Chem. Pharm. Bull.* **1998**, *46* (2), 314-318.
27. Ozawa, M.; Hasegawa, K.; Yonezawa, Y.; Sunada, H., Preparation of solid dispersion for ethenzamide-carbopol and theophylline-carbopol systems using a twin screw extruder. *Chem. Pharm. Bull.* **2002**, *50* (6), 802-807.
28. Marsac, P. J.; Li, T.; Taylor, L. S., Estimation of drug-polymer miscibility and solubility in amorphous solid dispersions using experimentally determined interaction parameters. *Pharm. Res.* **2009**, *26* (1), 139.
29. Mohapatra, S.; Samanta, S.; Kothari, K.; Mistry, P.; Suryanarayanan, R., Effect of Polymer Molecular Weight on the Crystallization Behavior of Indomethacin Amorphous Solid Dispersions. *Cryst. Growth Des.* **2017**, *17* (6), 3142-3150.
30. Pacułt, J.; Rams-Baron, M.; Chrzyszcz, B.; Jachowicz, R.; Paluch, M., Effect of polymer chain length on the physical stability of amorphous drug-polymer blends at ambient pressure. *Mol. Pharmaceutics* **2018**, *15* (7), 2807-2815.
31. Kothari, K.; Ragoonanan, V.; Suryanarayanan, R., The role of drug-polymer hydrogen bonding interactions on the molecular mobility and physical stability of nifedipine solid dispersions. *Mol. Pharmaceutics* **2014** *12* (1), 162-170.
32. Duong, T. V.; Van Humbeeck, J.; Van den Mooter, G., Crystallization kinetics of indomethacin/polyethylene glycol dispersions containing high drug loadings. *Mol. Pharmaceutics* **2015**, *12* (7), 2493-2504.
33. Frank, D. S.; Matzger, A. J., Probing the Interplay between Amorphous Solid Dispersion Stability and Polymer Functionality. *Mol. Pharmaceutics* **2018**, *15* (7), 2714-2720.
34. Baghel, S.; Cathcart, H.; O'Reilly, N. J., Polymeric amorphous solid dispersions: a review of amorphization, crystallization, stabilization, solid-state characterization, and aqueous solubilization of biopharmaceutical classification system class II drugs. *J. Pharm. Sci.* **2016**, *105* (9), 2527-2544.
35. Van Duong, T.; Van den Mooter, G., The role of the carrier in the formulation of pharmaceutical solid dispersions. Part II: amorphous carriers. *Expert Opin. Drug Delivery* **2016**, *13* (12), 1681-1694.
36. Biedermann, F.; Appel, E. A.; Del Barrio, J.; Gruending, T.; Barner-Kowollik, C.; Scherman, O. A., Postpolymerization modification of hydroxyl-functionalized polymers with isocyanates. *Macromolecules* **2011**, *44* (12), 4828-4835.
37. Mistry, P.; Amponsah-Efah, K. K.; Suryanarayanan, R., Rapid assessment of the physical stability of amorphous solid dispersions. *Cryst. Growth Des.* **2017**, *17* (5), 2478-2485.
38. Hancock, B. C.; Zografi, G., The relationship between the glass transition temperature and the water content of amorphous pharmaceutical solids. *Pharm. Res.* **1994**, *11* (4), 471-477.
39. Makower, B.; Dye, W., Sugar crystallization, equilibrium moisture content and crystallization of amorphous sucrose and glucose. *J. Agric. Food Chem.* **1956**, *4* (1), 72-77.
40. Andronis, V.; Yoshioka, M.; Zografi, G., Effects of sorbed water on the crystallization of indomethacin from the amorphous state. *J. Pharm. Sci.* **1997**, *86* (3), 346-351.

41. Mehta, M.; Kothari, K.; Ragoonanan, V.; Suryanarayanan, R., Effect of water on molecular mobility and physical stability of amorphous pharmaceuticals. *Mol. Pharmaceutics* **2016**, *13* (4), 1339-1346.
42. Mehta, M.; Suryanarayanan, R., Accelerated Physical Stability Testing of Amorphous Dispersions. *Mol. Pharmaceutics* **2016**, *13* (8), 2661-2666
43. Marsac, P. J.; Konno, H.; Rumondor, A. C.; Taylor, L. S., Recrystallization of nifedipine and felodipine from amorphous molecular level solid dispersions containing poly (vinylpyrrolidone) and sorbed water. *Pharm. Res.* **2008**, *25* (3), 647-656.
44. Konno, H.; Taylor, L. S., Ability of different polymers to inhibit the crystallization of amorphous felodipine in the presence of moisture. *Pharm. Res.* **2008**, *25* (4), 969-978.
45. Rowland, R. S.; Taylor, R., Intermolecular nonbonded contact distances in organic crystal structures: Comparison with distances expected from van der Waals radii. *J. Phys. Chem.* **1996**, *100* (18), 7384-7391.
46. Frank, D. S.; Matzger, A. J., Influence of Chemical Functionality on the Rate of Polymer-Induced Heteronucleation. *Cryst. Growth Des.* **2017**, *17* (8), 4056-4059.
47. Chen, Y.; Liu, C.; Chen, Z.; Su, C.; Hageman, M.; Hussain, M.; Haskell, R.; Stefanski, K.; Qian, F., Drug-polymer-water interaction and its implication for the dissolution performance of amorphous solid dispersions. *Mol. Pharmaceutics* **2015**, *12* (2), 576-589.
48. Chen, Y.; Pui, Y.; Chen, H.; Wang, S.; Serno, P.; Tonnis, W.; Chen, L.; Qian, F., Polymer mediated drug supersaturation controlled by drug-polymer interactions persisting in aqueous environment. *Mol. Pharmaceutics* **2018**.
49. Surwase, S.; Itkonen, L.; Aaltonen, J.; Saville, D.; Rades, T.; Peltonen, L.; Strachan, C., Polymer incorporation method affects the physical stability of amorphous indomethacin in aqueous suspension. *Eur. J. Pharm. Biopharm* **2015**, *96*, 32-43.
50. Ullah, M.; Hussain, I.; Sun, C. C., The development of carbamazepine-succinic acid cocrystal tablet formulations with improved in vitro and in vivo performance. *Drug Dev. Ind. Pharm.* **2016**, *42* (6), 969-976.
51. Qian, F.; Wang, J.; Hartley, R.; Tao, J.; Haddadin, R.; Mathias, N.; Hussain, M., Solution behavior of PVP-VA and HPMC-AS-based amorphous solid dispersions and their bioavailability implications. *Pharm. Res.* **2012**, *29* (10), 2766-2776.
52. Jacobi, E.; Schuttenberg, H.; Schulz, R. C., A new method for gel permeation chromatography of polyamides. *Makromol. Chem. Rapid. Comm.* **1980**, *1* (6), 397-402.
53. Hoffman, J. D., Thermodynamic driving force in nucleation and growth processes. *J. Chem. Phys.* **1958**, *29* (5), 1192-1193.
54. Rowland, R. S.; Taylor, R., Intermolecular nonbonded contact distances in organic crystal structures: Comparison with distances expected from van der Waals radii. *J. Phys. Chem.* **1996**, *100* (18), 7384-7391.

Chapter 5. Probing the Interplay between Amorphous Solid Dispersion Stability and Polymer Functionality[†]

5.1 Introduction

The amorphous form of a pharmaceutical can display dramatically improved solubility compared to crystalline forms.^{1, 2} However, the amorphous state is metastable³ and additives are often necessary to delay crystallization and reap the benefits of this high energy state in pharmaceutical formulations.⁴ Polymers have shown promise as crystallization inhibitors, yet there is no consensus on the most relevant chemical factors that dictate the ability of a polymer to slow crystallization.^{5, 6} It has been proposed that polymers restrict crystallization by decreasing the molecular mobility of pharmaceuticals in the amorphous state.⁷ A decrease in mobility could stem from an anti-plasticizing effect where polymer raises the glass transition temperature of a pharmaceutical dispersion.⁸ In practice, there is not a direct relationship between the glass transition temperature of a polymer and its ability to inhibit crystallization.⁹⁻¹¹ Strong intermolecular interactions (e.g. hydrogen bonding) between drug molecules and polymer chains have been shown to occur in systems showing low mobility and slow kinetics of crystallization.¹²⁻¹⁶ However, these functional group trends derive from a few examples, and although the ability of specific polymers to stabilize against crystallization has been studied for a number of drug molecules, such studies employ a diverse set of polymeric materials in order to draw broad chemical conclusions; the validity of such structure-function relationships may be convoluted with parameters such as polymer molecular weight and backbone chain chemistry.

[†] Adapted from Frank, D. S.; Matzger, A. J. *Mol. Pharmaceutics* **2018**, *15*(7), 2714-2720.

In order to elucidate the relationship between functional groups within a polymer and the ability of a polymer to inhibit amorphous form crystallization, a series of polymers was synthesized on a common scaffold. This was accomplished via functionalization of a single batch of poly(chloromethylstyrene-*co*-styrene) such that average degree of polymerization and backbone chemistry could all be held constant. As shown in Figure 5.1, functionalities were selected to explore the impact of hydrogen bonding on the stability of dispersions and test—without influencing other structural parameters—how modulating the interaction strength between polymer and drug alters the kinetics of crystallization. Nabumetone, a Biopharmaceutics Classification System (BCS) class II nonsteroidal anti-inflammatory drug,¹⁷ was selected as a model pharmaceutical for this study because of its fast crystallization kinetics at room temperature and lack of degradation upon melting. This latter point is particularly critical for establishing generalizable conclusions, because individual drugs will have characteristic decomposition products that may vary depending on polymer and will almost certainly influence crystallization kinetics. By comparing polymers with protic functionalities (which can donate a hydrogen bond to nabumetone) and their methylated counterparts (which cannot), the prevailing theory that hydrogen bonding imparts stability to an amorphous dispersion was tested for a set of otherwise equivalent polymers.

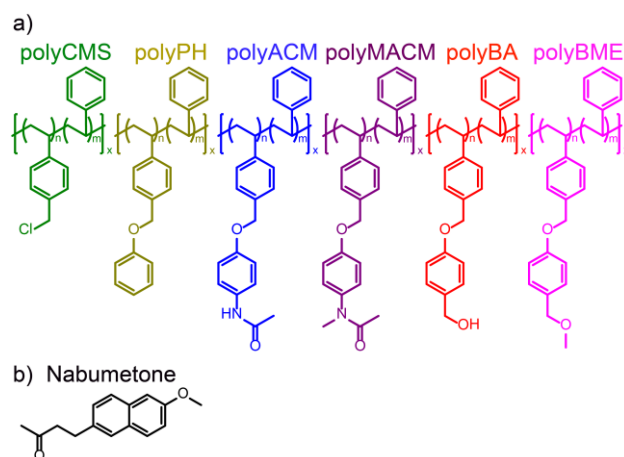


Figure 5.1 a) Series of statistical copolymers studied as crystallization inhibitors in amorphous solid dispersions with b) nabumetone. Each is given a name corresponding to functional groups on the polymers; polyCMS is the parent poly(chloromethylstyrene-*co*-styrene) polymer, polyPH has a phenyl group, polyACM bears an acetaminophen ligated through the phenol, polyMACM has bears a methylated acetaminophen, polyBA has a benzyl alcohol functionality, and polyBME has a benzyl methyl ether moiety.

5.2 Experimental

Poly(chloromethylstyrene-*co*-styrene) was synthesized by free radical polymerization in ethylbenzene, resulting in a parent polymer with a molecular weight of 9500 Da which contains 80% chloromethylstyrene repeat units (see Supporting Information for additional details on all experimental procedures). Functionalization was achieved by reacting linear polymer with a substituted phenol and cesium carbonate in dimethylacetamide and functionalization was verified with both Raman and NMR spectroscopies. All functionalized polymers in this study came from a single poly(chloromethylstyrene-*co*-styrene) batch to ensure a consistent polymer length for each sample. Molecular weights were measured using a Shimadzu GPC equipped with a diode array UV-vis detector. Glass transition temperatures were measured by differential scanning calorimetry (DSC) at a 20 °C/min scanning rate in a Q2000 from TA Instruments in hermetically sealed aluminum pans containing pinholes, where T_g was taken as the inflection point along a glass transition. Onset crystallization temperatures were measured at 20 °C/min in a Q20 DSC after quench cooling melts from 105 °C to -20 °C in pans containing pinholes.

Amorphous solid dispersions were prepared by dissolving equal amounts of drug and polymer in dichloromethane (10 mg/mL each) and evaporating 0.25 mL of solution among six regions on a glass slide.¹⁸ The material was heated to 105 °C for at least one minute before quench cooling to 30 °C, yielding amorphous islands which were monitored by time lapse photography for crystallization events. Quench cooling occurred within 19 ± 2 seconds as measured by an FLIR TG165 Spot Thermal Camera. The few crystallites which appeared after only one minute were discarded from statistical analysis, as these represent samples where drug was not adequately mixed with polymer. Crystallizations were run in duplicate with two glass slides for each run to give a minimum of twenty induction times for each polymer sample. Nabumetone displays rapid crystal growth rates relative to its nucleation rate at 30 °C; complete crystallization of amorphous droplets occurred within minutes of initial crystal appearance (Figure 5.2) and was verified to be crystalline nabumetone by polarized light microscopy and PXRD (see 5.12 for PXRD in Supporting Information). Therefore, the recorded induction time is approximated to be the induction time to nucleation without a considerable delay due to slow growth rates, obviating the need to detect nanometer sized nuclei and its associated difficulties.^{19, 20}

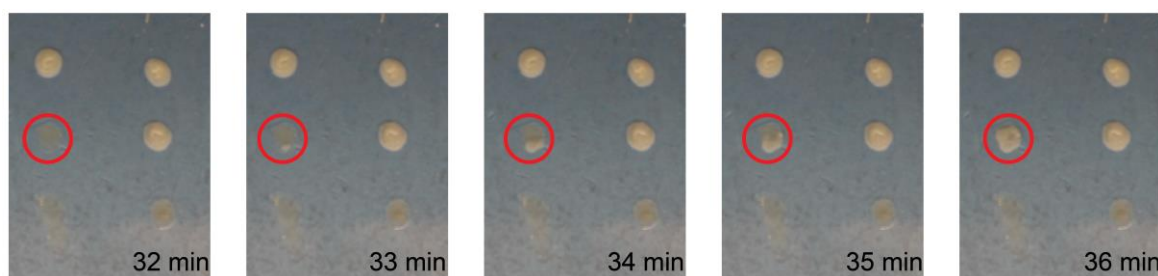


Figure 5.2 Crystal appearance of nabumetone dispersed in polymer (shown here in polyBME). As seen in the sample indicated with a red circle, within three minutes of initial nucleation ($t = 33$ min), crystallization occurs throughout the entire dispersion. Thus the induction time to nucleation is designated as the time to first crystal appearance in dispersions and delays due to growth rates are assumed to be negligible. The two samples at the bottom of the slide remain amorphous over this time period, and the other samples have undergone crystallization earlier in the trial.

5.3 Results

Figure 5.3 shows a probability plot of nabumetone crystallization in 50 wt% dispersions in polymer at 30 °C. In this plot, the percent of amorphous samples containing each polymer that have undergone crystallization is plotted against time to give a curve representing the nucleation rate of nabumetone from each amorphous solid dispersion (see Supporting Information for information on statistical significance). Without added polymer, nabumetone is a rapid crystallizer, and nucleation was recorded to occur on average in 13 minutes. The addition of unfunctionalized polyCMS extends induction times, but in order to dramatically inhibit crystallization, it is necessary to attach more strongly interacting functional groups to the polymer. A general ranking of polymers in their ability to stabilize against crystallization is shown in Figure 5.3. Side chain functionality on a polymer plays a crucial role in dictating the kinetics of nabumetone crystallization, apparent by the diversity of nucleation rates of amorphous solid dispersions, and in this series of polymers of equal size, structure-function relationships can be established without the influence of other polymer parameters. Although the strongest inhibitors of nucleation—polyBA and polyMACM—both contain polar functionalities, the presence of a polar side group on a polymer is not required for strong inhibition. PolyPH, a nonpolar polymer, outperforms both polyACM and polyCMS in stabilizing against crystallization. Many of the polymers which have been investigated in the literature as crystallization inhibitors are water soluble and polar. However, these results hint that nonpolar polymers may rival or outperform many of previously studied polymers to inhibit devitrification of a nonpolar drug such as nabumetone. Furthermore, complimentary hydrogen bonding accepting and donating groups on drug and polymer are not sufficient to ensure the inhibition of crystallization. Nabumetone is a hydrogen bond acceptor, yet the presence of a hydrogen bond donating functionality does not reliably predict which polymers

inhibit the nucleation of nabumetone. Both polyBA and polyACM contain hydrogen bond donating functionalities, yet polyACM is not a particularly strong inhibitor, and methylation of polyACM (and removal of its ability to hydrogen bond with nabumetone) does not result in a polymer with a reduced ability to inhibit crystallization. Neither the presence of a polar functionality nor a hydrogen bond donating side group are necessary to inhibit nucleation in these amorphous solid dispersions.

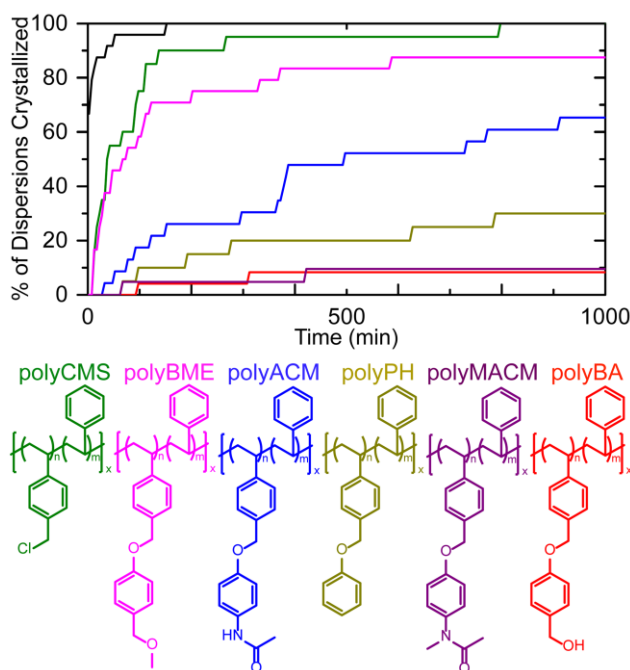


Figure 5.3 Rate of crystallization for nabumetone dispersed in each of the functionalized polymers at 30 °C. The black trace shows pure nabumetone crystallization from the amorphous state and each colored trace represents a 50 wt% dispersion of nabumetone in the corresponding colored polymer, ordered left-to-right according to their relative ability to inhibit crystallization.

The nucleation rates of dispersions were modeled after a Poisson distribution, where $P(t)$, the percent probability of nucleation in each sample after t minutes, is a function of time t and J , a fitted parameter representing the nucleation rate:²¹

$$P(t) = 100 - 100 * \exp(-Jt)$$

Table 1 shows the fitted nucleation rates from each sample. Dispersions were also characterized by differential scanning calorimetry. Glass transition temperatures of each pure polymer are shown in Table 1. Using the Fox equation, which predicts the glass transition temperature of miscible blends, the T_g of nabumetone was calculated and used to approximate T_g of each dispersion containing 50 wt% polymer. These T_g values were not directly measured due to devitrification at slow cooling rates but are proportional to the glass transition temperature of pure polymer.²² Comparing experimental T_g and the fitted nucleation rates shows that the glass transition temperature of pure polymer is a poor predictor of crystallization behavior. Although for nonpolar polymers (polyBME and polyPH) a higher glass transition temperature corresponds with stronger inhibition, for polymers with polar functionalities there is no trend relating the glass transition temperature and inhibition behavior. Such a discrepancy between T_g and crystallization inhibition has been observed in amorphous solid dispersions of water-soluble polymers;^{10, 11} however, this represents the first time the relationship has been established in a series of polymers of equivalent size, indicating a robust finding. Furthermore, although the onset crystallization temperature has been proposed as a gauge for stability of dispersions against crystallization,^{14, 23} it is apparent that the ability of a polymer to inhibit isothermal nucleation is not well approximated by extrapolating this parameter. The onset crystallization temperature was measured by cooling dispersions to -20 °C from 105 °C and recording the temperature of nabumetone crystallization upon heating. Comparing this parameter with the nucleation rate for dispersions, it is clear that the onset crystallization temperature does not approximate isothermal stability against nucleation at 30 °C. For instance, the onset crystallization temperature of unfunctionalized polyCMS dispersions is over 10 °C higher than that of polyPH dispersions in spite of the fact that nabumetone dispersed in polyPH has a nucleation rate thirty times slower than when dispersed in polyCMS. Accelerated

ageing techniques, such as this, thus should be interpreted with care and are not replacements for isothermal nucleation rate measurements.

Table 5.1 Glass transition temperatures for pure functionalized polymers, predicted T_g of polymeric dispersions from the Fox equation, and onset crystallization temperature of nabumetone dispersions (measured by DSC) compared with nucleation rate of dispersions. Values recorded by DSC shown with standard errors are the average of two experimental runs.

	polyCMS	polyBME	polyACM	polyPH	polyMACM	polyBA
$J \times 10^3$ (hr ⁻¹)	783.1 ± 13.1	338.7 ± 9.7	72.2 ± 0.7	25.8 ± 0.3	8.24 ± 0.1	7.48 ± 0.1
T_g Pure Polymer (°C)	107 ± 0.6	47.3 ± 2.7	105 ± 2.5	68 ± 1.3	94 ± 4.4	121.5
Predicted T_g 50 wt% Dispersion (°C)	11	-7	11	0	8	15
Onset Crystallization Temperature (°C)	14.1 ± 0.8	-1.9 ± 0.6	24 ± 0.4	1.1 ± 0.5	10.3 ± 0.1	15.5 ± 0.2

IR Spectroscopy

Hydrogen bonding between polymer and drug will cause peak shifts in the vibrational spectrum of dispersed pharmaceutical.²⁴ Pure amorphous nabumetone contains a carbonyl stretch at 1713.1 cm⁻¹. The transmission IR spectra of nabumetone dispersions in polymers with hydrogen bond donating functionalities show shifting to lower frequency for this carbonyl stretch (see Figure 5.4). This region in the IR does not contain significant peaks from pure polymer (see Supporting Information), thus such shifts can be attributed to intermolecular interaction. The extent of peak shifting—and presumably hydrogen bonding strength—between polymer and drug does not

directly correlate with stability in the amorphous state. While benzyl alcohol functionalities on polyBA donate a hydrogen to the carbonyl group on nabumetone (red-shifting the carbonyl peak frequency to 1711.1 cm^{-1}) and stabilize the dispersion against crystallization, a similar interaction originating from the amide hydrogen on polyACM does not result in lengthened induction times, although the presence of this hydrogen bond can be inferred from IR peak shifting (at 1712.7 cm^{-1}). That being said, the interaction strengths of these hydrogen bonds are weak; spectroscopic investigation of other amorphous pharmaceuticals have shown larger peak shifts when dispersed in polymer,¹⁶ and it is possible that the presence of stronger hydrogen bond donating functionalities would strongly bind to pharmaceutical and restrict crystallization. Furthermore, interactions between polymer and other functionalities on nabumetone might account for improved stability against nucleation although such interactions did not result in dramatic peak shifts of other vibrational modes. From a practical standpoint, although hydrogen bonding correlates with peak shifting in the infrared spectra of nabumetone dispersions, such peak shifting from hydrogen bonding between drug and polymer fails to predict the relative ability of polymer to inhibit the crystallization of nabumetone.

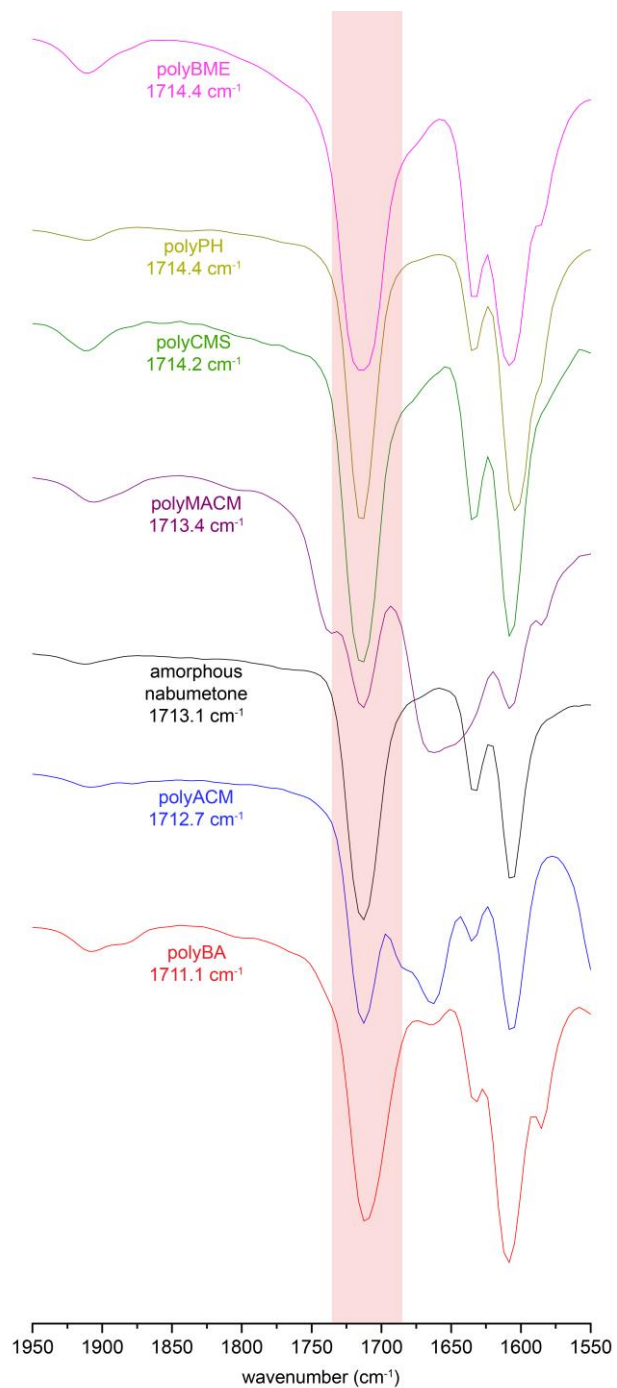


Figure 5.4 Overlaid transmission IR spectra of dispersions ranked top-to-bottom by decreasing peak frequency of the nabumetone carbonyl stretch, highlighted in red.

5.4 Discussion

Hydrogen bonding between polymer and pharmaceutical is a feature often cited to interpret the relative ability of polymers to inhibit crystallization.^{10, 14, 15} It was found that the rate of nucleation of nabumetone from polymeric dispersions depends on the character of hydrogen bond interactions between drug and polymer, and methylation of protic polymer functionalities leads to divergent effects on the stability of dispersions. For a hydroxy functionality, methylation resulted in weaker inhibition of crystallization. Comparing the performance of polyBA and polyBME (Figure 5.1), replacement of a hydroxy group with a methoxy in the polymer dispersion decreases stability (Table 1). It is proposed that the hydrogen bonds formed between hydroxy groups on polyBA and the carbonyl on nabumetone impart stability to the amorphous phase, in line with the classic framework correlating hydrogen bond strength and stability in amorphous solid dispersions.²⁵ However, polymers with hydrogen bond donating amide functionalities did not form dispersions with long-term stability against crystallization; polyACM (containing hydrogen bond donating secondary amide functionalities) is a less potent inhibitor of nucleation compared to polyMACM (containing tertiary amide functionalities which cannot donate a hydrogen bond). We consider two possible reasons for this observed deviation from expectations: limited polymer solubility in drug and polymer-induced heteronucleation from the amorphous phase.

First we examine the possibility that weak stability of dispersions containing polyACM stems from low polymer solubility in nabumetone. The solubility of small-molecule pharmaceuticals in a polymer carrier is regularly considered when addressing the stability of an amorphous dispersion^{26, 27}—high supersaturations of drug in polymer will lead to phase separation of drug and devitrification.²⁸⁻³⁰ However, the solubility of polymer in drug also plays an important role.³¹ Although increasing polymer concentration in a solid dispersion can decrease molecular mobility

and crystallization rates,^{32, 33} high concentration may lead to polymer phase separation or crystallization within the amorphous dispersion.^{31, 34} If polyACM has limited solubility in nabumetone at 50 wt% compared to other dispersed polymers, it would limit its ability to restrict crystallization. Evidence for this solubility discrepancy can be seen by DSC, where nabumetone (Form I) crystallized from polyACM shows less significant melting point depression compared to the crystalline material in polyMACM (see Supporting Information for DSC trace). To further investigate this phenomenon, amorphous solid dispersions containing 16 wt% polymer relative to nabumetone were prepared and their nucleation rates measured (Figure 5.5). At this lower concentration, polyACM is a stronger inhibitor of nucleation than polyMACM, in contrast to at higher weight loadings. We hypothesize that for 50 wt% dispersions of nabumetone in polyACM, polymer shows incomplete solubility in drug, while at a lower concentration, polyACM is fully dissolved in the amorphous phase. The enhanced stability of polyACM dispersions relative to polyMACM at 16 wt% polymer could then be attributed to intermolecular hydrogen bonding between nabumetone and polymer, and at higher weight percent loadings, because polyACM is not soluble in drug, it is less effective than other polymers to stabilize the amorphous phase. Furthermore, dispersions containing 16 wt% polyMACM show dramatically weaker stability than those containing 50 wt% polyMACM, suggesting that more incorporated polymer (when dissolved) corresponds to a higher barrier to nucleation of nabumetone from the amorphous phase.³⁵ As seen in these experiments, polymer solubility in drug plays a salient role in dictating the relationship between polymer functionality and stability of an amorphous dispersion at high weight percent polymer loadings. This point is particularly relevant when designing amorphous formulations for long-term stability—dispersions containing 50 wt% polyMACM show far slower nucleation rates than those containing either 16 wt% or 50 wt% polyACM. One explanation for

why polymer solubility in drug is rarely evoked to interpret the relative inhibitory ability of polymers is that many of the commercially available polymers employed in amorphous solid dispersions contain side chains with weaker homomeric interaction strength (carboxylate,^{36, 37} lactam,^{27, 38, 39} hydroxy⁴⁰) than those explored here, and the solubility of polymer in amorphous drug is seldom a limiting parameter in such systems. However, in this study, extending the scope of polymers to include those with stronger homomeric hydrogen bonding interactions gives rise to examples where solubility of polymer in drug may be a limiting parameter on the ability of a polymer to inhibit crystallization. As a result, stability is difficult to predict from accelerated ageing or spectroscopic data because it depends on both local drug-polymer interactions and global polymer solubility.

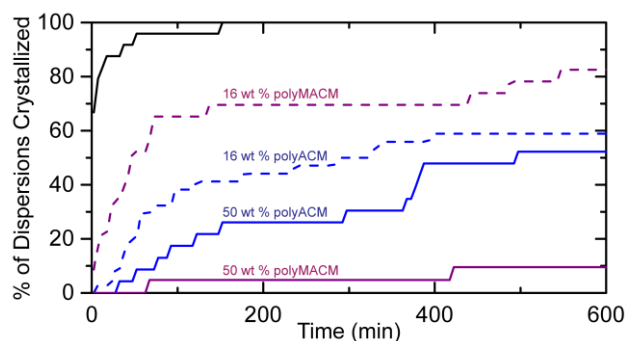


Figure 5.5 Probability plot of nabumetone nucleation from amorphous solid dispersions containing 16 wt% (dotted lines) and 50 wt% (solid lines) of polyACM (blue) and polyMACM (purple). Pure nabumetone crystallization is shown in black.

A second possible origin of the anomalously fast nucleation kinetics of nabumetone dispersed in polyACM is polymer-induced heteronucleation. Phase separation in an amorphous dispersion will lead to polymer-rich regions in contact with drug-rich regions, and this polymer-rich phase might provide a surface to seed crystallization of pharmaceutical. Heterogeneous nucleation on a polymer substrate, also known as polymer-induced heteronucleation, is a well-studied crystallization technique which can result in polymorphic phase direction and enhanced nucleation rates.⁴¹⁻⁴⁷

Although polymer-induced heteronucleation typically employs crosslinked polymers as heteronuclei, there is evidence that linear polymers can display the same effect to speed nucleation in both solution and in the amorphous phase.⁴⁸⁻⁵² Nabumetone is a compound with two known polymorphs.^{53,54} On glass, the thermodynamic polymorph (Form I) nucleates from the supercooled state; in the presence of stabilizing polymers, the metastable form (Form II) was found to appear as well. However, dispersions with polyACM resulted often in crystallizations containing only the thermodynamic form, hinting at the possibility that this polymer preferentially nucleates Form I (see Supporting Information for PXRD data). A common approach in the design of stable amorphous solid dispersions is to encode strong hydrogen bonding interactions between polymer and drug to restrict molecular mobility. However, these same functionalities may template nucleation upon phase separation, promoting more rapid crystallization than less strongly interacting functionalities.^{41, 43} Such a mechanism likely contributes to the weak stability in polyACM dispersions—phase separation in other dispersions may not result in such fast nucleation kinetics due to weaker interaction and weaker propensity to organize molecules from the amorphous phase.

5.5 Conclusion

This study stands out as the postulated relationships between polymer functionality and stability in amorphous solid dispersions have been probed in the absence of other physical differences between polymers, allowing testing of a number of hypotheses in the field.^{5, 55, 56} Two critical findings are: 1) thermal properties (T_g , onset crystallization temperature) are not strong predictors of the isothermal nucleation rate of nabumetone from dispersions, and 2) hydrogen bond donating functionalities are not necessary to stabilize the amorphous state of nabumetone, and at times lead to dispersions with reduced induction times to crystallization. This failure to inhibit crystallization

by polymers containing strongly interacting hydrogen bonding groups is attributed to limited solubility of polymer in amorphous drug—such an argument may explain the behavior of other amorphous solid dispersions, especially those comprising of polymers intended to strongly interact with drug to inhibit crystallization. Once deconvoluted from other physical factors, it is clear that the design for polymers to impart stability to an amorphous dispersion must consider a range of chemical interactions between polymer and drug, and that evaluation of these polymers as crystallization inhibitors cannot rely solely on structural predictions or accelerated ageing without isothermal nucleation rate experiments. Future work will investigate the influence of chemical functionality on stability for a broader range of hydrophobic drugs with the goal of a generalizable framework to predict the ability of a polymer to inhibit crystallization in any amorphous dispersion.

5.6 Supporting Information

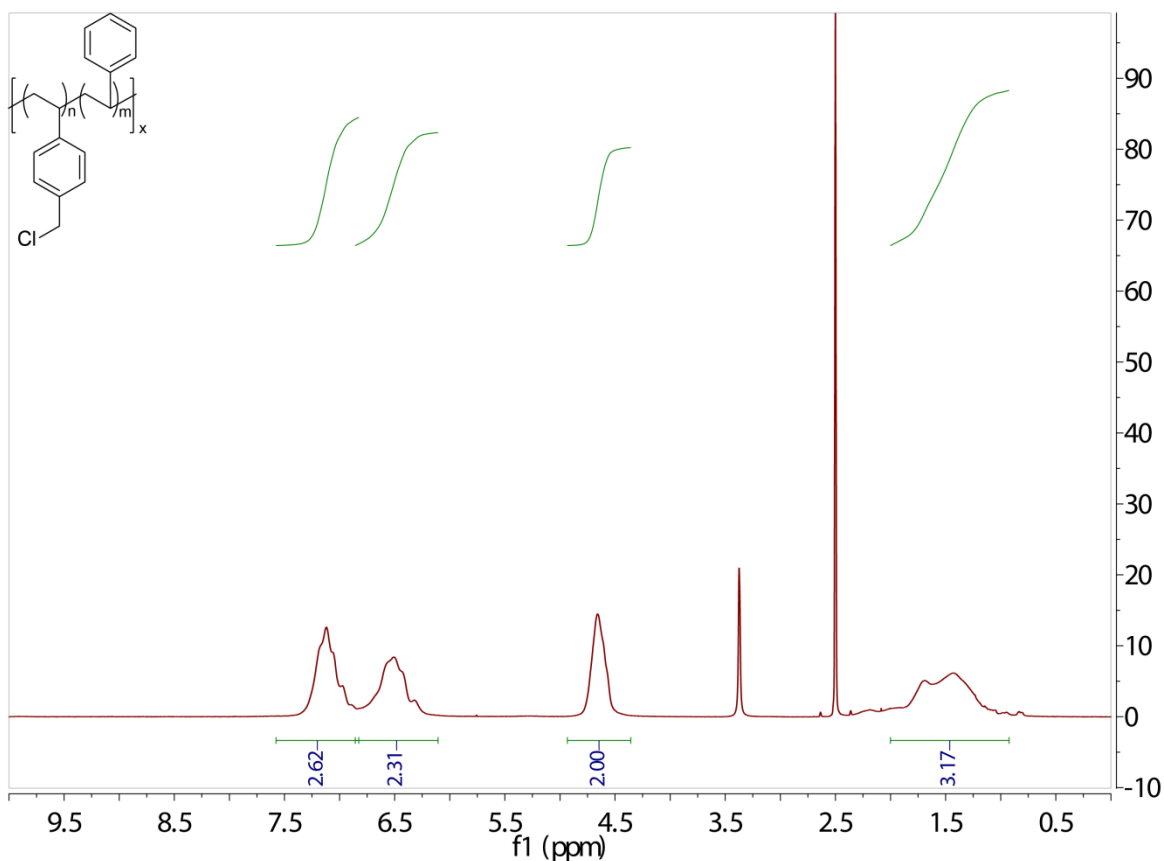
5.6.1 Synthesis and functionalization of poly(chloromethylstyrene-co-styrene)

Styrene (>99.5%) and chloromethylstyrene (90%) were obtained from Sigma Aldrich. Polymerization inhibitor was removed on a 4-tert-butylcatechol removal column prior to use; all other chemicals were used without purification. Phenol (ACS reagent grade) was purchased from Fisher Scientific; acetaminophen (99%) was purchased from MP Biomedicals; methyl-acetaminophen (95%) was purchased from EnamineStore; 4-hydroxybenzyl alcohol (97%) was purchased from Acros; 4-(methoxymethyl) phenol (97%) was purchased from ArkPharm.

Polymer Synthesis

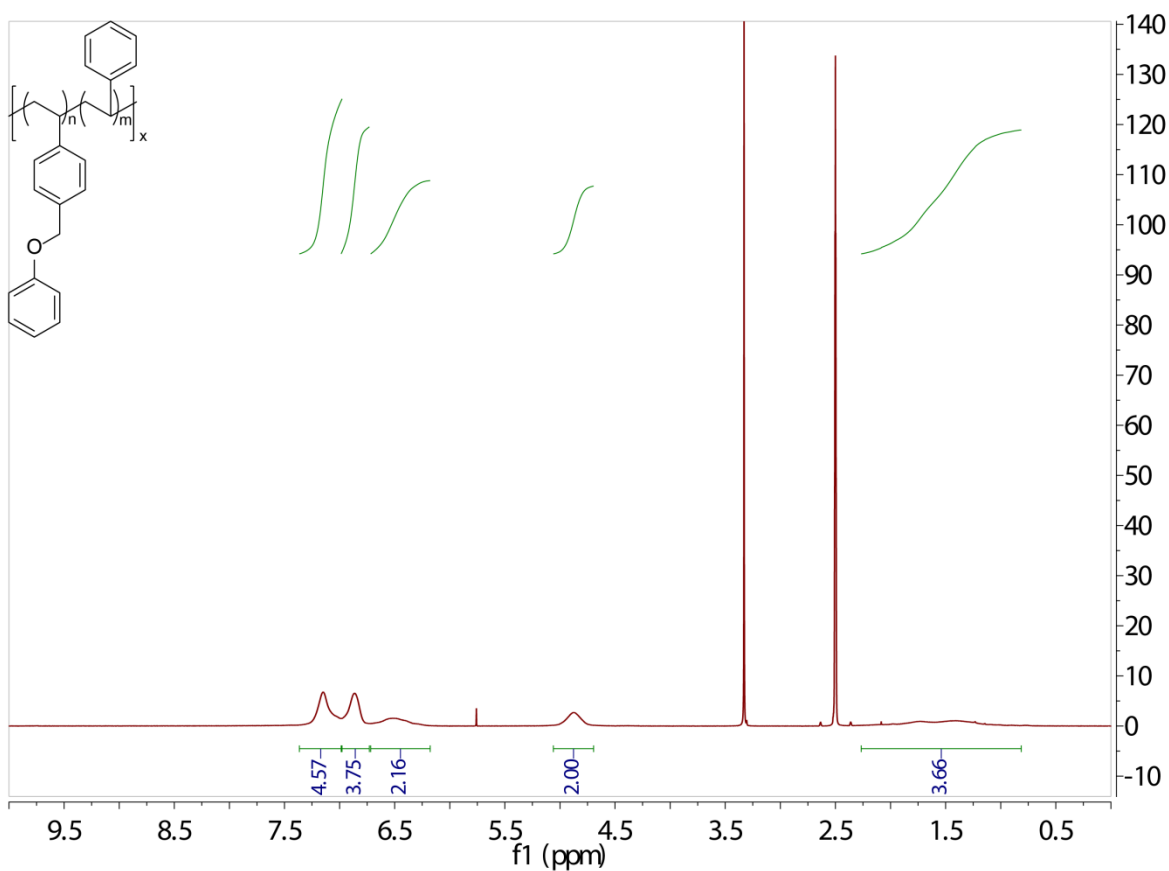
Poly(chloromethylstyrene) was synthesized by free radical polymerization in ethylbenzene. 2,2'-Azobisisobutyronitrile (0.292 mmol) dissolved in ethylbenzene (30 mL) was added to a mixture

of styrene (1.30 mL) and chloromethylstyrene (2.20 mL). The solution was heated at 65 °C for 20 hours under an inert nitrogen atmosphere to allow for polymerization. Polymer was then precipitated in cold hexanes, dissolved in CH₂Cl₂, and reprecipitated in hexanes to give a 1.62 g yield of white polymer. NMR spectroscopy was performed on a Varian Inova 500 MHz instrument and each spectrum was collected for 64 scans with a 2 sec relaxation delay. By NMR integration relative to chloromethyl protons, the resulting copolymer contains 80% chloromethylstyrene and 20% styrene repeat units. ¹H NMR (400 MHz, DMSO-*d*₆, ppm): δ 7.11 (*br*, 3H), δ 6.51 (*br*, 2H), δ 4.65 (*s*, 2H), δ 1.45 (*br*, 3H).



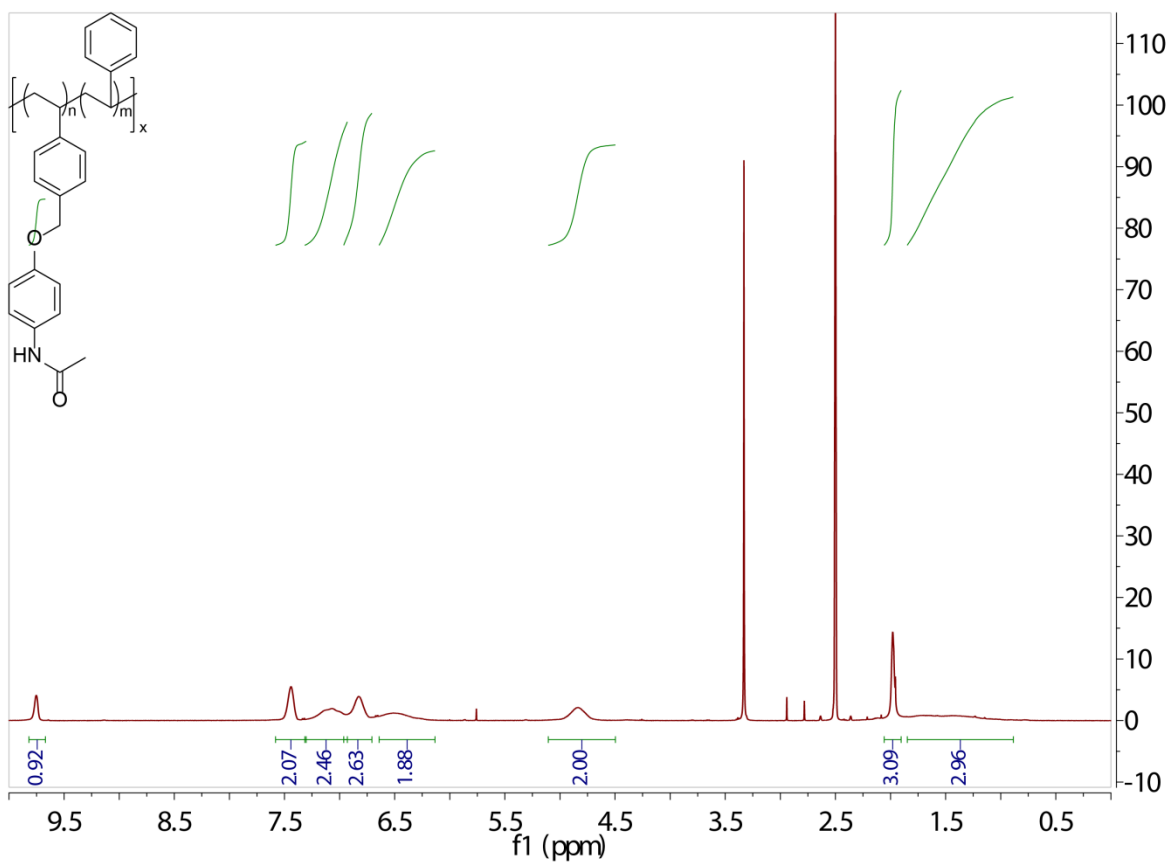
PolyPH

Poly(chloromethylstyrene) (144.3 mg) was reacted in dimethylacetamide (6 mL) with phenol (1.54 mmol) and cesium carbonate (1.38 mmol) under a nitrogen atmosphere for 20 hours at 85 °C. PolyPH was then precipitated in H₂O:MeOH (2:1), dissolved in tetrahydrofuran, reprecipitated in isopropanol, and dried before use. Yield: 71 mg. ¹H NMR (400 MHz, DMSO-*d*₆, ppm): δ 7.15 (*br*, 4H), δ 6.87 (*br*, 3H), δ 6.52 (*s*, 2H), δ 4.88 (*s*, 2H), δ 1.81 (*s*, 3H).



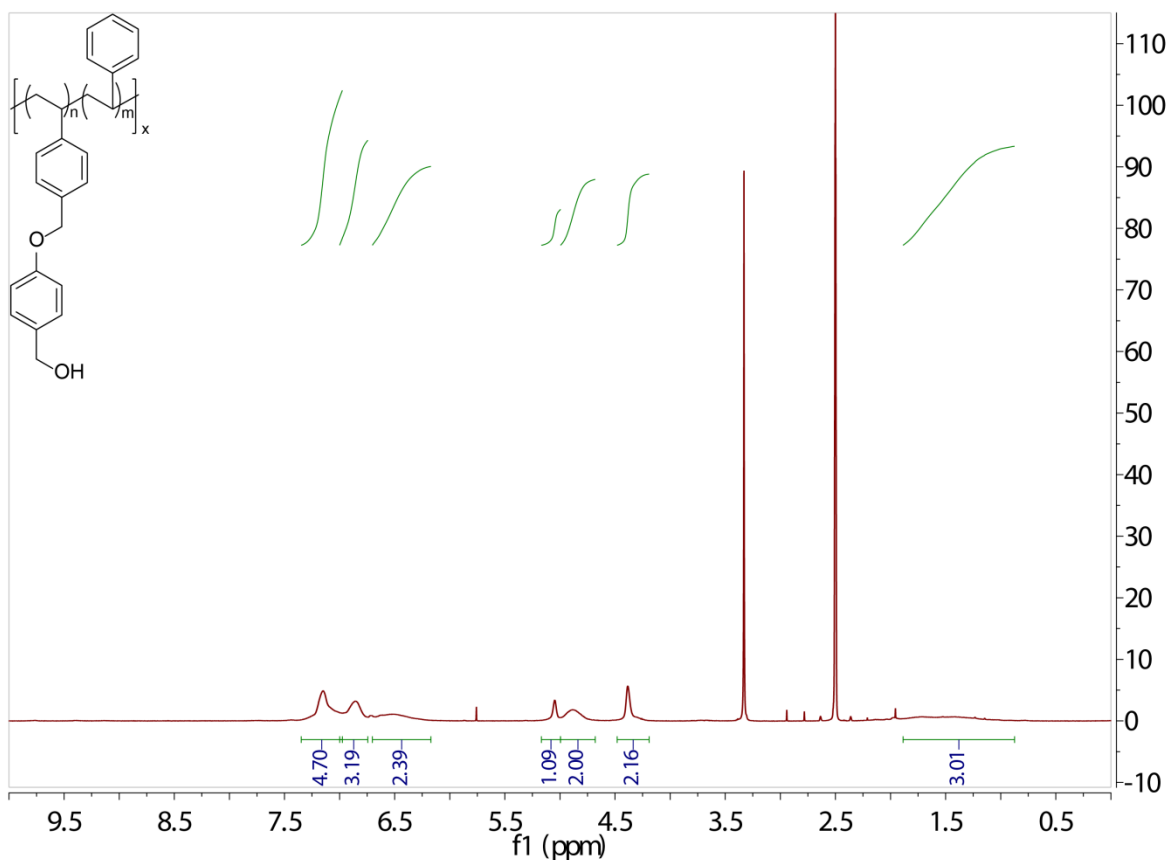
PolyACM

Poly(chloromethylstyrene) (59.9 mg) was reacted in dimethylacetamide (6 mL) with acetaminophen (1.02 mmol) and cesium carbonate (1.42 mmol) under a nitrogen atmosphere for 20 hours at 85 °C. PolyACM was then precipitated in H₂O:MeOH (2:1), dissolved in tetrahydrofuran, reprecipitated in hexanes, washed with ethanol, and dried before use. Yield: 82 mg. ¹H NMR (400 MHz, DMSO-*d*₆, ppm): δ 9.69 (*s*, 1H), δ 7.44 (*br*, 2H), δ 7.06 (*br*, 2H), δ 6.83 (*br*, 2H), δ 6.58 (*br*, 2H), δ 4.84 (*s*, 2H), δ 1.98 (*s*, 3H), δ 1.89 (*br*, 3H).



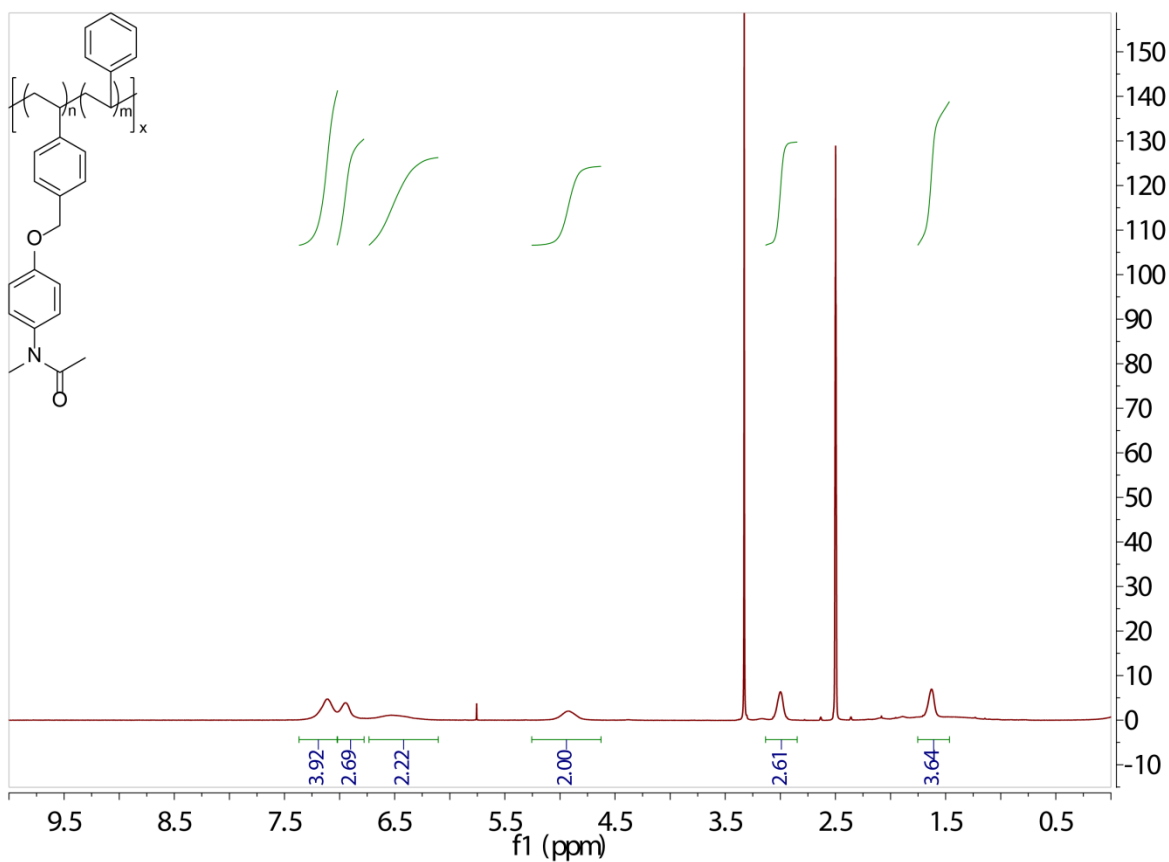
PolyBA

Poly(chloromethylstyrene) (121.5 mg) was reacted in dimethylacetamide (6 mL) with 4-hydroxybenzyl alcohol (1.11 mmol) and cesium carbonate (1.14 mmol) under a nitrogen atmosphere for 20 hours at 85 °C. PolyBA was then precipitated in H₂O:MeOH (2:1), dissolved in tetrahydrofuran, reprecipitated in hexanes, washed with ethanol, and dried before use. Yield: 101 mg. ¹H NMR (400 MHz, DMSO-*d*₆, ppm): δ 7.15 (*br*, 4H), δ 6.86 (*br*, 2H), δ 6.57 (*s*, 2H), δ 5.06 (*s*, 1H), δ 4.88 (*s*, 2H), δ 4.39 (*s*, 2H), δ 1.65 (*br*, 3H).



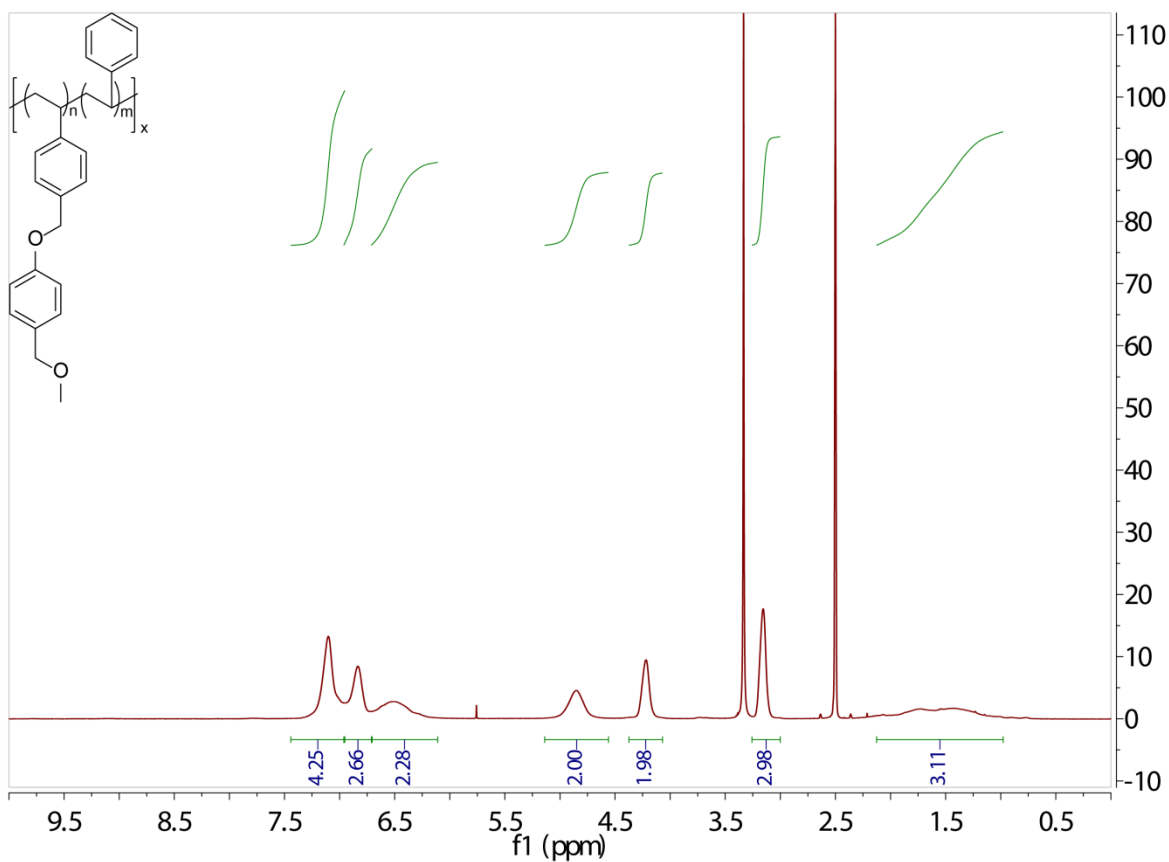
PolyMACM

Poly(chloromethylstyrene) (98.5 mg) was reacted in dimethylacetamide (6 mL) with methylacetaminophen (0.86 mmol) and cesium carbonate (0.89 mmol) under a nitrogen atmosphere for 20 hours at 85 °C. PolyMACM was then precipitated in H₂O:MeOH (2:1), dissolved in tetrahydrofuran, reprecipitated in hexanes, washed with ethanol, and dried before use. Yield: 97 mg. ¹H NMR (400 MHz, DMSO-*d*₆, ppm): δ 7.11 (*br*, 4H), δ 6.95 (*br*, 2H), δ 6.54 (*s*, 2H), δ 4.93 (*s*, 2H), δ 2.97 (*s*, 3H), δ 1.70 (*br*, 3H), δ 1.63 (*s*, 3H).



PolyBME

Poly(chloromethylstyrene) (140.2 mg) was reacted in dimethylacetamide (6 mL) with 4-(methoxymethyl) phenol (1.35 mmol) and cesium carbonate (1.31 mmol) under a nitrogen atmosphere for 20 hours at 85 °C. PolyBME was then precipitated in H₂O:MeOH (2:1), dissolved in tetrahydrofuran, reprecipitated in hexanes, washed with ethanol, and dried before use. Yield: 143 mg. ¹H NMR (400 MHz, DMSO-*d*₆, ppm): δ 7.11 (*br*, 4H), δ 6.77 (*br*, 2H), δ 6.52 (*s*, 2H), δ 4.86 (*s*, 2H), δ 4.22 (*s*, H2), δ 3.16 (*s*, H3), δ 1.66 (*s*, H3).



5.6.2 Raman spectroscopy and PXRD of functionalized polymers

The Raman spectra for all polymers except polyMACM were collected on a Renishaw inVia Raman microscope equipped with a RenCam CCD detector, 785 nm diode laser, 1200 lines/mm grating, and a 65 μm slit. The Raman spectrum for polyMACM was collected on a Renishaw inVia Raman microscope with a 633 nm diode laser, 1800 lines/mm grating, 50 μm slit, and a RenCam CCD detector to mitigate strong fluorescence. Spectra were analyzed using the WiRE 3.4 software package and calibrated with a silicon standard. Shown in Figure 5.6, the vibrational peak associated with a chloromethyl stretch at 676 cm^{-1} is not present after functionalization of the parent poly(chloromethylstyrene-co-styrene) polymer, indicating transformation of this functionality.

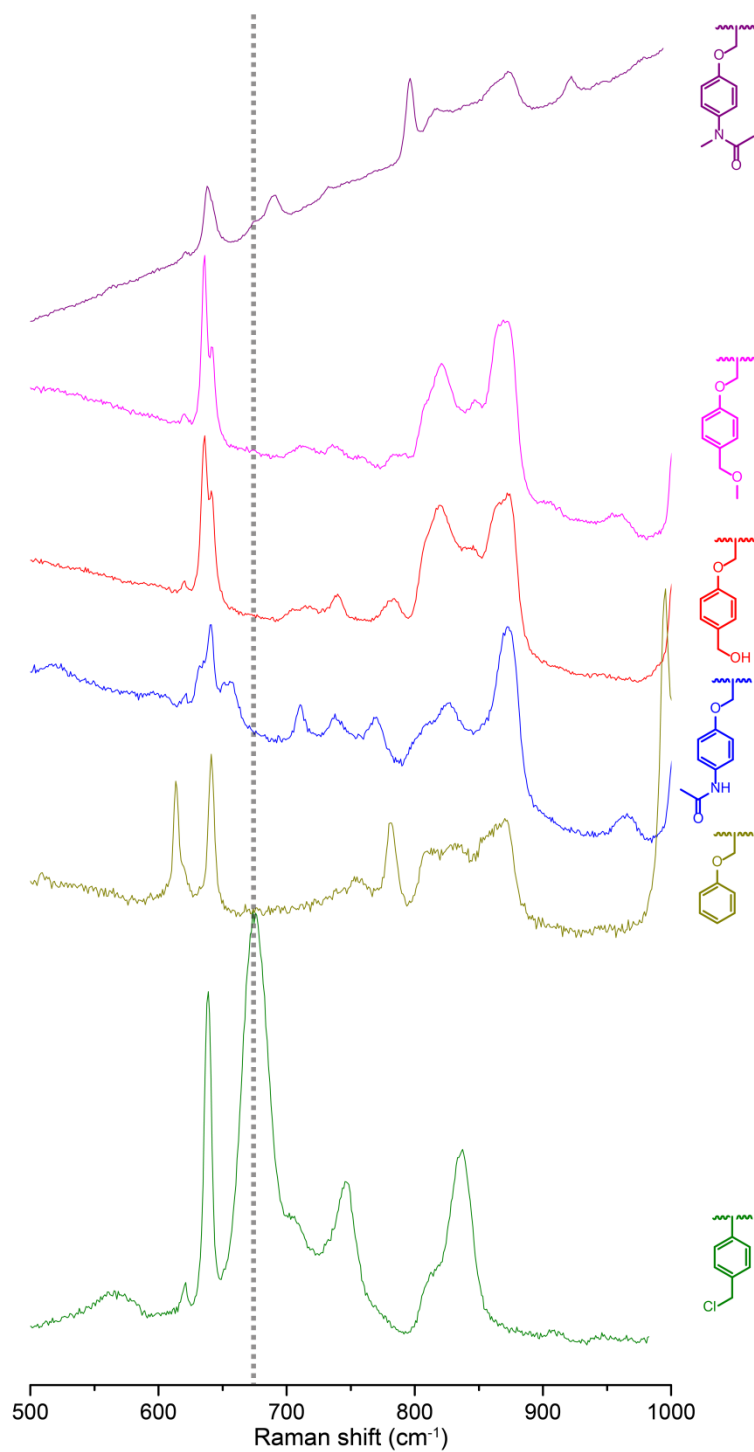


Figure 5.6. Raman spectra of functionalized poly(chloromethylstyrene-*co*-styrene) polymers used in this study, labeled by side-chain functionality.

Furthermore, synthesized polymers were evaluated by powder X-ray diffraction for the presence of crystallinity. PXRD data was collected on a Rigaku SmartLab X-ray diffractometer at 40 kV,

44 mA using CuK α radiation ($\lambda = 1.54187 \text{ \AA}$) from 5° to 60° 2θ with a scan speed of 1.5 s/step and a step size of 0.01° . As shown in Figure 5.7, all functionalized derivatives of polyCMS are amorphous.

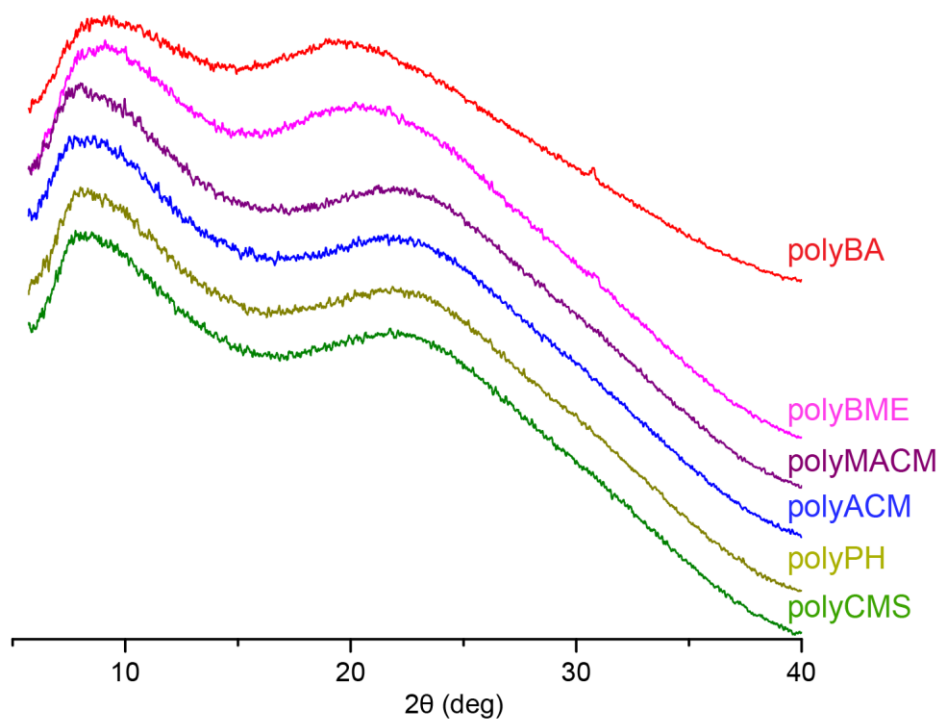


Figure 5.7. PXRD of functionalized polymers labelled by chemical name as designed in Figure 5.1 in the manuscript text.

5.6.3 GPC of functionalized polymers

GPC was collected on a Shimadzu GPC using THF as a solvent monitoring at 225 nm. Molecular weights were determined using polystyrene as a standard (see Figure 5.8 for GPC traces). All polymers functionalized for this study came from the same synthesized batch of poly(chloromethylstyrene-*co*-styrene). Differences in molecular weight as determined by GPC are likely due to changes in the hydrodynamic volume of these polymers rather than actual changes in number average molecular weight.

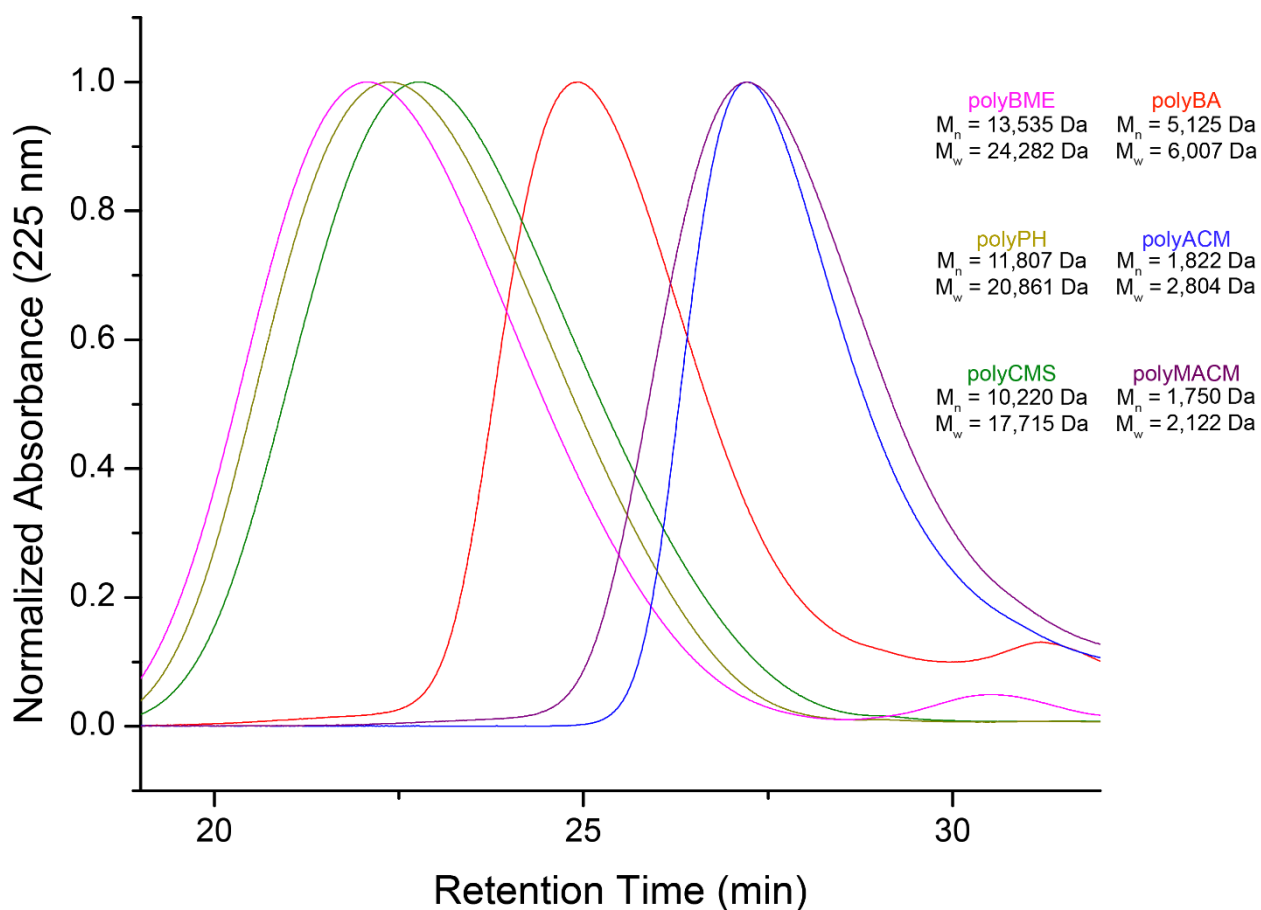


Figure 5.8. GPC traces for functionalized poly(chloromethylstyrene-*co*-styrene) polymers.

5.6.4 Transmission IR Spectroscopy of amorphous solid dispersions

IR spectra were collected on a Nicolet iN10 MX IR microscope in transmission mode on a glass cover slip. As shown in Figure 5.9, there are no intense peaks from polymer in the vicinity of the carbonyl stretch of amorphous nabumetone at 1713.1 cm^{-1} , which allows peak shifts to be a gauge for hydrogen bonding to this moiety on the drug.

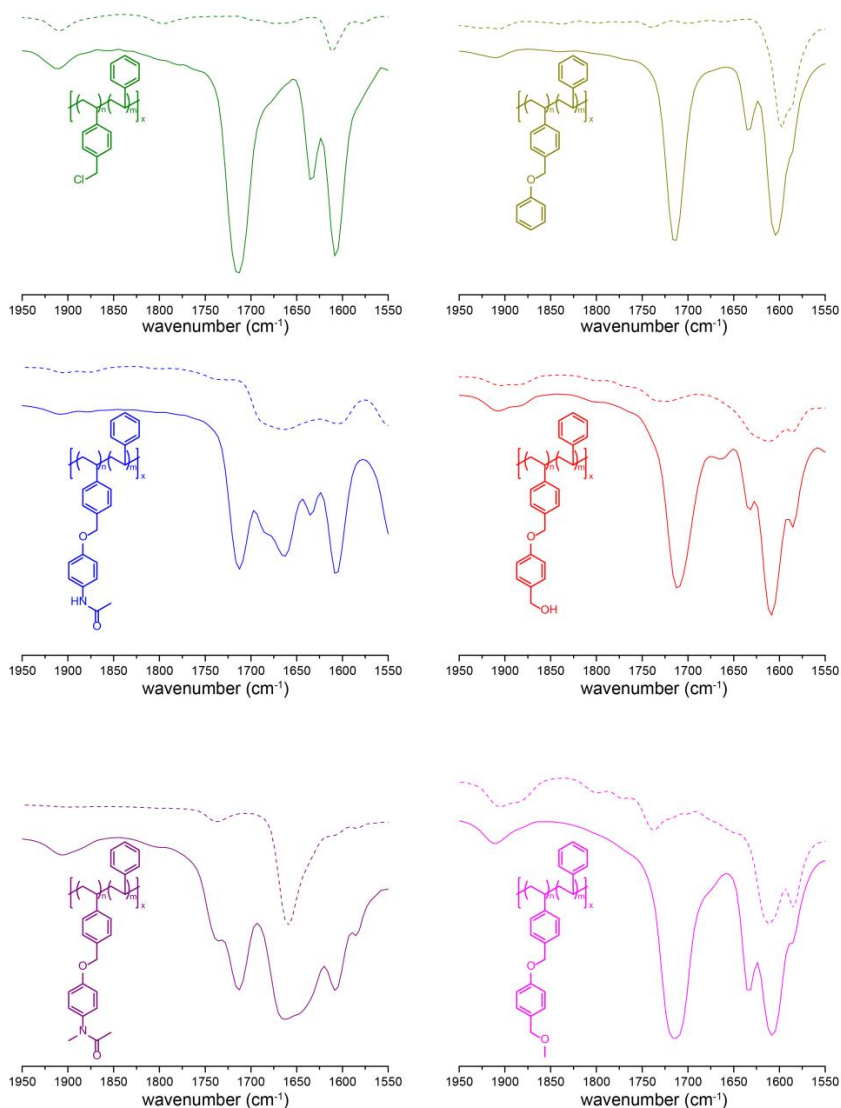


Figure 5.9. Transmission IR spectra comparing pure polymer (dotted line) and dispersion with nabumetone (solid line).

5.6.5 Methodology and statistical significance of induction time measurements

Table 5.2 shows the measured induction times for amorphous solid dispersions used to produce the probability plots shown in Figures 5.3 and 5.5 in the manuscript.

Table 5.2. Recorded induction times (in minutes) to crystallization for amorphous solid dispersion samples prepared in this work.

Control	50 wt% polyCMS	50 wt% polyPH	50 wt% polyACM	50 wt% polyMACM	50 wt% polyBA	50 wt% polyBME	16 wt% polyACM	16 wt% polyMACM
1	13	66	30	421	98	10	34	6
2	17	276	52	65	313	13	187	9
2	15	629	75	no crystals observed	1044	25	670	21
2	20	789	92	no crystals observed	no crystals observed	48	26	23
4	39	96	124	no crystals observed	no crystals observed	68	35	37
6	40	194	299	no crystals observed	no crystals observed	106	40	74
7	97	no crystals observed	383	no crystals observed	no crystals observed	370	48	27
7	136	no crystals observed	496	no crystals observed	no crystals observed	585	95	42
14	265	no crystals observed	734	no crystals observed	no crystals observed	10	285	47
35	796	no crystals observed	772	no crystals observed	no crystals observed	11	325	72
50	13	no crystals observed	1206	no crystals observed	no crystals observed	33	28	807
150	14	no crystals observed	1063	no crystals observed	no crystals observed	46	56	7
1	27	no crystals observed	152	no crystals observed	no crystals observed	114	72	10
1	39	no crystals observed	369	no crystals observed	no crystals observed	120	124	67
1	36	no crystals observed	388	no crystals observed	no crystals observed	201	179	485
4	69	no crystals observed	377	no crystals observed	no crystals observed	20	1185	549

4	92	no crystals observed	911	no crystals observed	no crystals observed	32	no crystals observed	no crystals observed
4	94	no crystals observed	no crystals observed	no crystals observed	no crystals observed	75	no crystals observed	no crystals observed
1	96	no crystals observed	no crystals observed	no crystals observed	no crystals observed	99	no crystals observed	no crystals observed
2	111	no crystals observed	no crystals observed	no crystals observed	no crystals observed	331	no crystals observed	
3	114		no crystals observed	no crystals observed	no crystals observed	20	no crystals observed	
3			no crystals observed	no crystals observed		no crystals observed	no crystals observed	
3			no crystals observed	no crystals observed		no crystals observed	no crystals observed	
16				no crystals observed		no crystals observed	no crystals observed	
							no crystals observed	
							no crystals observed	
							no crystals observed	
							no crystals observed	
							no crystals observed	
							no crystals observed	
							no crystals observed	
							no crystals observed	
							no crystals observed	

To determine statistical significance, the average induction time, τ , and its associated standard error were determined by linear regression using the formula $\ln(P) = -t/\tau$, where P is the probability of no crystallization within time t , following procedures from Diao, et al.⁵⁷ As can be seen in Figure 5.10, the only samples with overlapping confidence intervals are polyCMS and polyBME.⁵⁸ That being said, statistical equivalence between polyCMS and polyBME does not alter the broader conclusions in the manuscript.

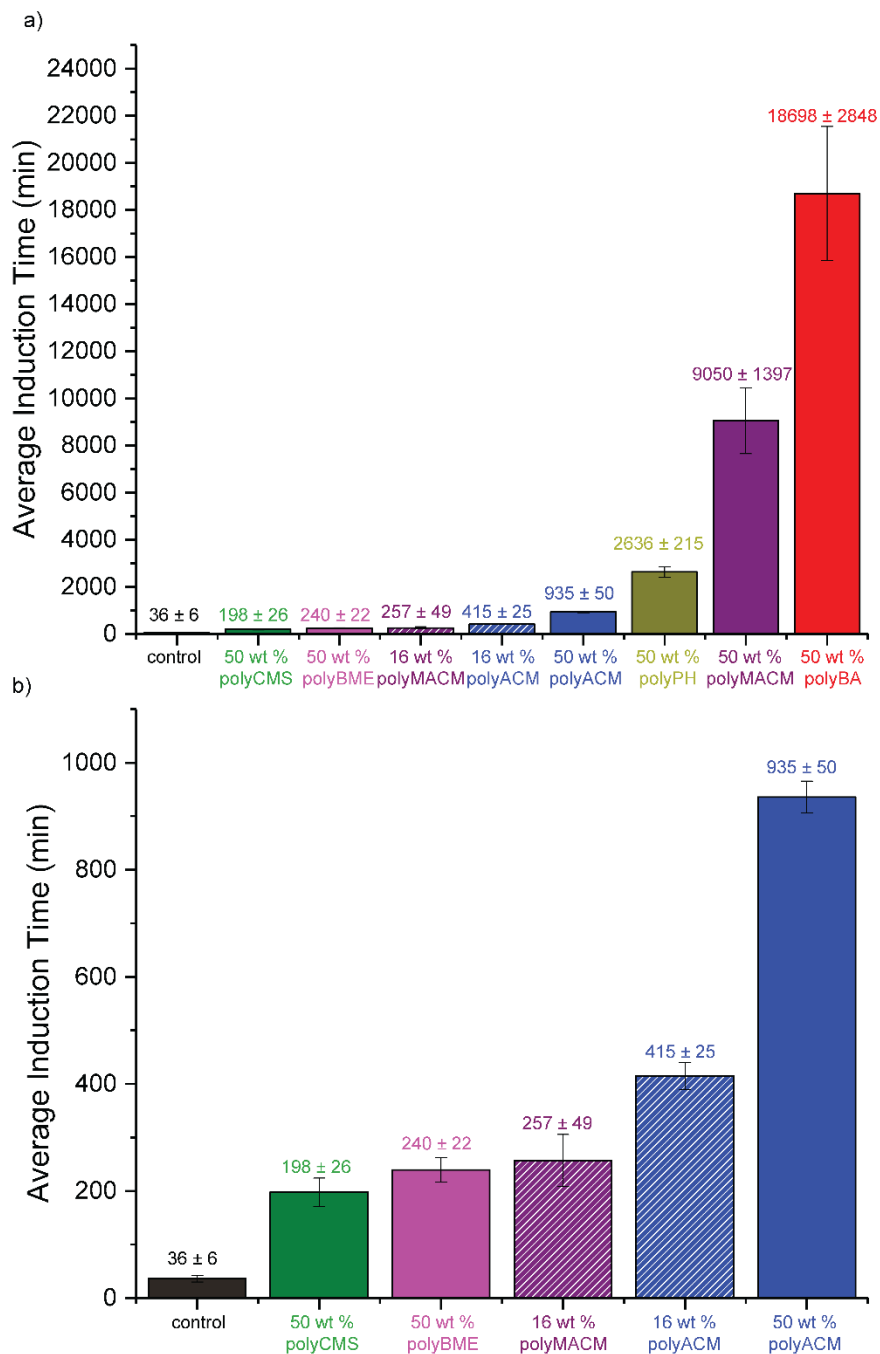


Figure 5.10. Average induction times to crystallization as determined by linear regression—standard errors were determined by standard error to slopes regressed in $\ln(P) = -t/\tau$. Plot a) compares across all polymers used as inhibitors in this study, while plot b) compares the fastest crystallizing samples.

5.6.6 Polarized light microscopy of amorphous solid dispersion crystallization

Polarized light microscopy was used to unambiguously verify that the growing turbid masses on amorphous dispersions were crystalline nabumetone. A crystallization of 50 wt% polyCMS dispersions was performed between polarizing filters while backlit by a Phlox White LED, supplied by Hirox, and imaged via time-lapse photography. This method did not guarantee a controlled temperature for isothermal crystallization, thus the induction time measurements were not included in the determination of the nucleation rate of dispersions. However, this technique does show that the turbid masses which appear are crystalline nabumetone. The accompanying video shows the crystallization over a period of 12 hours, where each second in the video corresponds to roughly 30 minutes of real-time crystallization.

5.6.7 Prediction of T_g of dispersions by the Fox Equation

To supplement thermal data on pure poly(chloromethylstyrene-*co*-styrene) derivatives, the glass transition temperature of 50 wt% dispersions was approximated. Because T_g values could not be collected directly due to devitrification at slow cooling rates, they were predicted by the Fox Equation, which estimates the glass transition temperature of miscible amorphous blends:

$$\frac{1}{T_{g,mix}} \sim \sum_i \frac{w_i}{T_{g,i}}$$

Dispersions of polyCMS containing varied wt% of nabumetone were prepared and their glass transition temperatures measured to approximate the T_g of pure nabumetone, shown in Figure 5.11.

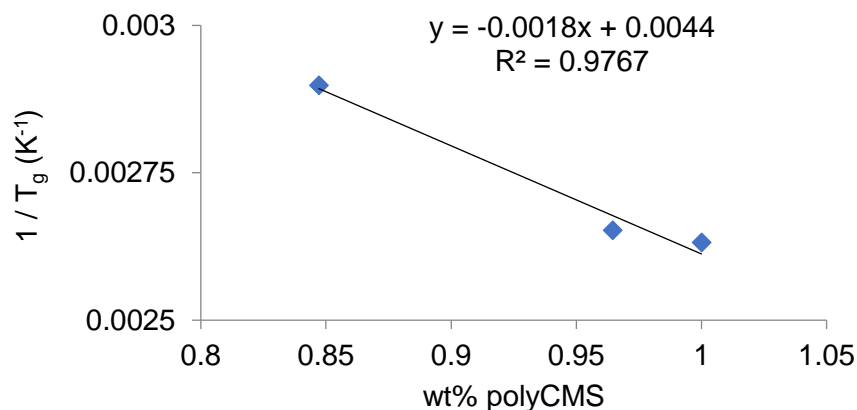


Figure 5.11. Measured T_g of nabumetone dispersions in polyCMS with extrapolated plot to determine the T_g for pure nabumetone.

This method gave a T_g for nabumetone of -46 °C, which is in accordance with predicted values based on the melting temperature of the pharmaceutical.⁵⁹ The glass transition temperature of 50 wt% dispersions can be calculated by reapplying the Fox Equation and are shown in Table 5.1 in the manuscript.

5.6.8 Powder X-Ray Diffraction of nabumetone crystallized from amorphous solid dispersions

PXRD data were collected on a Rigaku SmartLab X-ray diffractometer at 40 kV, 44 mA using CuK α radiation ($\lambda = 1.54187 \text{ \AA}$) from 5° to 35° 2θ with a scan speed of 0.6 s/step and a step size of 0.01° . Nabumetone from the amorphous phase crystallizes in its thermodynamic polymorph (Form I), indicated by an intense peak at 22° ; the kinetic form (Form II) can be identified by peaks at 6.5° and 9.8° 2θ .⁵³ As can be seen in Figure 5.12, all dispersions except polyACM seed growth of the metastable form of nabumetone (or some combination of both polymorphs) whereas polyACM results predominately in the thermodynamic polymorph. That being said, Form II of nabumetone did appear in some dispersions of polyACM, albeit in low concentration. This observation leads us to believe that a heteronuclear seeding effect in polyACM dispersions contributes to higher than expected nucleation rates of pharmaceutical.

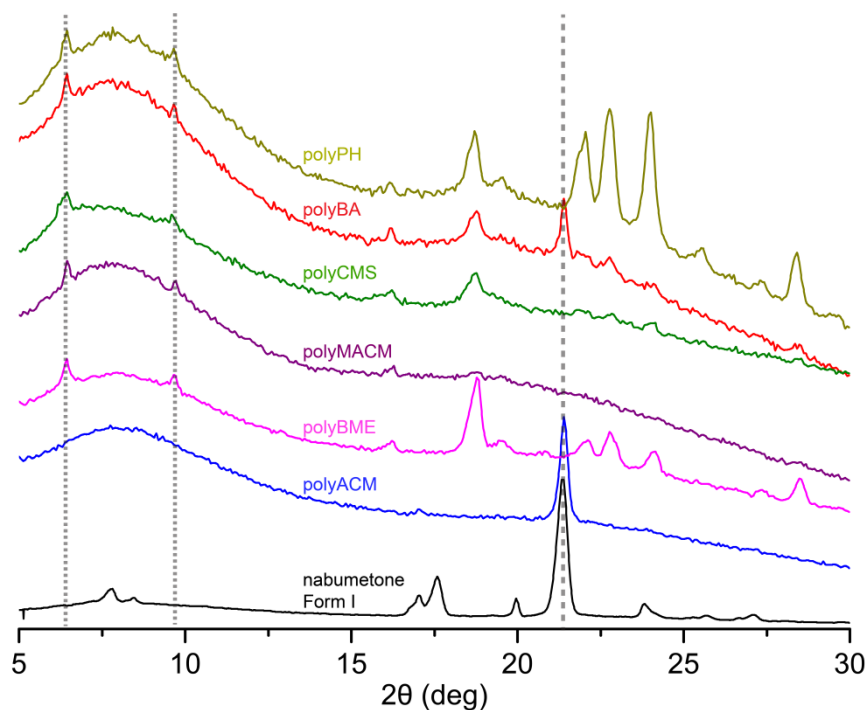


Figure 5.12. PXRD traces for nabumetone crystallites formed from amorphous dispersions—plots correspond to the dispersion labeled above to each curve.

5.6.9 Melting point depression of nabumetone

The melting point for nabumetone Form I was collected for both pure pharmaceutical as well as in dispersions containing 50 wt% polyMACM and 50 wt% polyACM, shown below in Figure 5.13. There is a larger melting point depression of nabumetone in dispersions of polyMACM than polyACM, indicating that polyMACM is more soluble in amorphous nabumetone than polyACM. These traces were collected by heating devitrified dispersions and are normalized to equal enthalpies of fusion.

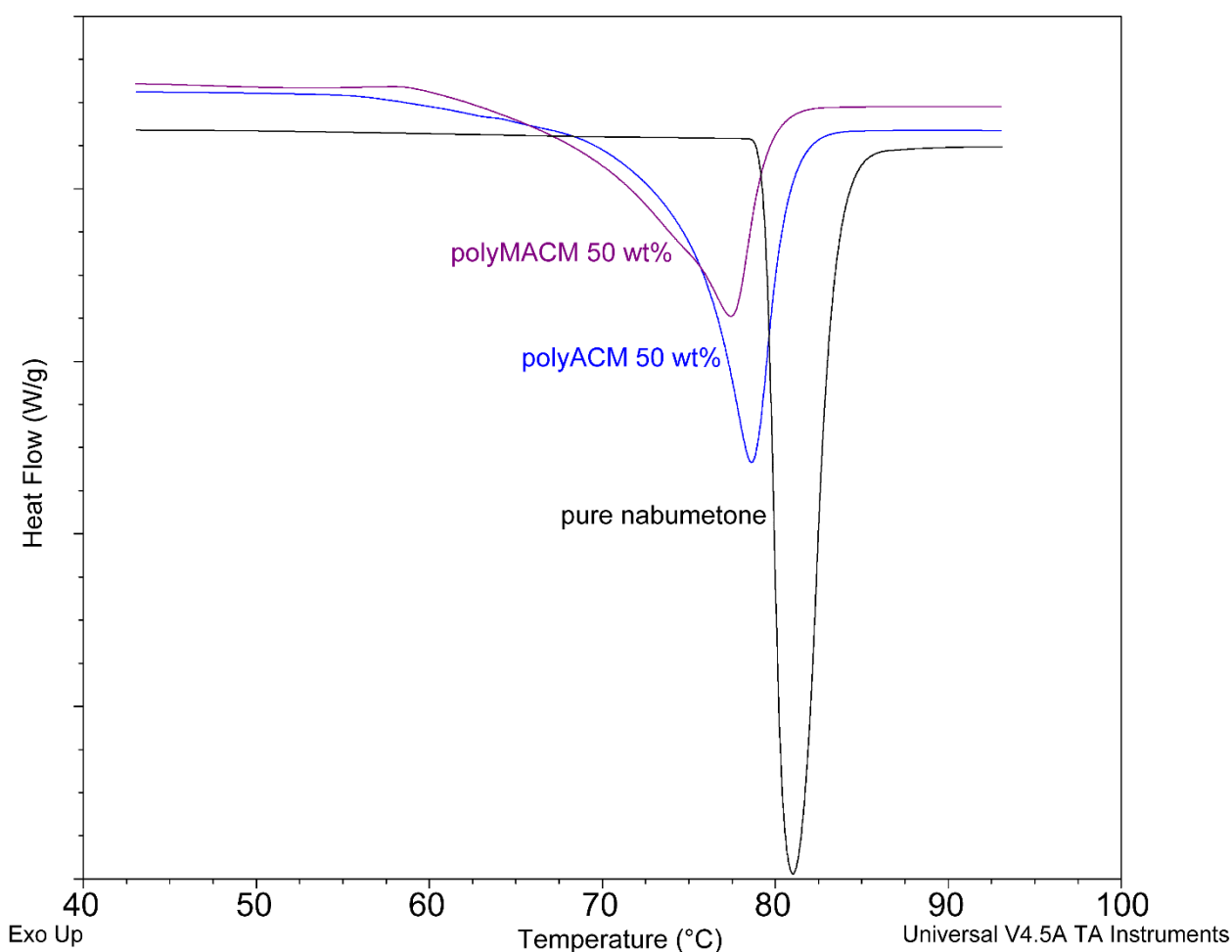


Figure 5.13. DSC of nabumetone Form I showing melting point depression in the presence of polymers.

5.7 References

1. Chiou, W. L.; Riegelman, S., Preparation and dissolution characteristics of several fast-release solid dispersions of griseofulvin. *J. Pharm. Sci.* **1969**, 58 (12), 1505-1510.0.

2. Hancock, B. C.; Parks, M., What is the True Solubility Advantage for Amorphous Pharmaceuticals? *Pharm. Res.* **2000**, *17* (4), 397-404.
3. Hancock, B. C.; Zografi, G., Characteristics and Significance of the Amorphous State in Pharmaceutical Systems. *J. Pharm. Sci.* **1997**, *86* (1), 1-12.
4. Hancock, B. C., Disordered drug delivery: destiny, dynamics and the Deborah number. *J. Pharm. Pharmacol.* **2002**, *54* (6), 737-746.
5. Vasconcelos, T.; Sarmiento, B.; Costa, P., Solid dispersions as strategy to improve oral bioavailability of poor water soluble drugs. *Drug Discovery Today* **2007**, *12* (23-24), 1068-1075.
6. Ting, J. M.; Porter III, W. W.; Mecca, J. M.; Bates, F. S.; Reineke, T. M., Advances in Polymer Design for Enhancing Oral Drug Solubility and Delivery. *Bioconjugate Chem.* **2018**.
7. Yu, L., Amorphous pharmaceutical solids: preparation, characterization and stabilization. *Adv. Drug Deliv. Rev.* **2001**, *48* (1), 27-42.
8. Hancock, B. C.; Shamblin, S. L.; Zografi, G., Molecular Mobility of Amorphous Pharmaceutical Solids Below Their Glass Transition Temperatures. *Pharm. Res.* **1995**, *12* (6), 799-806.
9. Baird, J. A.; Taylor, L. S., Evaluation of amorphous solid dispersion properties using thermal analysis techniques. *Adv. Drug Deliv. Rev.* **2012**, *64* (5), 396-421.
10. Konno, H.; Taylor, L. S., Influence of Different Polymers on the Crystallization Tendency of Molecularly Dispersed Amorphous Felodipine. *J. Pharm. Sci.* **2006**, *95* (12), 2692-2705.
11. Matsumoto, T.; Zografi, G., Physical Properties of Solid Molecular Dispersions of Indomethacin with Poly(vinylpyrrolidone) and Poly(vinylpyrrolidone-co-vinyl-acetate) in Relation to Indomethacin Crystallization. *Pharm. Res.* **1999**, *16* (11), 1722-1728.
12. Chauhan, H.; Kuldipkumar, A.; Barder, T.; Medek, A.; Gu, C.-H.; Atef, E., Correlation of Inhibitory Effects of Polymers on Indomethacin Precipitation in Solution and Amorphous Solid Crystallization Based on Molecular Interaction. *Pharm. Res.* **2014**, *31* (2), 500-515.
13. Kothari, K.; Ragoonanan, V.; Suryanarayanan, R., The Role of Drug–Polymer Hydrogen Bonding Interactions on the Molecular Mobility and Physical Stability of Nifedipine Solid Dispersions. *Mol. Pharm.* **2014**, *12* (1), 162-170.
14. Mistry, P.; Mohapatra, S.; Gopinath, T.; Vogt, F. G.; Suryanarayanan, R., Role of the Strength of Drug–Polymer Interactions on the Molecular Mobility and Crystallization Inhibition in Ketoconazole Solid Dispersions. *Mol. Pharm.* **2015**, *12* (9), 3339-3350.
15. Mistry, P.; Suryanarayanan, R., Strength of Drug–Polymer Interactions: Implications for Crystallization in Dispersions. *Cryst. Growth Des.* **2016**.
16. Taylor, L. S.; Zografi, G., Spectroscopic Characterization of Interactions Between PVP and Indomethacin in Amorphous Molecular Dispersions. *Pharm. Res.* **1997**, *14* (12), 1691-1698.
17. Turner, S.; Ravishankar, J.; Fassihi, R., Method for improving the bioavailability of orally delivered therapeutics. US20060068010 A1, March 30, 2006.
18. Polymers with polar functionalities (polyBA and polyACM) required an additional few drops of methanol to completely dissolve polymer.
19. Ricarte, R. G.; Lodge, T. P.; Hillmyer, M. A., Detection of pharmaceutical drug crystallites in solid dispersions by transmission electron microscopy. *Mol. Pharm.* **2015**, *12* (3), 983-990.
20. Ricarte, R. G.; Lodge, T. P.; Hillmyer, M. A., Nanoscale Concentration Quantification of Pharmaceutical Actives in Amorphous Polymer Matrices by Electron Energy-Loss Spectroscopy. *Langmuir* **2016**, *32* (29), 7411-7419.

21. Jiang, S.; ter Horst, J. H., Crystal Nucleation Rates from Probability Distributions of Induction Times. *Cryst. Growth Des.* **2010**, *11* (1), 256-261.
22. Fox, T. G.; Flory, P. J., The Glass Temperature and Related Properties of Polystyrene. Influence of Molecular Weight. *J. Polym. Sci. A.* **1954**, *14* (75), 315-319.
23. Bhugra, C.; Shmeis, R.; Krill, S. L.; Pikal, M. J., Prediction of Onset of Crystallization from Experimental Relaxation Times. II. Comparison between Predicted and Experimental Onset Times. *J. Pharm. Sci.* **2008**, *97* (1), 455-472.
24. Tang, X. C.; Pikal, M. J.; Taylor, L. S., A Spectroscopic Investigation of Hydrogen Bond Patterns in Crystalline and Amorphous Phases in Dihydropyridine Calcium Channel Blockers. *Pharm. Res.* **2002**, *19* (4), 477-483.
25. Serajuddin, A. T., Solid Dispersion of Poorly Water-Soluble Drugs: Early Promises, Subsequent Problems, and Recent Breakthroughs. *Adv. Drug Deliv. Rev.* **1999**, *88* (10), 1058-1066.
26. Marsac, P. J.; Shamblin, S. L.; Taylor, L. S., Theoretical and Practical Approaches for Prediction of Drug–Polymer Miscibility and Solubility. *Pharm. Res.* **2006**, *23* (10), 2417.
27. Tao, J.; Sun, Y.; Zhang, G. G.; Yu, L., Solubility of Small-Molecule Crystals in Polymers: d-Mannitol in PVP, Indomethacin in PVP/VA, and Nifedipine in PVP/VA. *Pharm. Res.* **2009**, *26* (4), 855-864.
28. Qian, F.; Huang, J.; Hussain, M. A., Drug–Polymer Solubility and Miscibility: Stability Consideration and Practical Challenges in Amorphous Solid Dispersion Development. *J. Pharm. Sci.* **2010**, *99* (7), 2941-2947.
29. Vasanthavada, M.; Tong, W.-Q.; Joshi, Y.; Kislalioglu, M. S., Phase Behavior of Amorphous Molecular Dispersions I: Determination of the Degree and Mechanism of Solid Solubility. *Pharm. Res.* **2004**, *21* (9), 1598-1606.
30. Vasanthavada, M.; Tong, W.-Q. T.; Joshi, Y.; Kislalioglu, M. S., Phase Behavior of Amorphous Molecular Dispersions II: Role of Hydrogen Bonding in Solid Solubility and Phase Separation Kinetics. *Pharm. Res.* **2005**, *22* (3), 440-448.
31. Duong, T. V.; Van Humbeeck, J.; Van den Mooter, G., Crystallization Kinetics of Indomethacin/Polyethylene Glycol Dispersions Containing High Drug Loadings. *Mol. Pharm.* **2015**, *12* (7), 2493-2504.
32. Kothari, K.; Ragoonanan, V.; Suryanarayanan, R., The Role of Polymer Concentration on the Molecular Mobility and Physical Stability of Nifedipine Solid Dispersions. *Mol. Pharm.* **2015**, *12* (5), 1477-1484.
33. Wegiel, L. A.; Mauer, L. J.; Edgar, K. J.; Taylor, L. S., Crystallization of Amorphous Solid Dispersions of Resveratrol during Preparation and Storage—Impact of Different Polymers. *J. Pharm. Sci.* **2013**, *102* (1), 171-184.
34. Rumondor, A. C.; Wikström, H.; Van Eerdenbrugh, B.; Taylor, L. S., Understanding the Tendency of Amorphous Solid Dispersions to Undergo Amorphous–Amorphous Phase Separation in the Presence of Absorbed Moisture. *AAPS PharmSciTech* **2011**, *12* (4), 1209-1219.
35. Marsac, P. J.; Li, T.; Taylor, L. S., Estimation of Drug–Polymer Miscibility and Solubility in Amorphous Solid Dispersions Using Experimentally Determined Interaction Parameters. *Pharm. Res.* **2009**, *26* (1), 139.
36. Weuts, I.; Kempen, D.; Verreck, G.; Peeters, J.; Brewster, M.; Blaton, N.; Van den Mooter, G., Salt formation in solid dispersions consisting of polyacrylic acid as a carrier and three basic model compounds resulting in very high glass transition temperatures and constant dissolution properties upon storage. *Eur. J. Pharm. Sci.* **2005**, *25* (4-5), 387-393.

37. Mesallati, H.; Umerska, A.; Paluch, K. J.; Tajber, L., Amorphous Polymeric Drug Salts as Ionic Solid Dispersion Forms of Ciprofloxacin. *Mol. Pharm.* **2017**, *14* (7), 2209-2223.
38. Simonelli, A.; Mehta, S.; Higuchi, W., Dissolution Rates of High Energy Polyvinylpyrrolidone (PVP)-Sulfathiazole Coprecipitates. *J. Pharm. Sci.* **1969**, *58* (5), 538-549.
39. Mahlin, D.; Berggren, J.; Gelius, U.; Engström, S.; Alderborn, G., The influence of PVP incorporation on moisture-induced surface crystallization of amorphous spray-dried lactose particles. *Int. J. Pharm.* **2006**, *321* (1-2), 78-85.
40. Leuner, C.; Dressman, J., Improving drug solubility for oral delivery using solid dispersions. *Eur. J. Pharm. Biopharm.* **2000**, *50* (1), 47-60.
41. Frank, D. S.; Matzger, A. J., Influence of Chemical Functionality on the Rate of Polymer-Induced Heteronucleation. *Cryst. Growth Des.* **2017**, *17* (8), 4056-4059.
42. López-Mejías, V.; Kampf, J. W.; Matzger, A. J., Polymer-Induced Heteronucleation of Tolfenamic Acid: Structural Investigation of a Pentamorph. *J. Am. Chem. Soc.* **2009**, *131* (13), 4554-4555.
43. Pfund, L. Y.; Price, C. P.; Frick, J. J.; Matzger, A. J., Controlling Pharmaceutical Crystallization with Designed Polymeric Heteronuclei. *J. Am. Chem. Soc.* **2015**, *137* (2), 871-875.
44. Price, C. P.; Grzesiak, A. L.; Matzger, A. J., Crystalline Polymorph Selection and Discovery with Polymer Heteronuclei. *J. Am. Chem. Soc.* **2005**, *127* (15), 5512-5517.
45. Diao, Y.; Helgeson, M. E.; Myerson, A. S.; Hatton, T. A.; Doyle, P. S.; Trout, B. L., Controlled Nucleation from Solution Using Polymer Microgels. *J. Am. Chem. Soc.* **2011**, *133* (11), 3756-3759.
46. Diao, Y.; Helgeson, M. E.; Siam, Z. A.; Doyle, P. S.; Myerson, A. S.; Hatton, T. A.; Trout, B. L., Nucleation under Soft Confinement: Role of Polymer–Solute Interactions. *Cryst. Growth Des.* **2011**, *12* (1), 508-517.
47. Diao, Y.; Whaley, K. E.; Helgeson, M. E.; Woldeyes, M. A.; Doyle, P. S.; Myerson, A. S.; Hatton, T. A.; Trout, B. L., Gel-Induced Selective Crystallization of Polymorphs. *J. Am. Chem. Soc.* **2011**, *134* (1), 673-684.
48. Trasi, N. S.; Oucherif, K. A.; Litster, J. D.; Taylor, L. S., Evaluating the influence of polymers on nucleation and growth in supersaturated solutions of acetaminophen. *CrystEngComm* **2015**, *17* (6), 1242-1248.
49. Liu, X., Interfacial Effect of Molecules on Nucleation Kinetics. *J. Phys. Chem. B* **2001**, *105* (47), 11550-11558.
50. Poornachary, S. K.; Han, G.; Kwek, J. W.; Chow, P. S.; Tan, R. B., Crystallizing Micronized Particles of a Poorly Water-Soluble Active Pharmaceutical Ingredient: Nucleation Enhancement by Polymeric Additives. *Cryst. Growth Des.* **2016**, *16* (2), 749-758.
51. Lang, M.; Grzesiak, A. L.; Matzger, A. J., The Use of Polymer Heteronuclei for Crystalline Polymorph Selection. *J. Am. Chem. Soc.* **2002**, *124* (50), 14834-14835.
52. Trasi, N. S.; Taylor, L. S., Effect of polymers on nucleation and crystal growth of amorphous acetaminophen. *CrystEngComm* **2012**, *14* (16), 5188-5197.
53. Price, C. P.; Grzesiak, A. L.; Lang, M.; Matzger, A. J., Polymorphism of Nabumetone. *Cryst. Growth Des.* **2002**, *2* (6), 501-503.
54. Chyall, L. J.; Tower, J. M.; Coates, D. A.; Houston, T. L.; Childs, S. L., Polymorph Generation in Capillary Spaces: The Preparation and Structural Analysis of a Metastable Polymorph of Nabumetone. *Cryst. Growth Des.* **2002**, *2* (6), 505-510.

55. Janssens, S.; Van den Mooter, G., Physical Chemistry of Solid Dispersions. *J. Pharm. Pharmacol.* **2009**, *61* (12), 1571-1586.
56. Bhugra, C.; Pikal, M. J., Role of Thermodynamic, Molecular, and Kinetic Factors in Crystallization from the Amorphous State. *J. Pharm. Sci.* **2008**, *97* (4), 1329-1349.
57. Diao, Y.; Myerson, A. S.; Hatton, T. A.; Trout, B. L., Surface design for controlled crystallization: The role of surface chemistry and nanoscale pores in heterogeneous nucleation. *Langmuir* **2011**, *27* (9), 5324-5334.
58. To fit polyMACM data, outliers at the end of the crystallization trials were removed from regression analysis.
59. Alzghoul, A.; Alhalaweh, A.; Mahlin, D.; Bergström, C. A., Experimental and computational prediction of glass transition temperature of drugs. *J. Chem. Inf. Model.* **2014**, *54* (12), 3396-3403.

Chapter 6. Conclusions and Future Directions

6.1 Summary of Work

The preceding chapters describe the effect of polymer functionality on the ability of a polymer to impact crystallization. Chapter 2 investigates the use of crosslinked polymers to catalyze crystallization from solution. It was found that key fundamental parameters such as interaction strength between polymer and drug and interaction strength between polymer and solvent dictate the ability of a polymer to serve as a site for heterogeneous nucleation. The ideal application of this technology is to assist in the crystallization of novel drug substances which prove difficult to obtain an initial crystalline form, possibly due to their molecular weight or conformational flexibility. Polymer-induced heteronucleation has shown great success in screening solid forms for polymorphism. In the future, this technology might also show success to seed crystallization for new molecular entities without known crystal structures. By utilizing the principles discussed in this chapter, scientists involved in the solid-state characterization of new compounds will be able to design polymers which can accelerate the isolation of crystalline phases for potential therapeutics.

Chapter 3 showed how polymer-induced heteronucleation can be leveraged for the discovery of polymeric inhibitors of precipitation. Functionalities identified as effective accelerators of nucleation when tethered to insoluble, crosslinked polymers were then incorporated in water-soluble, linear polymers. It was found that functionalities determined to be the best enhancers of nucleation on crosslinked polymers were the best inhibitors of crystallization when tethered to water-soluble polymers. Thus, the best functional groups to include on precipitation inhibitors can

be discovered using relative rates of nucleation acceleration using heterogeneous templates. This work could be applied in the large-scale screening of functionalities to serve as precipitation inhibitors for pharmaceutical crystallization. The discovery of potent inhibitors of crystallization is a major bottleneck in the development of amorphous drug products. In contrast to screening the ability of polymers to inhibit crystallization, which often must be done on the time frame of days to weeks, identifying functionalities that accelerate crystallization can be achieved in the timescale of minutes. This work also demonstrates how manipulating polymer solubility changes the effect of a polymer on the kinetics of crystallization, where insoluble polymers accelerate nucleation, in contrast to soluble polymers which inhibit crystallization.

Inhibiting crystallization from solution and from the amorphous phase are both necessary to ensure fast dissolution rates and high solubility of amorphous solid dispersions. Chapter 4 investigates the relationship between polymers synthesized to inhibit precipitation from solution and those optimized to inhibit crystallization from the amorphous solid-state with the goal of development excipients that contribute to both suppressing nucleation in solution and stabilizing the amorphous phase. In the case of these polymers, for the hydrophobic drug ethenzamide, it was found that maximizing polymer hydrophobicity—while maintaining aqueous solubility—generated excipients that imparted the greatest stability to both supersaturated solutions and to the amorphous phase. This work thus posits that improvements in the design of polymers to inhibit nucleation during precipitation might be applied in the development of polymers to maintain physical stability in amorphous solid dispersions.

Chapter 5 investigates factors determining the ability of linear polymers to inhibit crystallization of amorphous pharmaceutical. A series of polymers synthesized from parent poly(styrene-*co*-chloromethylstyrene) were employed to stabilize the amorphous phase of the hydrophobic drug,

nabumetone. A variety of previously reported metrics correlating with solid-state stability, such as the glass transition temperature and the onset crystallization temperature, were not found to correlate with stability of amorphous solid dispersions when controlled for number-average chain length of polymer excipients. Furthermore, it was found that the solubility of a polymer dispersant in the amorphous phase of drug dictates stability. This insight would imply that there is an impetus to engineer polymers with low cohesive strength to maximize solubility in amorphous drug. Such systems, which were not explored in this paper, might include charged polymers interacting with charged pharmaceutical (care would have to be taken to avoid hygroscopicity of dispersions and to ensure rapid release in solution) or to prepare polymers containing nanostructured domains that can absorb drug in an amorphous blend.

Overall, the structure-function relationships that dictate the impact of a polymer on pharmaceutical crystallization provide insight into the development of novel technologies in the pharmaceutical industry as well as in the basic, mechanistic understanding of crystallization. Post-polymerization functionalization is a useful tool to deconvolute the effects of functional group chemistry on how a polymer impacts crystallization independent of other parameters such as polymer chain length or backbone chain chemistry. Work in this thesis not only provides elements that can be applied in the design of commercial pharmaceutical formulations but also serves to elucidate the role of an additive to alter the kinetic barrier to crystallization.

6.2 Future Directions

One broad conclusion of these studies is that the chemical factors that dictate how a polymer impacts crystallization—be it the polymer accelerating nucleation from solution, inhibiting precipitation, or stabilizing against amorphous phase devitrification—are quite similar. It is demonstrated that the ability of cross-linked polymers to accelerate nucleation and soluble

polymers to inhibit crystallization follow the same rank order of functional groups (Chapter 3). Furthermore, it is shown that hydrophobicity of polymers correlates with stability in both the amorphous phase and in solution (Chapter 4). Future work in this area would be well-positioned to connect the ability of insoluble polymers to heteronucleate crystallization and linear polymers to stabilize the amorphous phase. In the development of amorphous drug products, there is a substantial bottleneck in the stability testing of polymer excipients to stabilize against solid-state crystallization, which must be inhibited on the time order of months to years. Despite some advances in computational prediction and accelerated stability testing, a key deficiency is the lack of an experimental probe that can predict the ability of a polymer to inhibit nucleation from the amorphous phase. Future work might use polymer-induced heteronucleation to investigate how linear polymers can inhibit crystallization from the amorphous phase.

Another dimension of future work would be to investigate not only the stability of amorphous solid dispersions but also dissolution and drug release rates of amorphous solid dispersions with respect to polymer functionality. The ideal polymer to include in a formulation can restrict crystallization both during storage and upon administration. Yet, some polymeric excipients form such strong complexes with pharmaceutical that dissolution and drug release are negatively impacted, leading to limits on the improved bioavailability possible by administering drug in its amorphous form. In these cases, it is necessary to develop both precipitation inhibitors that can adequately release drug in solution as well as amorphous stabilizers of sufficient hydrophilicity that can undergo efficient wetting and dissolution. The relationship between functional group chemistry on a polymer and the ability of a polymer to dissolve and release drug in solution are primarily assessed empirically, similar to the relationship between functional group chemistry and stability. The ability of heteronucleation to probe these other properties of polymers has yet to be

explored. In general, assays to predict structure-function properties of excipients are of substantial need to streamline the design and discovery of polymers in formulation in the pharmaceutical industry.

Finally, the most ambitious goal relevant to this thesis is a predictive model relating the chemical structure of a molecular additive and its impact on the crystallization kinetics of a given compound. The papers in this thesis, as well a larger host of scientific research, discuss the engineering of additives to control the kinetics of crystallization. The mode of action of an additive—either to perturb nucleation, block crystal growth, decrease pharmaceutical diffusivity, or alter the solution structure of dissolved pharmaceutical—is not well understood with reference to a particular molecular additive. In the future, it would be advantageous to understand how additive structure affects nucleation and growth kinetics independently, as well as to investigate how other polymer parameters such as persistence length, molecular weight, backbone chain chemistry, and polymeric architecture contribute to the ability of a polymer to impact crystallization.